Aachener Verfahrenstechnik Series
AVT.CVT – Chemical Process Engineering
Volume 41 (2023)

Jens Rubner

Plasma-Coated Membranes for Gas Separation

DOI: 10.1007/RWTH-2023-09417

Plasma-Coated Membranes for Gas Separation

Plasmabeschichtete Membranen für die Gastrennung

Von der Fakultät für Maschinenwesen der Rheinisch-Westfälischen Technischen Hochschule Aachen zur Erlangung des akademischen Grades eines Doktors der Ingenieurwissenschaften genehmigte Dissertation

vorgelegt von

Jens Rubner

Berichter:
Univ.-Prof. Dr.-Ing. Matthias Wessling
apl. Prof. Dr. rer. nat. Rainer Dahlmann

Tag der mündlichen Prüfung: 26.06.2023

Diese Dissertation ist auf den Internetseiten der Universitätsbibliothek online verfügbar.

Parts of this thesis have previously been published:

Kleines, L., Wilski, S., Alizadeh, P., Rubner, J., Wessling, M., Hopmann, C., & Dahlmann, R. *Structure and gas separation properties of ultra-smooth PE-CVD silicon organic coated composite membranes*, Surface and Coatings Technology, 2021 DOI: 10.1016/j .surfcoat.2021.127338

Kleines, L., Wilski, S., Alizadeh, P., Rubner, J., Wessling, M., Hopmann, C., & Dahlmann, R. *Evaluation of the membrane performance of ultra-smooth silicon organic coatings depending on the process energy density*, Thin Solid Films, 2022 DOI: 10.1016/j .tsf.2022.139169

Jens Rubner, Soukaina Skribbe, Hannah Roth, Lara Kleines, Rainer Dahlmann, Matthias Wessling *On the Mixed Gas Behavior of Organosilica Membranes Fabricated by Plasma-Enhanced Chemical Vapor Deposition (PECVD)* , Membranes, 2022 DOI: 10.3390/membranes12100994

Jens Rubner, Leonie Stellmann, Ann-Kathrin Mertens, Maik Tepper, Hannah Roth, Lara Kleines, Rainer Dahlmann, and Matthias Wessling *Organosilica coating layer prevents aging of a polymer with intrinsic microporosity*, Plasma processes and polymers, 2022 DOI: 10.1002/ppap.202200016

Titel: Plasma-Coated Membranes for Gas Separation
Plasmabeschichtete Membranen für die Gastrennung

Autor: Jens Rubner

Reihe: Aachener Verfahrenstechnik Series
AVT.CVT - Chemical Process Engineering
Volume: 41 (2023)

Herausgeber: Aachener Verfahrenstechnik
Forckenbeckstraße 51
52074 Aachen
Tel.: +49 (0)241 8095470
Fax.: +49 (0)241 8092252
E-Mail: secretary.cvt@avt.rwth-aachen.de
https://www.avt.rwth-aachen.de/AVT

Volltext verfügbar: https://doi.org/10.18154/RWTH-2023-09417

Nutzungsbedingungen:
Die Universitätsbibliothek der RWTH Aachen University räumt das unentgeltliche, räumlich unbeschränkte und zeitlich auf die Dauer des Schutzrechtes beschränkte einfache Recht ein, das Werk im Rahmen der in der Policy des Dokumentenservers „RWTH Publications“ beschriebenen Nutzungsbedingungen zu vervielfältigen.

Universitätsbibliothek
RWTH Aachen University
Templergraben 61
52062 Aachen
https://www.ub.rwth-aachen.de

Danksagung

Diese Arbeit ist das Ergebnis der Zusammenarbeit und der Beiträge Vieler, die in den letzten sechs Jahren mit mir zusammengearbeitet haben. Es wäre unmöglich gewesen, all diese Ideen und Ergebnisse ohne die Unterstützung zahlreicher Personen zu generieren.

Daher möchte ich mich bei meinem Doktorvater Matthias Wessling, meinem zweiten Doktorvater Rainer Dahlmann, meiner zwischenzeitlichen Gruppenleiterin Hannah Roth, all meinen KollegInnen am Lehrstuhl für Chemische Verfahrenstechnik und Freunden, die mich tagtäglich beraten und unterstützt haben, bedanken. Außerdem, möchte ich mich bei allen Studierenden bedanken, die an meinen Projekten mitgewirkt und damit intensiv zu meiner persönlichen Entwicklung und den hier vorgestellten Ergebnissen beigetragen haben: Ann-Kathrin Mertens, Petar Peric, Jenny Ling, Lena Riechers, Bethany Conroy, Jennifer Birke, Soukaina Skribbe, Jacques Hofmann, Yuqing He, Ben Doehmen, Sarah Wolters, Roman Zündorff, Leonie Stellmann, Dominik Schäfer, Alina Kuhlen, Felix Schulze-Hoeing, Paul Salomon, Philipp Säger, Cedric Rösel, Andreas Mielke und Felix Schott.

Zu guter Letzt möchte ich meinen Eltern, Claudia und Günther, sowie meiner Schwester Sonja, danken. Ihr habt mich zu dem gemacht was ich bin. Ihr wart immer für mich da und habt mich in allen Situationen bestmöglich unterstützt. Es ist toll euch im Rücken zu haben und zu wissen, dass ihr immer für einen da seid.

Winning is a choice!

- Gustav Iden

Contents

Danksagung **i**

Abstract **v**

Zusammenfassung **vii**

1. Introduction **1**

1.1. Introduction 1

1.2. Hypothesis and Outline 2

2. Fundamentals on Gas Permeation and Plasma Processes **7**

2.1. Gas separation principles 10

2.1.1. Solution diffusion mechanism 10

2.1.2. Permeation in thin film composite membranes 14

2.1.3. Temperature dependence 17

2.1.4. Time dependence (physical aging) 18

2.1.5. Permeance measurement techniques 20

2.2. Plasma processes in membrane fabrication 23

2.2.1. Fundamentals on plasmas and plasma chemistry 24

2.2.2. Plasma-enhanced chemical vapor deposition 25

2.2.3. Structural properties of plasma polymers 28

2.2.4. Transport properties of plasma polymers 30

2.2.5. Fabrication of membranes by plasma-enhanced chemical vapor deposition 31

3. PECVD Parameter Optimization for the Fabrication of Gas Separation Membranes **35**

3.1. Introduction 37

3.2. Experimental 38

3.3. Results and Discussion 41

3.3.1. Chemical analysis 41

3.3.2. Pure gas permeation . . . 45
3.4. Conclusion . . . 52

4. On the mixed gas behavior of organosilica fabricated by plasma-enhanced chemical vapor deposition 55
4.1. Introduction . . . 57
4.2. Experimental . . . 60
4.2.1. Materials . . . 60
4.2.2. PECVD membrane fabrication . . . 61
4.2.3. XPS measurements . . . 61
4.2.4. FTIR measurements . . . 62
4.2.5. Ellipsometry measurements . . . 62
4.2.6. Permeation measurements . . . 63
4.3. Results and discussion . . . 64
4.3.1. Chemical analysis of the organosilica layer . . . 64
4.3.2. Temperature dependent permeation behavior . . . 66
4.3.3. Mixed gas behavior . . . 68
4.4. Conclusion . . . 74

5. Physical aging mitigation by plasma-polymerized organosilica layers 77
5.1. Introduction . . . 79
5.2. Experimental . . . 81
5.3. Results and discussion . . . 85
5.3.1. Chemical analysis . . . 85
5.3.2. Physical aging monitoring via ellipsometric analysis . . . 89
5.4. Conclusion . . . 100

6. Conclusion and perspectives 103
6.1. Summary . . . 105

A. Appendix 109
A.1. Pure gas permeation . . . 110

Bibliography 113

Abstract

The increase in global energy demand for chemical reactions and subsequent downstreaming processes boosts greenhouse gas emissions and accelerates climate change. Applying polymeric gas separation membranes instead of thermally driven processes offers great potential in enhancing the processes' energy efficiency. Since commercial membranes still lack the necessary separation performance for many applications, researchers have developed many new membrane materials over the past decades. Unfortunately, the synthesis routes for those materials are often complex, challenging to scale up, and the polymers tend to exhibit strong non-ideal effects. As a result, none of those new materials made the step into industrial application.

Unlike most published membrane materials, this work builds upon an already-established technology. So-called plasma-enhanced chemical vapor deposition (PECVD) is used to deposit barrier coatings on polymer films. In this process, monomers and auxiliary gases are injected into a low-pressure vacuum chamber; a plasma is ignited, thereby triggering a chemical reaction. This results in the deposition of an organosilica polymer on a substrate. This thesis aims to utilize PECVD to produce organosilica films with tailored chemical and permeation properties. The deposited films shall be used as highly selective membranes for gas separation and physical aging mitigation coatings.

Nanometer-thin organosilica films were deposited on a polydimethylsiloxane (PDMS) composite membrane or polymers with intrinsic microporosity (PIMs). The thesis investigated the influence of the plasma parameters on the chemical structure and membrane performance of the organosilica layer. The membranes prepared with low plasma energy input showed the lowest oxygen and highest carbon concentrations. Moreover, they exhibited superior size sieving behavior and high permeances. With the gained knowledge, highly selective gas separation membranes were fabricated. These were then tested in various pure and mixed gas environments. Although the deposited organosilica membranes showed signs of voids in their structure, they had excellent helium separation properties. In addition, the influence of organosilica layers on the physical aging behavior of PIMs was investigated. Here, highly oxidized films showed excellent protection against rapid aging for films as thin as 10 nm. They reduced the physical aging velocity by more than two orders of magnitude.

Thus, this thesis shows the capability of PECVD to fabricate highly size-selective gas separation membranes and effective physical aging mitigation layers. Furthermore, since the PECVD process is already established in the industry as continuous roll-to-roll process, the findings open a promising route to fabricating nanometer-thin membranes by a tunable plasma-assisted process and utilizing them in currently challenging separation tasks.

Zusammenfassung

Der weltweite Energiebedarf für chemische Reaktionen und nachfolgende Prozesse war noch nie so hoch wie heute. Mit dem Anstieg des Energieverbrauchs haben auch die Treibhausgasemissionen stetig zugenommen, was den Klimawandel beschleunigt. Eine Möglichkeit den Energiebedarf zu senken besteht darin thermisch betriebene Trennverfahren zu ersetzen. Polymermembranen für die Gastrennung sind ein möglicher Alternativprozess. Da kommerzielle Membranen für viele Anwendungen immer noch nicht die nötige Trennleistung aufweisen, haben Forscher in den letzten Jahrzehnten viele neue Membranmaterialien entwickelt. Leider sind die Synthesewege für diese Materialien oft komplex und schwierig hochzuskalieren, und die Polymere neigen dazu starke nicht-ideale Effekte zu zeigen. Daher wird bisher noch keines dieser neuen Materialien industriell eingesetzt.

Im Gegensatz zu den meisten veröffentlichten Membranmaterialien baut diese Arbeit auf einer bereits etablierten Technologie auf. Die so genannte plasmaunterstützte chemische Gasphasenabscheidung (PECVD) wird zur Abscheidung von Barriereschichten auf Polymerfilmen unter anderem in Rolle-zu-Rolle-Verfahren verwendet. Dabei werden Monomere und Hilfsgase in eine Niederdruck-Vakuumkammer injiziert, ein Plasma gezündet und dadurch eine chemische Reaktion ausgelöst. Dies führt zur Abscheidung eines Organosilica-Polymers auf einem Substrat.

Diese Arbeit zielt darauf ab, PECVD als Verfahren zur Herstellung von Organosilica-Schichten mit maßgeschneiderten chemischen und Permeationseigenschaften zu nutzen. Die abgeschiedenen Schichten sollen als hochselektive Membranen für die Gastrennung und physikalische Alterungsschutzschichten eingesetzt werden.

Nanometerdünne Organosilica-Schichten wurden auf einer Polydimethylsiloxan-Verbundmembran und Polymeren mit intrinsischer Mikroporosität (PIMs) abgeschieden. In der Arbeit wurde der Einfluss der Plasmaparameter auf die chemische Struktur und die Membraneigenschaften der Organosilia-Schicht untersucht. Die Membranen, die mit geringem Plasmaenergieeinsatz hergestellt wurden, zeigten die geringsten Sauerstoff- und höchsten Kohlenstoffkonzentrationen. Darüber hinaus wiesen sie hohe Heliumpermeanzen und -selektivitäten und damit die besten Membraneigenschaften auf. Mit den gewonnenen Erkenntnissen wurden hochselektive Gastrennmembranen hergestellt. Diese wurden anschließend in verschiedenen Rein- und Mischgasumgebungen auf ihre Permeationseigenschaften untersucht. Obwohl die abgeschiedenen Organosilica-Membranen Anzeichen von Defekten in ihrer Struktur aufwiesen, hatten sie hervorragende Heliumtrenneigenschaften. Darüber hinaus wurde der Einfluss von Organosilica-Schichten auf das physikalische Alterungsverhalten von PIMs untersucht. Hier zeigten hoch oxidierte Schichten bereits ab einer Dicke von 10 nm hervorragenden Schutz vor schneller Alterung.

Diese Arbeit zeigt somit die Fähigkeit der plasmaunterstützten chemischen Gasphasenabscheidung zur Herstellung von hochgradig größenselektiven Gastrennmembranen und effektiven physikalischen Alterungsschutzschichten. schichten. Da Rolle-zu-Rolle-Verfahren in der Industrie bereits etabliert sind, eröffnen die Ergebnisse einen neuen Weg zur Herstellung von nanometerdünnen Membranen durch einen einstellbaren plasmagestützten Prozess und deren Einsatz in derzeit herausfordernden Trennaufgaben.

1. Introduction

1.1. Introduction

Membranes are semi-permeable layers fabricated out of polymers, ceramics or metals. Membrane separation processes are one of the basic operations in process engineering. Compared to classical thermally driven separation processes, they stand out due to their low energy demand. Sholl and Lively stated in 2016 that using non-thermally driven purification processes, like membranes, leads to a drastic reduction in energy use, emissions, and pollution [Shol2016]. Currently, membranes are applied in specific fields of water treatment, food and beverage processing, gas separation, and medical applications. Still, they have great potential for application in other processes and to tackle many global challenges of the 21st century. However, improvement of production and process costs and intrinsic membrane properties is needed to increase its market share in industrial applications.

In gas separation, intense research in polymer synthesis has been carried out during the last decades to develop new materials with improved permeability and selectivity. As a result, researchers invented and focused on new membrane material classes like mixed matrix membranes (MMM), polymers with intrinsic microporosity (PIM), carbon molecular sieves (CMS), and others. Nowadays, these materials dominate scientific journals and further push the boundaries of membrane properties. However, the membrane's synthesis and production processes become more complex to achieve these excellent results. Hence, upscaling the fabrication is challenging and often prevents testing of these materials in pilot-scale scenarios. Furthermore, the polymers often show strong permeance or selectivity changes over time caused by non-ideal effects. Thus, none of the promising membrane materials developed over the last two decades is on the market.

This thesis utilizes plasma-enhanced chemical vapor deposition (PECVD) to overcome the challenges of classical polymer chemistry. It is a method already applied in industry to fabricate nanometer-thin coatings for, e.g., coating glass plates, plastic bottles or plastic foils in batch and roll-to-roll processes.. However, in all these applications, the methodology is only used to fabricate barrier coatings. In contrast, this thesis aims to tailor the film's permeation properties by tuning the fabrication parameters to produce highly permeable and selective gas separation membranes.

1.2. Hypothesis and Outline

This thesis deals with the utilization of plasma-enhanced chemical vapor deposition (PECVD) for the fabrication of polymeric thin film composite gas separation membranes or as mitigator of physical aging in polymers of intrinsic microporosity. So far, different research groups published data on gas separation membranes fabricated by PECVD. However, they either used ceramic support membranes to achieve highly selective but very costly membranes or achieved only low selectivities when using polymeric support membranes. Within this work, the aim is to deposit a highly selective PECVD layer on a polymeric support membrane which has both, good membrane properties and production costs comparable to state-of-the-art polymeric gas separation membranes.

As visualized in Figure 1.1, the outline of this thesis consists of 4 scientific chapters:

Chapter 2 introduces the fundamentals of membrane based gas separation and plasma processes. It establishes the solution diffusion mechanism and explains how temperature and time can influence the permeation mechanism. Furthermore, it introduces the two measurement techniques used in this thesis: the pressure increase and the constant pressure method. In addition, the chapter introduces the fundamentals of plasmas and plasma chemistry. It explains the basics of plasma-assisted chemical vapor deposition processes and the influence of different process parameters. It illustrates the evolving structural properties

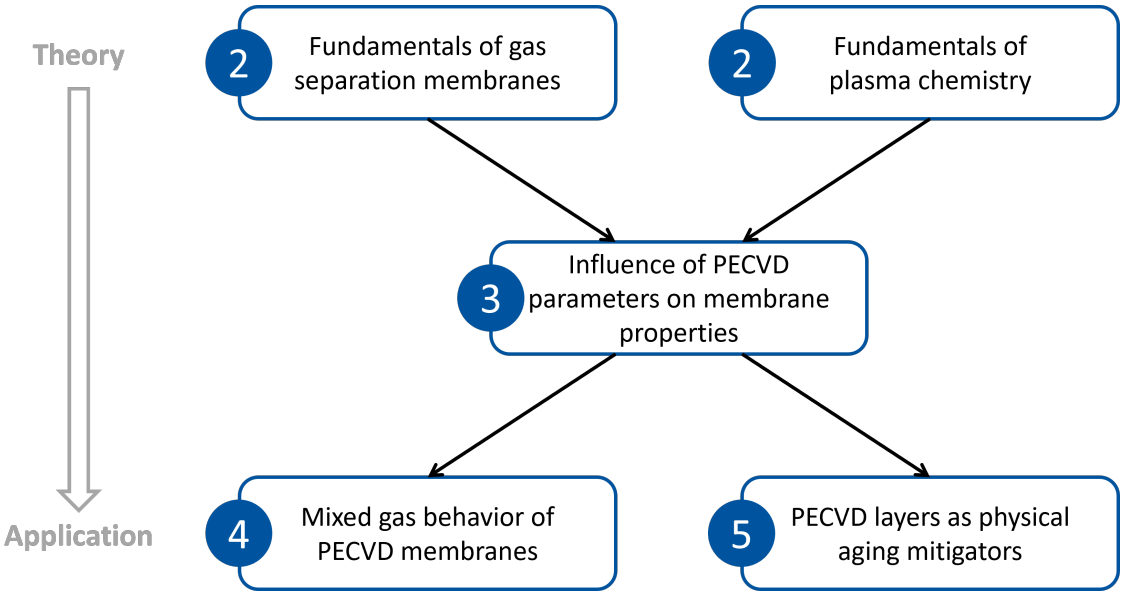


Figure 1.1.: Outline of the thesis.

of the deposited plasma polymers and the resulting transport properties of them. Finally, it describes the monomer, setup and process used for the fabrication of membranes in this thesis.

Chapter 3 evaluates the influence of different plasma process parameters on the gas separation properties of the deposited films. Therefore, the monomer to oxygen ratio, the microwave input power, and the plasma pulse length are varied. The fabricated films are analyzed regarding their chemical structure and gas permeation properties. The chapter elucidates the connections between changes in the chemical composition or energy density in the plasma reactor and the membrane performance of the fabricated membranes. Thereby, it determines optimal fabrication parameters for the utilized reactor. With the knowledge gained in Chapter 3, the best performing membrane is chosen to perform in-depth membrane performance tests.

Therefore, **Chapter 4** investigates the temperature dependent pure gas behavior of the organosilica membrane for Helium (He), carbon-dioxide (CO_2), nitrogen (N_2), methane (CH_4), and propane (C_3H_8) in a range from 0 to 60°C. In addition, it also examines more application-like process conditions by doing mixed gas experiments for He/CO_2, He/CH_4, and CO_2/CH_4 and studying the influence of

humidity on the He, and CO_2 pure gas permeance.

In contrast to the previous chapters, **Chapter 5** utilizes the PECVD-fabricated organosilica layer as non-selective physical aging mitigator instead of a selective membrane layer. Therefore, it investigates the physical aging behavior of a polymer with intrinsic microporosity via spectroscopic ellipsometry. It studies the influence of two different organosilica layers with distinct chemical composition on the physical aging behavior of the underlaying polymer. One layer has high carbon content and the other is deposited in a highly oxidized state. Furthermore, it examines the influence of different organosilica layer thicknesses for both depositions to determine a lower thickness limit.

Finally, **Chapter 6** summarizes the findings of this thesis. It further gives an outlook on future potentials of PECVD as fabrication method for gas separation membranes and remaining questions on the fabricated membranes' properties.

This thesis includes contributions of the following student theses written under the supervision of Jens Rubner:

- Jennifer Birke, 2020, Bachelor thesis, Investigation of the permeation behavior of HMDSO plasma coated membranes
- Ben Doehmen, 2020, Master thesis, Entwicklung neuartiger Gaspermeationsmembranen mittels Plasmatechnologie
- Sarah Wolters, 2020, Master thesis, Evaluation of the controllability of gas separation properties of plasma
- Soukaina Skribbe, 2020, Bachelor thesis, Fabrication and characterization of Mono- and Multilayer PECVD Membranes
- Roman Zuendorff, 2021, Master thesis, Optimization of PECVD gas permeation membranes using machine learning
- Leonie Stellmann, 2021, Bachelor thesis, Mitigating physical aging of PTMSP by PECVD coating

- Philipp Saeger, 2022, Bachelor thesis, Investigation of the influence of polymer coatings on PECVD-coated membranes
- Felix Schott, 2022, Bachelor thesis, CO_2 and H_2 separation from real gas mixtures - Investigation of the mixed gas behavior new gas permeation membranes

1

2. Fundamentals on Gas Permeation and Plasma Processes

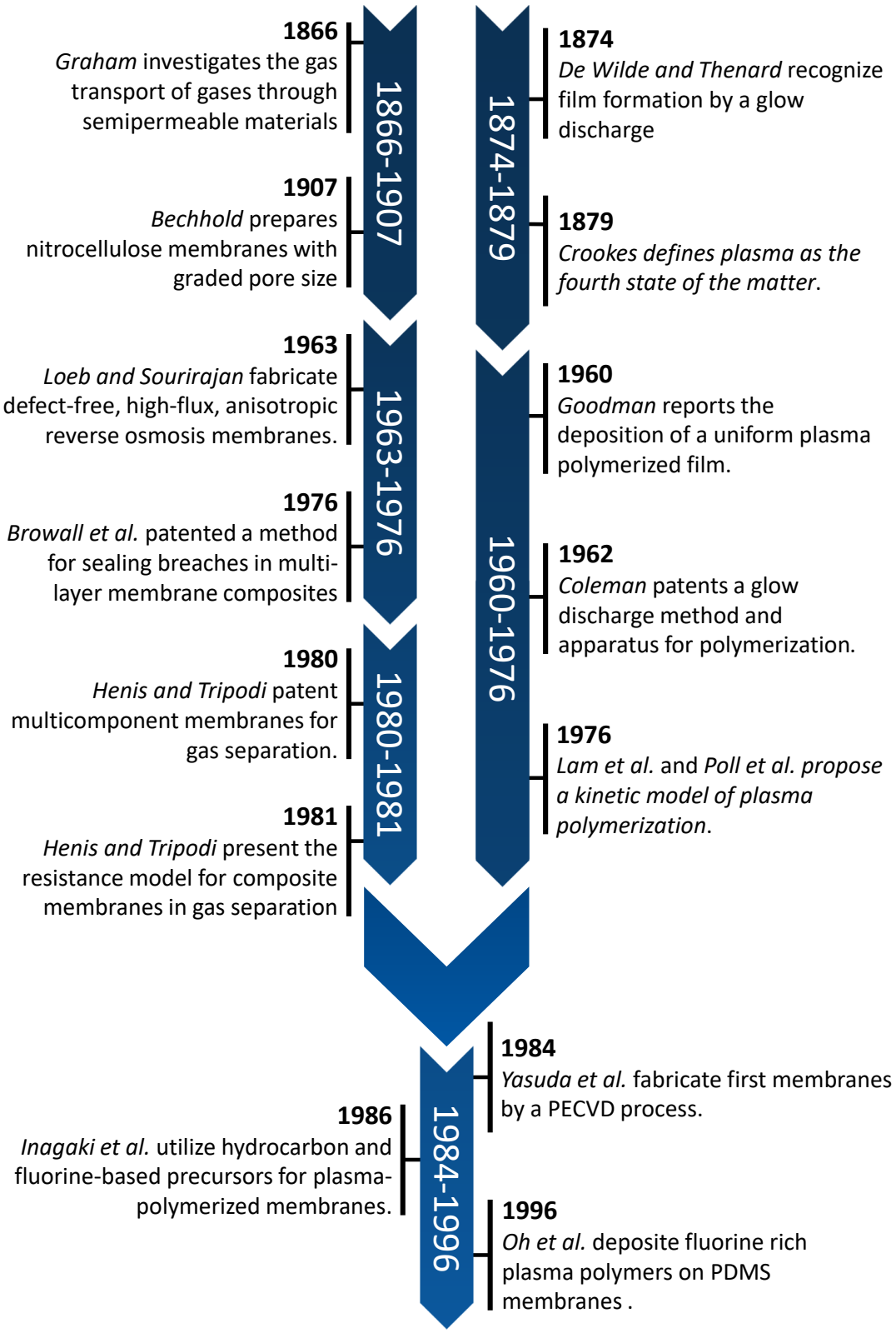


Figure 2.1.: Overview of research on membranes for gas separation, the development of plasma-assisted polymer deposition processes, and their combination in current research. Overview of development in the fabrication of membranes for gas separation and plasma-assisted polymer deposition processes leading to their combination and current research.

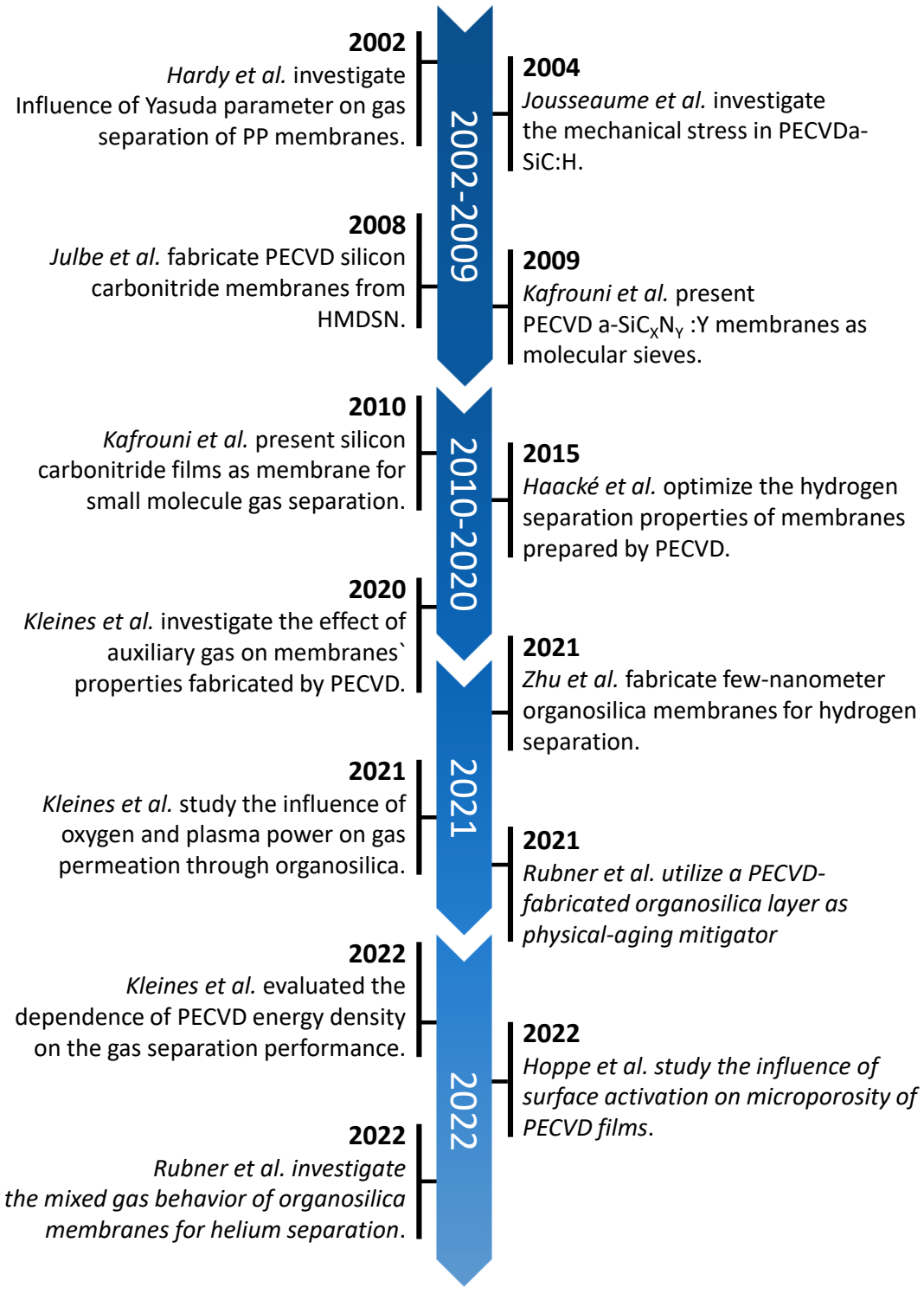


Figure 2.2.: Overview of research on membranes for gas separation, the development of plasma-assisted polymer deposition processes, and their combination in current research. Overview of development in the fabrication of membranes for gas separation and plasma-assisted polymer deposition processes leading to their combination and current research.

2.1. Gas separation principles

This section introduces the basic principles of gas separation. It starts by deriving the solution diffusion model used for gas permeation through dense polymeric films. Afterward, it establishes temperature- and time-dependent phenomena in polymeric membranes and presents the used gas permeation measurement techniques and setups.

2.1.1. Solution diffusion mechanism

Non-porous polymeric membranes transport gases and vapors according to a solution-diffusion mechanism first proposed by Graham [Mitc1995]; [Grah1866]. The model is based on three subsequent steps: adsorption of the penetrants at the upstream membrane surface, diffusion through the membrane, and desorption at the downstream membrane surface. The following derivation of the model is adapted from Wijmans and Baker [Wijm1995]. It assumes the chemical potential as the only driving force for mass transport through the membrane with

$$\dot{n}_i'' = -L_i \cdot \frac{d\mu_i}{dz}, \tag{2.1}$$

where $\dot{n}_i''$ is the molar flux of component i at any position within the membrane normalized to time and membrane area. L_i is a proportional factor, μ_i is the chemical potential of component i in the membrane, and z is the coordinate vertical to the membrane surface. Hence, $\frac{d\mu_i}{dz}$ describes the change of chemical potential through the membrane. If the chemical potential is limited to pressure and concentration gradients, it simplifies to

$$d\mu_i = R \cdot T \cdot \ln(\gamma_i \cdot c_i) + v_i \cdot dp, \tag{2.2}$$

where c_i is the molar concentration (mol/mol) and v_i is the molar volume of component i, γ_i is the activity coefficient linking concentration with activity, and p is the pressure. Further, the solution diffusion model assumes the pressure in the dense phase of the membrane to be equal to the pressure of the upstream side,

which implies $dp = 0$. Combining equations 2.1 and 2.2 results in the following:

$$\dot{n}_i'' = -\frac{RTL_i}{c_i} \cdot \frac{dc_i}{dz}. \tag{2.3}$$

Here, the term $\frac{RTL_i}{c_i}$ can be replaced by the Fickian diffusion coefficient D_i. Therefore the assumption of a constant D_i for low c_i values has to be made. This leads to

$$\dot{n}_i'' = -D_i \cdot \frac{dc_i}{dz}. \tag{2.4}$$

This differential equation can be solved by integration over the membrane thickness δ:

$$\int_0^{\delta} \dot{n}_i'' dz = -D_i \cdot \int_{c_{i,feed}}^{c_{i,permeate}} dc_i, \tag{2.5}$$

where $c_{i,feed}$ and $c_{i,permeate}$ are the concentrations of component i on the feed and permeate side of the membrane. For steady-state conditions, meaning constant mass transport rate over the whole membrane, the equation gives:

$$\dot{n}_i'' = -D_i \cdot \frac{c_{i,feed} - c_{i,permeate}}{\delta}. \tag{2.6}$$

Furthermore, an equilibrium on both membrane surfaces is assumed to be expressed by:

$$c_i = f(f_i), \tag{2.7}$$

where f_i is the fugacity of component i in the gas phase. Here, the function $f()$ describes the sorption equilibrium between the gas and membrane (solid) phase.

By assuming a Henry relation [Henr1803], the equation simplifies to:

$$c_i = S \cdot f_i. \tag{2.8}$$

There, the fugacity can be described by

$$f_i = x_i \cdot p \cdot \phi_i, \tag{2.9}$$

where ϕ_i is the fugacity coefficient. For ideal gases, it equals 1. With this assumption, the concentration c_i is linearly dependent on the partial pressure p_i, and equation 2.6 simplifies to:

$$\dot{n}_i'' = \frac{D_i \cdot S_i}{\delta} \cdot (x_i \cdot p_f - y_i \cdot p_p)\,. \tag{2.10}$$

The product of diffusion D_i and Henry coefficient S_i is called permeability

$$P_i = D_i \cdot S_i. \tag{2.11}$$

The permeability P_i is a material- and penetrant-specific property, independent of thickness and stated in the unit Barrer:

$$[P_i] = 10^{-10} \frac{\mathrm{cm}^3_{(STP)}\ \mathrm{cm}}{\mathrm{cm}^2\ \mathrm{s}\ \mathrm{cmHg}} = 1 \text{ Barrer}\ . \tag{2.12}$$

To describe the permeation property of a specific membrane, we use the permeance Q, which is defined as

$$Q_i = \frac{P_i}{\delta} = \frac{D_i \cdot S_i}{\delta}. \tag{2.13}$$

Compared to the permeability, the permeance can be measured directly and

implicitly contains the thickness of the membrane. In the field of gas separation, the permeance Q_i is stated in gas permeation units (GPU) with

$$[Q_i] = 10^{-6} \frac{\mathrm{cm}^3_{(STP)}}{\mathrm{cm}^2 \ s \ \mathrm{cmHg}} = 1 \frac{\mathrm{Barrer}}{\mu m} = 1\mathrm{GPU}. \tag{2.14}$$

Besides the permeability or permeance, another important parameter, which describes the separation performance of a membrane, is the selectivity $\alpha_{i,j}$ and is defined as [Robe1991]

$$\alpha_{ij} = \frac{P_i}{P_j} = \frac{Q_i}{Q_j}. \tag{2.15}$$

It gives the ratio of permeabilities or permeances for different pure gases or components in mixed gases. Together, the permeability and selectivity of a polymer are essential properties to evaluate the performance of a newly developed membrane material. In the 1980s, various research groups noted that an increasing permeability P generally leads to a lower selectivity α. In 1991, Robeson analyzed literature data and found an upper-bound relationship for various gas mixtures [Robe1991]. Figure 2.3 shows the so-called "Robeson plot" for O_2/N_2, including their upper bound. The upper bound represents a linear relationship in the log-log plot of selectivity over permeability. At the time it was defined, no value existed above the upper bound. Since several newly developed polymers have passed the Robeson upper bound over the last decades, the relationship was redefined in 2008 by Robeson and in 2015 and 2019 by Swaidan, Ghanem, and Pinnau and Comesaña-Gándara et al. [Robe2008]; [Swai2015]; [Come2019]. The Robeson plot is still the state-of-the-art plot to benchmark new membrane materials and is also used in this thesis. Nevertheless, most of the data points shown in the Robeson plot are from pure gas measurements with bulk polymer materials. However, in all industrial applications, thin film membranes are used in a mixed gas environment, where many non-ideal effects can occur. Hence, the Robeson plot can only give a first glimpse of the performance of a newly developed material, and tests in more application-like environments must be done to

evaluate the real potential of the membrane material.

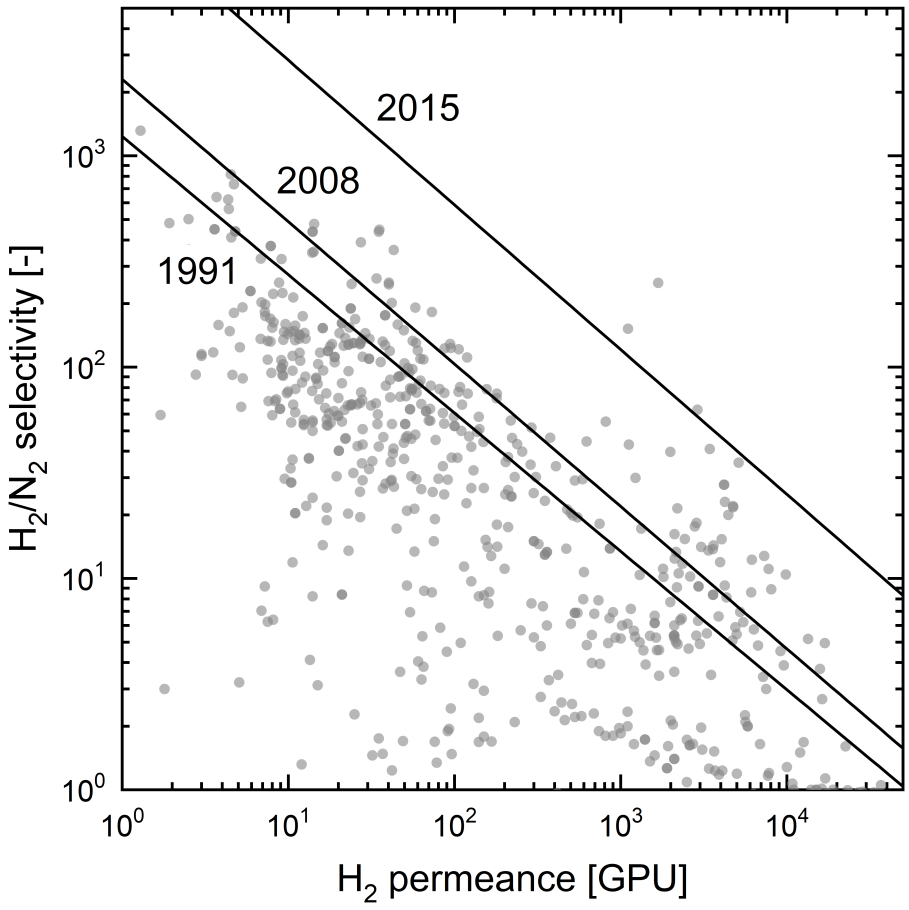


Figure 2.3.: Robeson plot for H_2 to N_2 with the upper bounds from 1991 [Robe1991], 2008 [Robe2008] and 2015 [Swai2015].

2.1.2. Permeation in thin film composite membranes

The permeance Q, as defined in section 2.1.1, describes the property of a specific membrane. In research, this membrane is often a free-standing polymer film consisting of only one layer. Since the membrane must have a specific mechanical stability, those films generally have 10 to 100 µm thicknesses. Researchers use such films to determine the permeability of a polymer. However, as the permeance of a membrane is directly connected to the layer thickness (see equation 2.13), membrane producers try to reduce the membrane thickness as much as possible. Since the mechanical stability of the membrane suffers from the reduction in thickness, the membrane functionalities of gas separation and mechanical stability are divided between two different components: the dense selective layer

and the porous mechanical support layer.[Bake2014]
Since the pore size of mechanically stable support structures (e.g., non-woven fabric) is often too big to directly coat the nanometer-thin selective layer, a transition layer with pore sizes around 10 nm is needed. This approach enables the industry to fabricate dense gas separation membranes with selective layer thicknesses drastically below one µm, maximizing their permeance. Still, preparing a defect-free selective top layer is challenging.[Bake2014]

On the one hand, microscopic defects (pinholes) can lead to a viscous and/or Knudsen flow through them and significantly decrease the membrane's selectivity. This effect of the pinholes can be eliminated by a subsequent coating of the selective layer with another thin layer of a highly permeable polymer such as polydimethylsiloxane (PDMS) or poly[1-(trimethylsilyl)-1-propyne] (PTMSP). They seal the pinholes and increase the membrane selectivity with almost no permeability drop. [Brow1976]; [Pinn1988]
On the other hand, penetration of the polymer solution into the pores of the support layer during fabrication has another negative effect on the membrane's performance. The penetrated polymer causes pore blockage, and penetrating gas molecules must pass a significantly longer distance in the low-permeable polymer. To avoid pore intrusion, manufacturers can introduce a "gutter" layer between the selective, low-permeable layer and the porous support. It does not just avoid pore intrusion but also prevents the formation of pinholes. Furthermore, it also decreases the effective thickness of the selective layer by providing a rapid penetration of gas molecules from the low-permeable selective layer to the closest pore.[Pete2009] As done in electrical engineering, the membrane can be modeled as a series and/or parallel connection of resistances to calculate the overall membrane permeance for each particular gas [Heni1980]. In the case of membranes, the resistance of a membrane corresponds to the reciprocal of the permeance,

$$R_{mem} = \frac{1}{P_{mem}}. \tag{2.16}$$

Figure 2.4 schematically shows the application of the calculation by resistances in series and parallel. In the case of a multilayer membrane structure, as shown

on the left, the resistance of the membrane is calculated by summing up the resistances of each layer. Generally, the resistance of the support structure (R_S) is significantly lower than the ones of the subsequently coated layers (R_1 and R_2). The resistances of R_1 and R_2 are individual for each gas. Hence, either R_1 or R_2 could be the resistance limiting the permeation of a particular gas. In the case of this thesis, for all gases, the resistance of the developed selective plasma coating is at least five times higher than for the underlying thin film composite PDMS membrane. Therefore, the measured permeance of the plasma-coated thin film composite (TFC) membrane is assumed to be the permeance of the plasma coating.[Heni1980]

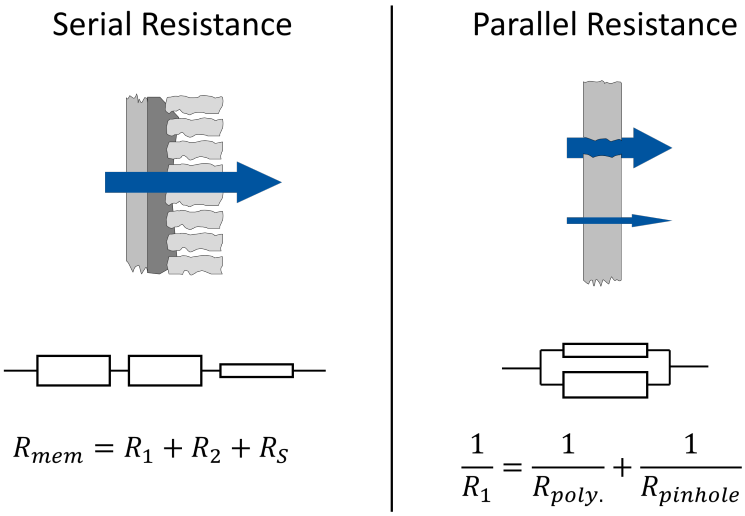


Figure 2.4.: Schematic of a thin film composite membrane (left) and a membrane's polymer layer with a pinhole (right) and the mathematical relationship between the total resistance and the individual resistors.[Heni1980]

The series in parallel calculation has to be applied in case of varying permeances in one specific layer. This modeling approach has to be applied in case of significantly varying thicknesses over the membrane area or even more pronounced if pinholes are present in the polymer layer (see Fig. 2.4). In this case, the reciprocal of the total membrane resistance corresponds to the sum of the reciprocal resistance of the polymer ($R_{pol.}$) and the reciprocal resistance of the pinhole ($R_{pinhole}$). This thesis assumes a pinhole-free plasma coating, although it cannot rule out defects in the plasma layer.

2.1.3. Temperature dependence

Permeation of molecules through dense membranes strongly depends on the operating temperature since diffusion D and sorption S depend on it.
A penetrant molecule has to perform numerous elementary acts to permeate through a membrane. In the polymer matrix, it has to "jump" from one equilibrium position into another (neighboring) one. To pass between those "microcavities" or "cells", it has to overcome forces of attraction between the chains of the macromolecules. Hence, the diffusing penetrant molecule must overcome an energy barrier [Theo2006]. This barrier can be considered an activation energy of diffusion E_d and can be described by the Arrhenius type equation

$$D(T) = D_0 \cdot \exp\left(\frac{-E_d}{RT}\right). \tag{2.17}$$

$D(T)$ is the diffusion coefficient at temperature T, D_0 the pre-exponential factor, R the universal gas constant and E_d the activation energy of diffusion. Since E_d is always positive, the diffusivity always increases with increasing temperature. In rubbery polymers, the energy barrier for diffusion is significantly lower than in glassy polymers. Hence, penetrant molecules' diffusivity is orders of magnitude higher in rubbery polymers.
As for diffusion, the temperature dependence of sorption also follows an Arrhenius type equation and is described by Van't Hoff's formula for the solubility coefficient

$$S(T) = S_0 \cdot \exp\left(\frac{-H_s}{RT}\right). \tag{2.18}$$

$S(T)$ is the solubility coefficient at temperature T, S_0 the pre-exponential factor and H_s the sorption enthalpy. In contrast to equation 2.17, this equation does not describe a thermodynamic activation. Hence, H_s can take positive and negative values.

The combination of equations 2.11,2.17 and 2.18 leads to

$$P(T) = P_0 \cdot \exp\left(\frac{-E_p}{RT}\right). \tag{2.19}$$

It describes the temperature-dependent permeability $P(T)$ in dependence on the pre-exponential factor P_0 and the apparent activation energy of permeation E_p. The latter is described by

$$E_p = E_d + H_s. \tag{2.20}$$

In most cases, E_p is positive, but for negative H_s values which exceed E_d, the apparent activation energy of permeation is negative.

2.1.4. Time dependence (physical aging)

Besides temperature dependence, polymer membranes can also differ in their permeation behavior because of different production and use histories. The essential time-dependent behavior investigated in this thesis is the so-called physical aging. Polymers consist of two distinct portions that make up the specific volume: occupied and free volume. The occupied volume is the volume occupied by the atoms of the polymer. The voids between those atoms are the free volume and depend on how efficiently the polymer chains can pack. The amount of free volume determines the diffusivity of molecules [Cohe1959].
As shown in Figure 2.5, polymers can exist in two states: rubbery and glassy.
In a rubbery polymer, thermal motion allows portions of the polymer chains to move freely and for segments of the polymer backbone to rotate around their axis. Hence, they can arrange in their thermodynamic equilibrium state.

In contrast, in a glassy polymer, rotation and free movement of polymer segments are inhibited by steric hindrance along the polymer backbone. Hence, all morphological changes in glassy polymers happen by diffusive processes on a long time scale. Due to these restrictions, a fresh polymer can not settle in a minimal

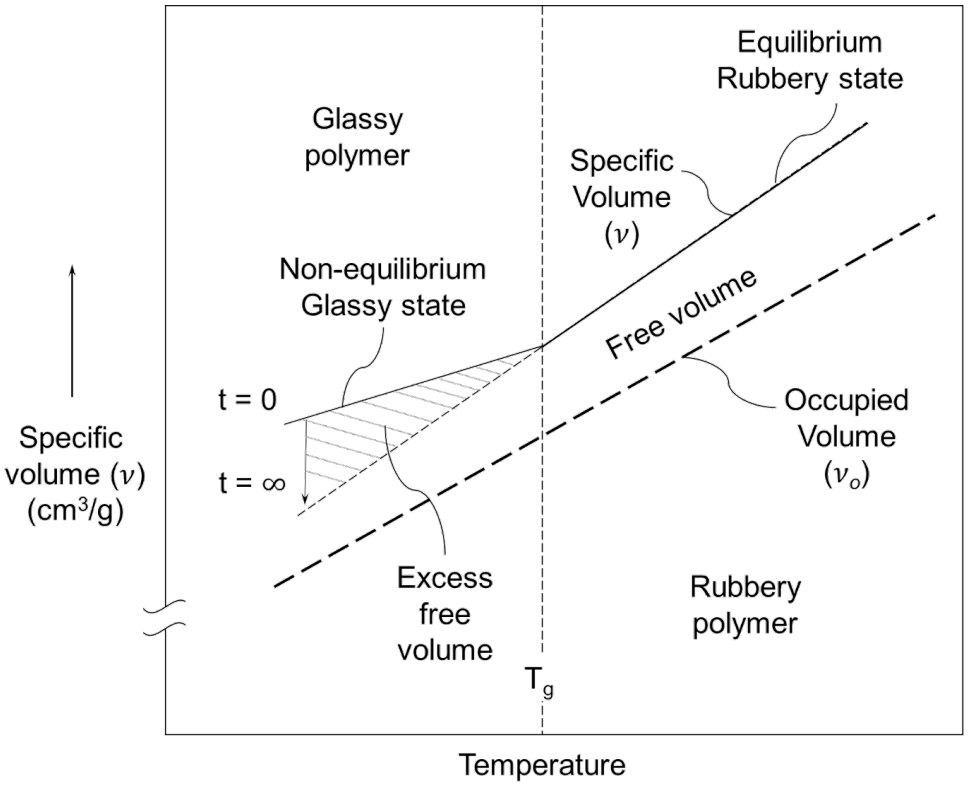


Figure 2.5.: Change in specific volume as a funtion of temperature for a typical polymer. Adapted from Yampolskii, Pinnau, and Freeman [Yamp2006].

energy state but is in a non-equilibrium glassy state. As a result, a significant amount of additional free volume, so-called excess free volume, is present in a fresh polymer (t = 0). By the diffusional rearrangement of the polymer chains, this excess free volume first vanishes quickly until it slowly approaches the equilibrium state (t = ∞). This time-dependent process is known as "physical aging" [Bake2014].

Regarding the solution diffusion mechanism, the (excess) free volume plays a key role since it determines both the diffusivity and solubility. Thus, dramatic changes in permeance and selectivity can happen over time. Cohen and Turnbull described the original free volume theory for amorphous polymers, where the diffusivity of a molecule is linked to the fractional free volume V_f in the polymer

by [Cohe1959]

$$D = R \cdot T \cdot A \cdot \exp\left(\frac{-B_d}{V_f}\right). \tag{2.21}$$

D is the diffusion coefficient, R is the ideal gas constant, and T is the absolute temperature. A and B_d are constants of which the latter correlates with the molecular size of the penetrants [Lin2006]. Therefore, the diffusion increases with a bigger fractional free volume. Besides the temperature (cf. Figure 2.5), the pressure and the sorption of penetrant molecules in the polymer matrix can also change the fractional free volume of a polymer.

2.1.5. Permeance measurement techniques

Several methods exist to measure the permeance of membranes [Sadr2018]. This section explains the two methods used in this thesis. They are both integral permeation methods and are designed for permeate pressures below or equal to atmospheric pressure. One setup uses the variable pressure constant volume method, also called pressure increase method. It is specifically designed to measure the permeances of pure gases. The other setup uses the variable volume constant pressure method and is able to measure pure as well as mixed gas permeances. Both setups are briefly explained below.

Pressure increase method

The principle of the pressure increase method is, as the name already suggests, the pressure increase of a confined, known volume V of the membrane module's permeate side. At the beginning of the measurement, the permeate volume is evacuated to a specific value. Then the valve connecting the vacuum pump and permeate volume is closed. Since gas is permeating through the membrane, the pressure in the permeate volume increases and is measured by a pressure transducer. The permeating mole flux $\dot{n}$ can be calculated using the ideal gas law

$$\frac{\partial p}{\partial t} \cdot V = \dot{n} \cdot R \cdot T \tag{2.22}$$

where $\frac{\partial p}{\partial t}$ is the pressure increase over time, R the gas constant and the temperature T. The permeance P can be calculated by inserting the mole flux into equation 2.10.

Figure 2.6 shows the flowsheet of the setup using the pressure increase method. Gas bottles supply the setup with pure gases. The complete setup is placed in an oven to perform experiments at room or slightly elevated temperatures up to 60 °C. The setup consists of four membranes connected in series to allow a fast acquisition of membranes produced with different parameters. Two temperature and two pressure sensors measure the conditions in the feed stream. A rotameter at the feed outlet controls the gas overflow on the feed side. On the permeate side, each membrane module has a fixed volume separated from the vacuum pump by a computer controlled valve and a pressure sensor. Before the first measurement, the setup is evacuated. Subsequently, the feed pressure and overflow are adjusted. Then, the permeate side is evacuated, the permeate valves are closed and the pressure increase as well as the feed pressure and temperatures are recorded. The setup is computer controlled and automatically conducts multiple measurements to be able to judge the reproducibility. At least three, but mostly six pressure increase cycles are measured per sample and gas.

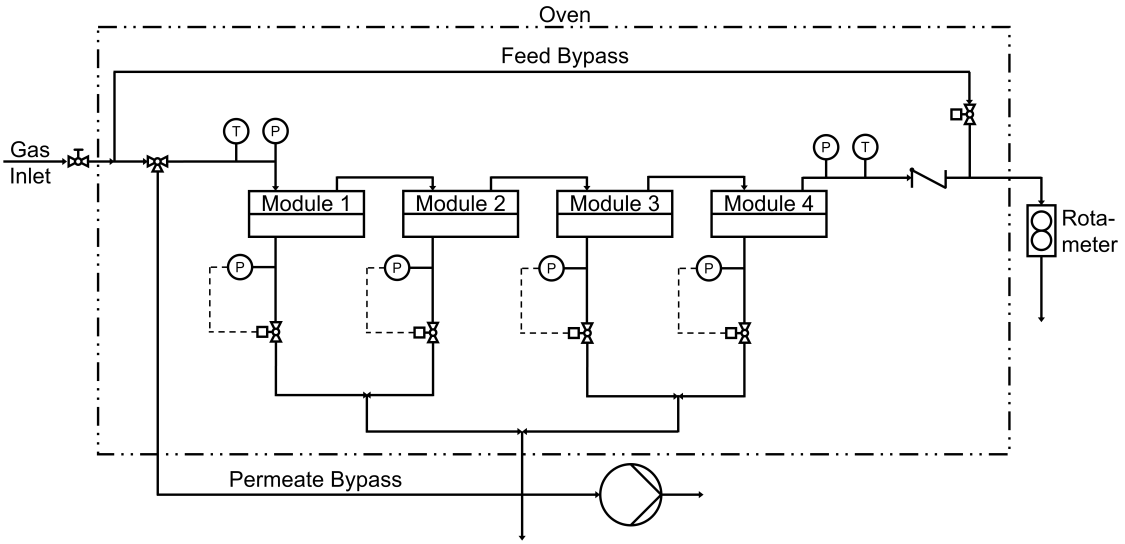


Figure 2.6.: Flowsheet of the pure gas multi membrane permeation setup.

Constant pressure method

Since the mass transport characteristics of membranes can significantly change in the presence of gas mixtures, it is important to investigate the permeation behavior under realistic operation conditions. Figure 2.7 shows a simplified flowsheet of the mixed gas permeation setup. The membrane module is located in an air conditioned cabinet (Memmert GmbH), which enables experiments in the temperature range from -40 °C to +200 °C. The diameter of the membrane is 65 mm. The feed pressure is regulated with an automated back pressure regulator (Bürkert GmbH) and the permeate pressure is always set to ambient pressure.

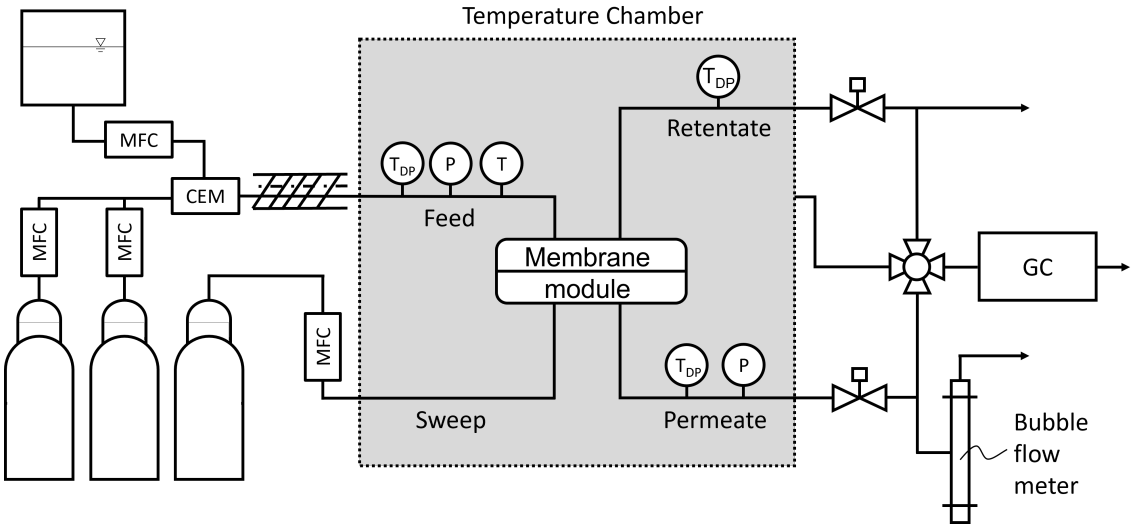


Figure 2.7.: Flowsheet of the mixed gas permeation setup.

The gas mixtures are produced from pure gas cylinders with the required composition controlled through mass flow controllers (Bronkhorst EL-Flow). To determine the gas compositions of the feed, retentate and permeate stream, a gas chromatograph (Agilent Technologies 7890A) is connected to the gas permeation setup which consists of a thermal conductivity detector and argon as carrier gas. For experiments with water vapor, a controlled evaporation and mixing device (CEM Evaporator W-101A from Bronkhorst GmbH) is used. The water vapor content is measured using dew point mirrors (Michell Optidew) in the feed, retentate and permeate channels. The measured dew points are converted into water vapor pressures using the Antoine equation [Anto1888]. With this value,

the water activity a_w is calculated as follows:

$$a_w = \frac{p_{H2O,gas}}{p_{H2O,sat}(T)}, \tag{2.23}$$

where $p_{H2O,gas}$ is the water vapor pressure of the gas stream measured with the dew point sensor and $p_{H2O,max}(T)$ is the saturation water vapor pressure at the temperature of the gas stream.
A manual bubble flow meter or mass flow meters (Alicat Scientific, TrigasDM GmbH) are used to determine the permeate flux. The permeances are calculated with:

$$Q_i = \frac{\dot{V}_P x_{P_i} \left(\frac{T_F}{273.15+T_R}\right)}{A_m \left(p_{F_i} - p_{P_i}\right)}, \tag{2.24}$$

where Q_i is the permeance, $\dot{V}_P$ the average permeate volume flux, x_{P_i} the mole fraction of gas i in the permeate stream, T_F the feed temperature, T_R the room temperature, A_m the membrane surface area and $(p_{F_i} - p_{P_i})$ the partial pressure difference between feed and permeate side.

2.2. Plasma processes in membrane fabrication

This section gives an overview of the use of plasma processes in membrane fabrication. Therefore, it first defines the term plasma and introduces its chemical properties. Afterward, it presents plasma-enhanced chemical vapor deposition, which is the method utilized for this work. Next, it gives schematic representations of the processes taking place during polymer formation in the plasma and how they connect to the structural properties of the deposited layer. At last, it introduces the transport properties of the plasma polymers and gives detailed information on the used plasma reactor.

2.2.1. Fundamentals on plasmas and plasma chemistry

In 1879, Crookes defined plasma as the fourth state of matter [Croo1879]. Plasma is a partially ionized and overall neutral medium generated by an electric field. The electric field transfers its energy to free electrons, which collide with gas molecules. Thereby, the electrons induce the ionization of gas molecules. Those ionized species again initiate a high number of complex reactions like ionization, excitation, neutralization, recombination, and deexcitation constituting a so-called glow discharge. The glow discharge consists of a wide variety of species like electrons, negative and positive ions, radicals, neutral atoms and molecules, and photons.
Plasmas are characterized by their energy and electronic density and can be classified into two categories: hot plasmas and cold plasmas. An arc discharge generates hot plasmas at atmospheric pressure or above. They are widespread in nature in the form of comets, galaxies, light flashes, or lightning and characterized by a high frequency of collisions between electrons and gas molecules and have a temperature of thousands of degrees Celsius.
In contrast, cold plasmas have a gas temperature near the ambient while the electronic temperature (kinetic energy of free electrons) is still at several thousands of degrees Celsius. Artificial plasmas are generated at low (25-450 kHz), radio (1-500 MHz) and microwave (500 MHz - some GHz) frequency ranges and low pressures between 10^{-2} and 10 Torr. Furthermore, they have a degree of ionization lower than 10^{-3}, so the gas phase mainly consists of neutral species in an excited state (radicals).

Several effects can occur simultaneously or consecutively when a cold plasma and a substrate interact. The four major effects are etching, functionalization, cross-linking, and formation of a deposit. The latter happens by recombining a reactive species adsorbed on the substrate's surface. The nature of the gas subjected to the electric discharge mainly determines the occurrence of one of the four mentioned effects. In the case of noncondensable gases (mono- or diatomic gases), the surface is etched, functionalized or cross-linked - processes known as plasma treatment. In contrast, a deposition only occurs if condensable gases (organic, inorganic or organometallic compounds) are present in the

plasma. The fragments of the reagent gases deposit on the substrate and form a three-dimensional randomly structured matrix. The related process is called plasma-enhanced chemical vapor deposition (PECVD). For gases of organic compounds, as used in this thesis, it is also called plasma polymerization.
Besides the specific gases used, many other parameters influence the effects on the substrate. One of these factors is the geometry of the reactor. There, the size and shape of the reactor chamber, the location, nature, and morphology of the electrodes, and the localization of the gas inlet(s) and pumping outlet have a substantial influence on the deposition process. Moreover, many phenomenological parameters affect the plasma's nature. The electric discharge frequency controls the charged species' kinetic energy. The power of the electric discharge determines the degree of fragmentation of the species [Yasu1985]. The gas(es) reactivity and flow rate(s) define the residence time of the species in the plasma. Furthermore, the ratio of different gases and the working pressure control the residence time but also the average energy of the electrons, the mean free path of the species, and the gas density. Additionally, the temperature of the substrate determines the mobility, absorption and desorption of the active species on the surface of the substrate. All the listed parameters must be controlled rigorously to reliably manufacture a tailor-made material. [Roua2017]; [Niem2012]; [Zani2007]; [Soll2002]

2.2.2. Plasma-enhanced chemical vapor deposition

Already in 1874, de Wilde and Thenard recognized the film formation by a glow discharge polymerization. Until the 1950s, polymers were considered by-products of an electric discharge and only a little attention was paid to them. It took until the 1960s when various researchers recognized the beneficial properties of glow discharge-assisted deposition processes (later called plasma-enhanced chemical vapor deposition) [Arqu1962]; [Cole1962]; [Stua1963]; [Brad1963]; [Ster1965]; [Swan1967]. The PECVD process is mainly used nowadays for the fabrication of inorganic, polymer-like or hybrid thin layers. Since mostly organic precursors are used to fabricate membranes, the process is often called plasma polymerization instead of PECVD.

PECVD differs strongly from classic polymerization since it has a poor selectivity of fragmenting molecules in the plasma which leads to many side reactions. Since the process has a variety of active species, reaction steps, and dependences on plasma parameters, the deposition mechanism is not yet well understood because of its complexity. Researchers have proposed several kinetic models of plasma polymerization. The most popular ones involve a competitive ablation and polymerization mechanism, trying to account for the complex and interrelated influences of the fragmented elements in the deposition of plasma polymers [Poll1976]; [Lam1976]; [Yasu2000].
Figure 2.8 displays the rapid stepgrowth polymerization mechanism and hence explains how the polymer is formed in the plasma. First, the monomer is activated by the plasma and then gets fragmented into differently sized radicals. Then, the essential reactions are the stepwise recombination of free radicals and stepwise addition or intrusion via hydrogen abstraction by impinging free radicals (not shown in Figure 2.8). Nevertheless, those elementary reactions do not form a polymer themselves but are oligomerization reactions. A certain number of those steps have to be repeated on the surface to form a polymeric deposition. During this plasma polymerization, the activated species may attack the growing polymer layer. Thereby, the plasma can decompose, extend the cross-linking, or cause the ablation of the deposited polymer. These polymerization and ablation processes proceed competitively. Hence, the overall plasma deposition rate is dependent on the PECVD parameters.

Among the various process parameters stated in Section 2.2.1, the ones directly affecting the fragmentation of the monomer are the most influential. The most pronounced effects are induced by the nature of the precursor (represented by its molecular weight M), the power of the electric discharge W, and the precursor flow rate F. Using these three parameters, the extent of fragmentation can be determined as introduced by Yasuda [Yasu2012]. He defined the energy-input level as the Yasuda parameter Y, where

$$Y = \frac{W}{F \cdot M} \tag{2.25}$$

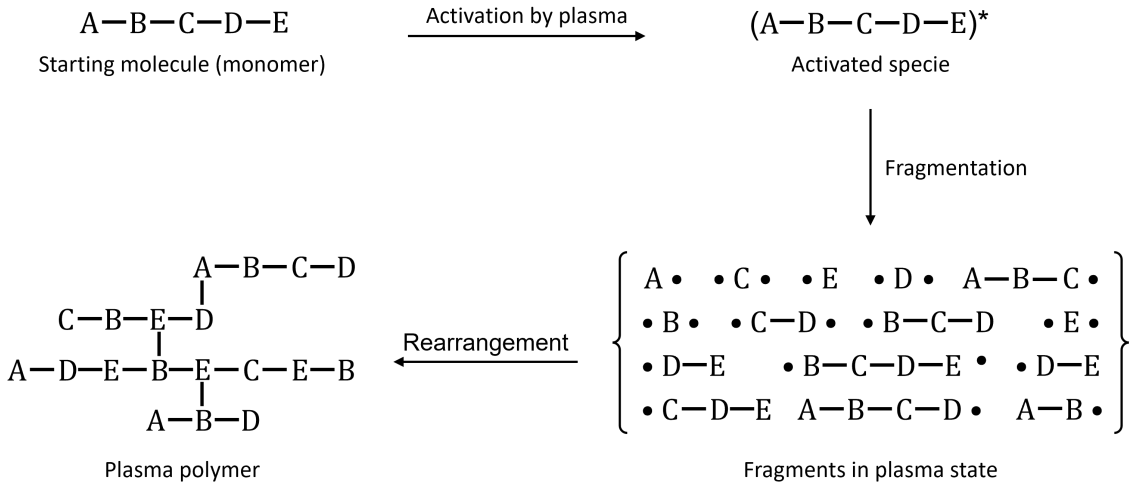


Figure 2.8.: Schematic representation of plasma polymerization, adapted from Inagaki [Inag2014].

gives the energy per mass of monomer. This parameter predominantly determines the extent of the fragmentation of the molecule. Figure 2.9 displays the plasma polymer deposition rate dependent on the Yasuda parameter Y. At low Y, the concentration of activated species is lower than that of monomers. Hence, in this "monomer sufficient region", the number of activated species and, thereby, the deposition rate increases with increasing Y. In the "competition region", the quantity of monomers introduced into the plasma is equal to the ones likely to be activated. Hence, the deposition rate is at its maximum. For higher Y values, the deposition rate decreases with increasing Y because of a lack of monomer molecules likely to be activated.[Roua2010] There, the monomers are subjected to heavy fragmentation, and plasma polymers with much rearrangement and a significant loss of weakly bound groups are formed [Inag2014].

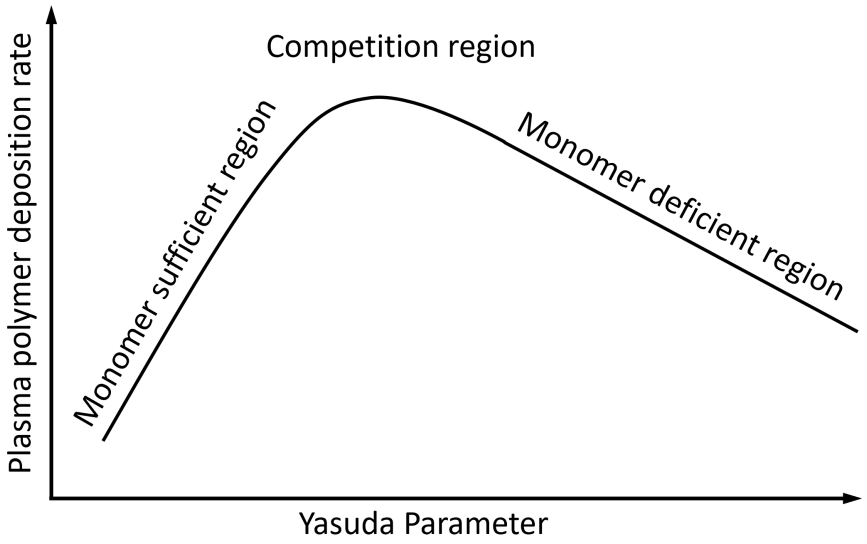


Figure 2.9.: Domains of plasma polymer deposition dependent on the Yasuda parameter, adapted from Inagaki [Inag2014]

2.2.3. Structural properties of plasma polymers

The repetition of monomers builds up the structure of a conventional polymer, as shown in Figure 2.10. In contrast, plasma polymers are formed in a disorganized way. Their thin films consist of short and branched chains, which often do not resemble the precursor but new moieties.

Plasma polymers have many advantages over polymer films fabricated by liquid route synthesis or other vacuum deposition techniques, with regard to material properties. Plasma polymers can be deposited in films of a few nanometers with deposition rates up to several µm/min, making the process ideal for industrial applications [Kim2003]; [Stor1997]. Furthermore, the process runs at ambient temperatures, making it possible to coat temperature sensitive materials. The coatings also adhere well to polymers, glasses, semiconductors, ceramics and metals. They generally are dense, amorphous and have a three-dimensional, highly cross-linked structure. The latter leads to specific properties like chemical inertia, good thermal stability and an anticorrosive character. Additionaly, plasma polymerization enables the adjustment of the deposited materials' physical and chemical properties by varying the process parameters in a broad range. However, this adjustability also necessitates rigorous control of the process parameters.

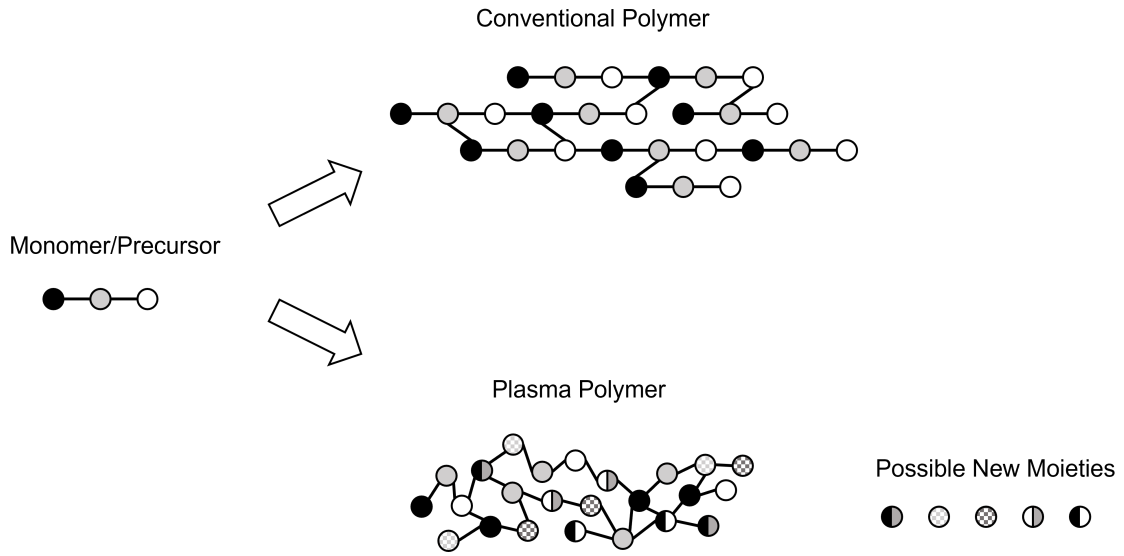


Figure 2.10.: Schematic crosslinking comparison of conventional and plasma polymers. Adapted from Roualdes and Rouessac [Roua2017]

The Yasuda parameter Y plays the biggest role in tuning the microstructural properties of the plasma polymer. In the monomer sufficient region, the plasma fragments the monomer only to a small degree and the molecule only loses some groups, such as hydrogen, methyl, hydroxyl, and carbonyl groups. Hence, the plasma polymer retains its monomer structure and resembles a conventional polymer due to its organic and loosely cross-linked structure. In contrast, monomers in processes with high Y values (monomer deficient region) are fragmented heavily. Polymers with a higher degree of rearrangement and a larger loss of especially carbon-based groups are formed. These polymers are harder, more inorganic and more highly cross-linked (ceramic-like). In the competition region, the plasma process can form a wide range of hybrid plasma polymers.
Figure 2.11 schematically shows the structure of plasma polymers from the precursor hexamethyldisiloxane (HMDSO) fabricated under conditions of low (see Fig. 2.11a) and high (see Fig. 2.11b) Y values as well as a conventional PDMS polymer as reference (see Fig. 2.11c). The polymer fabricated in soft plasma conditions (see Fig. 2.11a) shows a structure close to interconnected HMDSO monomers. It is also similar to its closest conventional polymer, PDMS (see Fig. 2.11c). Despite having a higher cross-linking density, the density of the plasma polymer itself is almost identical with about 1.1 g/cm^3. In contrast, the plasma film obtained in hard plasma conditions (see Fig. 2.11b) is similar to amorphous

hydrogenated silica. Compared to the PDMS-like polymer, it has a substantially higher density of up to 2.2 g/cm^3.

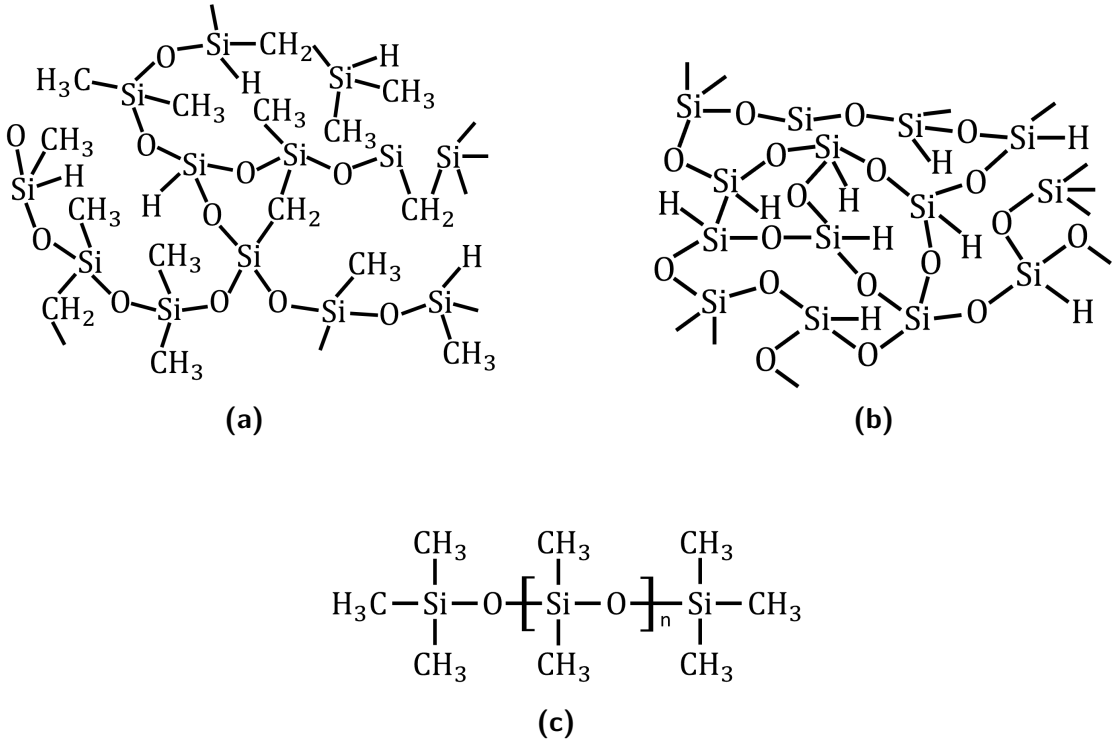


Figure 2.11.: Schematic chemical structures of a plasma polymer fabricated in the monomer sufficient 2.11a and monomer deficient 2.11b region in comparison to a conventional PDMS polymer 2.11c. Adapted from Roualdes and Rouessac [Roua2017]

Although plasma polymers are considered dense materials, they have free volumes comparable to ultramicroporous films with chain spacing lower than 0.7 nm. Changes in the plasma parameters can tune these free volumes together with their chain flexibility. To achieve enhanced free volume and chain flexibility, for example, the Yasuda factor can be decreased or the plasma can be pulsed to reduce the plasma-on time. Furthermore, a Faraday cage around the substrate, the use of monomers containing polymerizable doubles bounds or a cold substrate can have similar effects.

2.2.4. Transport properties of plasma polymers

As stated in section 2.2.3, plasma polymers have a ultramicroporous structure with free volumes smaller than 0.7 nm. Together with their high cross-linking

degree, this makes them a promising material to use as membrane for separation of molecules by size-sieving. In the 1980s, Yasuda was the first researcher to utilize plasma polymers as membranes [Yasu1984]. Besides the aforementioned properties, plasma polymers also show an excellent chemical and thermal stability, making them applicable in harsh or hot environment. Furthermore, the PECVD process allows the deposition of thin layers and exactly tunable thicknesses in the nanometer range.

Since plasma polymers are not self-supporting, they must be deposited on a substrate which acts as mechanical support. Researchers use dense or porous membranes with a symmetric or asymmetric structure for the fabrication of plasma polymer membranes [Wang2017]; [Klei2020]; [Char2016]; [Roua1999]; [Bosc2003]; [Lo2010]; [Ngam2013]; [Naga2013]. The pore size and roughness of the chosen support membrane also dictate the minimum plasma polymer layer thickness, which should be at least in the same size range. In contrast to other coating methods, PECVD only coats the surface and, depending on the pore size, the mouth of the pore, but not the inner pore walls. If a homogeneous coating is deposited, the transport properties are mainly dictated by the intrinsic properties of the plasma polymer. They can either feature a solution-diffusion, microporous surface diffusion, or molecular size-sieving behavior. Since plasma polymers are highly cross-linked, on the one hand, they generally posses a lower permeability compared to conventional polymers. Hence, the fabrication should aim for the minimum layer thickness and a high free volume composition with high chain flexibility. On the other hand, plasma polymers have high selectivities, usually found in inorganic membranes, thus, outperforming most polymers.

2.2.5. Fabrication of membranes by plasma-enhanced chemical vapor deposition

After describing the fundamentals of plasma processes, this section gives detailed information on the used setup and monomer. The layer deposition via PECVD was conducted in a low-pressure plasma reactor (LAMPS, Large Area Microwave Plasma System) located at the Institute of Plastics Processing at RWTH Aachen

University. Figure 2.12 schematically shows the setup. The vacuum/plasma chamber has a volume of 220 L and a rotary vane pump connected to a subsequent turbomolecular pump. A magnetic sample transfer system is mounted to the vacuum chamber to enable a fast exchange of samples and avoid impurities from the ambient air. Four microwave magnetrons generate pulsed microwaves with a frequency of 2.45 GHz and a maximum power of 4000 W. The microwaves are fed into the reaction chamber via four quartz glass tubes (Duo-Plasmalines®, Muegge GmbH, Reichelsheim). The mass flow controller (MKS Instruments Deutschland GmbH, München) can dose auxiliary gases with a maximum flow rate of 1000 sccm into the chamber. Additionally, the precursor is vaporized in an evaporation unit vaporizes at a pressure of 30 Pa and a subsequently dosed by a mass flow controller with a maximum flow rate of 150 sccm. More detailed information about the reactor design can be found elsewhere [Bahr2013]; [Behm2016].

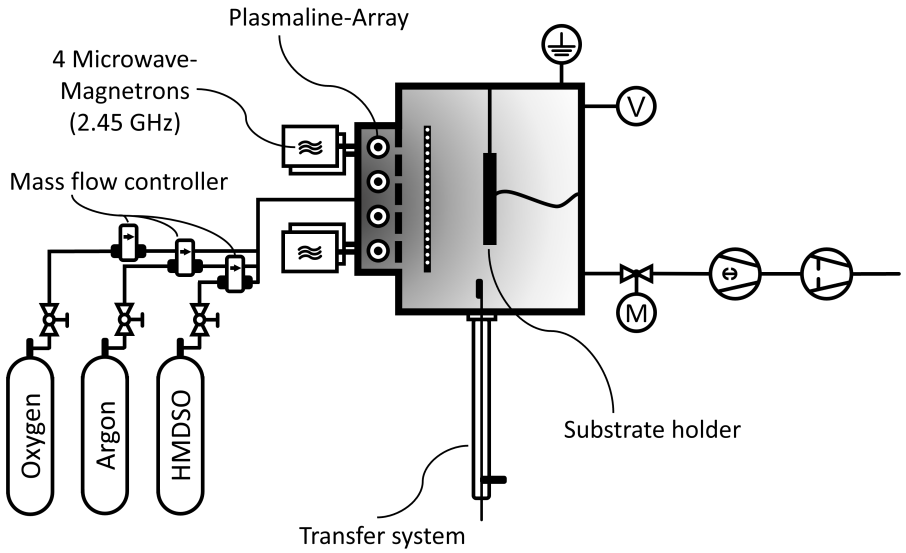


Figure 2.12.: Schematic representation of the low-pressure plasma reactor LAMPS.

All following studies use Hexamethyldisiloxane (HMDSO) as the precursor for PECVD due to its non-toxicity, good commercial availability and safe handling [Hege2014]. Because of its vapor pressure of 56 mbar, the monomer is liquid at standard conditions but easily vaporizable for use in PECVD processes [PUBC2022]. Figure 2.13 displays the chemical structure of HMDSO. As mentioned in Section 2.2.2, the monomer's fragmentation depends on the used plasma

power. Chemical bonds with lower binding energies need less energy to be broken and therefore are more likely to break at low plasma energy input. In the used HMDSO, the C-H and Si-C bonds have binding energies of about 3.5 eV and 4.7 eV, respectively, but the binding energy of the Si-O bonds is about 8.3 eV [Chen2003]; [Magn2001]. Hence, silicon and oxygen are most likely to remain in the plasma polymer in contrast to hydrogen and carbon atoms.

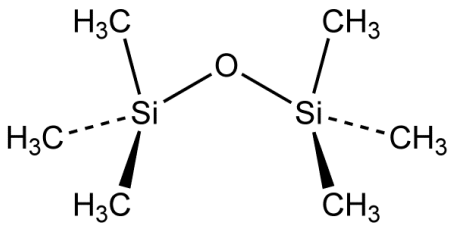


Figure 2.13.: Chemical structure of the Hexamethyldisiloxane (HMDSO) precursor.

2

3. PECVD Parameter Optimization for the Fabrication of Gas Separation Membranes

Parts of this chapter have been published as:
Kleines, L., Wilski, S., Alizadeh, P., Rubner, J., Wessling, M., Hopmann, C., & Dahlmann, R. *Structure and gas separation properties of ultra-smooth PE-CVD silicon organic coated composite membranes*, Surface and Coatings Technology, 2021 DOI: 10.1016/j .surfcoat.2021.127338

Kleines, L., Wilski, S., Alizadeh, P., Rubner, J., Wessling, M., Hopmann, C., & Dahlmann, R. *Evaluation of the membrane performance of ultra-smooth silicon organic coatings depending on the process energy density*, Thin Solid Films, 2022 DOI: 10.1016/j .tsf.2022.139169

3.1. Introduction

Plasma-enhanced chemical vapor deposition (PECVD) can produce ultra-thin coatings for a wide range of applications, such as sensors, implant coatings, scratch-resistant surfaces, barriers, corrosion protection, passivating layer in photovoltaic cells, and many others [Sloc2006]; [Förc2007]; [Meno2008]; [Baxa2009]; [Vasu2013]. The coating's properties strongly depend on the fabrication parameters in the process. Hence, different coating parameters for an organosilicon monomer like hexamethyldisiloxane (HMDSO) can lead to the formation of widely differing coatings. The properties range from soft, weakly cross-linked and elastic silicon organic coatings to hard, strongly cross-linked, glass-like silicon oxide coatings [dAgo1990]; [Behm2016]; [Roua2017]. As stated in Section 2.2, many parameters influence the layer deposition and the evolving chemical structure. On the one hand, the process' chemical properties are mainly influenced by the structure of the monomer, the chemical and morphological properties of the substrate, and the composition of the process gas for example by addition of auxiliary gases. On the other hand, the plasma energy impact for each molecule depends, among others, on the reactor geometry, the plasma excitation mode, and the power input. [dAgo1990]; [Hube1997]; [Li1999]; [Hipp2008]; [Roua2017]

Besides the aforementioned applications, researchers in the field of membrane separations also endeavored to utilize the flexibility of the PECVD process concerning structural properties for the deposition of selective layers. The same plasma reactor can produce tailor-made membranes only by adjusting the chemical and energetical environment in the reactor. Hence, researchers investigated the influence of different monomers [Naga2015]; [Roua1999]; [Roue2004]; [Naga2014], process gas flows and compositions [Li1999]; [Kafr2010]; [Enna2010]; [Haac2015]; [Cous2014]; [Kafr2009]; [Naga2013]; [Zuza2022], multilayer depositions [Tsur2011]; [Naga2013], energy inputs [Li1999]; [Lo2010]; [Roua2002]; [Kafr2010]; [Roua1999]; [Enna2010]; [Kafr2009]; [Lo2009]; [Zuza2022]and process pressures [Wang2018] on the membrane properties.

As stated in Section 2.2 a plasma can be created at different frequencies. Most of the cited studies were conducted with radio frequency (RF) plasma sources. In contrast to RF plasmas, microwave-driven plasmas have the advantage of a

higher ion density resulting in shorter process times during layer deposition. This leads to increased economic efficiency and allows easier upscaling of the process. In addition, the low-pressure atmosphere decreases the presence of gas impurities in the reactor chamber and thereby leads to a more homogeneous and stable deposition since less atoms are in the reactor chamber. To enable the application of those process advantages, more knowledge on microwave-driven low-pressure plasma processes for the fabrication of gas separation membranes is needed. Furthermore, reactor geometry and size have a significant influence on the deposited layers. Therefore, parameters can not be directly taken from the literature, but the optimal parameters have to be determined for the specific reactor.

Thus, this chapter on the one hand investigates the influence of a chemical composition change in the PECVD reactor gas by varying the HMDSO monomer and O_2 auxiliary gas content. On the other hand it studies the impact of differing microwave input powers and plasma pulse-on times, which both change the energy input per molecule in the plasma reactor. As performance indicators for the coated membranes, this study investigates the pure gas permeance for helium (He), nitrogen (N_2), carbon dioxide (CO_2), methane (CH_4), and propane (C_3H_8). Furthermore, the resulting gas selectivity, and the chemical structure of the fabricated layers is evaluated.

3.2. Experimental

A thin film composite membrane is the substrate for depositing the organosilica layers. The membrane consists of a polyester fleece, a porous polyacrylonitrile (PAN) layer and an about 160 nm thin, dense and defect-free polydimethylsiloxane (PDMS) layer. The Helmholtz-Zentrum Hereon Geesthacht (Germany) fabricated and kindly supplied the membrane. Its homogeneous, smooth and defect-free surface enables an optimal deposition of the organosilica layer. The PECVD process uses hexamethyldisiloxane (Sigma-Aldrich, St. Louis, Missouri, USA; purity 98%) as a monomer and oxygen (purity 5.0) as a reactive auxiliary gas to deposit organosilica layers.

The deposition is conducted in the LAMPS reactor described in Section 2.2.5.

The process pressure is 5 Pa for all fabrications. Before the deposition of the organosilica layer, all substrates are pre-treated for 5 s with an O_2 plasma having an O_2 flow of 100 sccm with a microwave input power of 4 kW and a pulse-on/-off time of 4 and 45 ms, respectively.
To investigate the influence of the O_2 auxiliary gas fraction in the reaction chamber as well as the microwave input power, membranes with the parameters listed in Table 3.1 are fabricated. The pulse-on and pulse-off times are kept constant at 3 and 45 ms, respectively. This study uses microwave input powers of 1, 2, and 3 kW. The deposition time is adjusted to target an organosilica layer thickness of about 100 nm for all parameter sets.

Table 3.1.: PECVD coating parameters for the investigation of O_2 gas fraction and microwave input power influence.

HMDSO flow [sccm]	Oxygen flow [sccm]	O_2 fraction in HDMSO [-]	Pulse on/off [ms]	Microwave input power [W]
150	0	0	3/45	1000; 2000; 3000
94	94	0.5	3/45	1000; 2000; 3000
68	136	0.66	3/45	1000; 2000; 3000
38	188	0.83	3/45	1000; 2000; 3000

To keep the Yasuda parameter Y (energy input per molecule) constant, the gas flow rates of HMDSO and O_2 into the plasma chamber have to be adjusted depending on the gas composition. Therefore, the volume flow F in the Yasuda parameter has to be extended to include the influence of both the monomer volume flow F_M and the auxiliary gas volume flow F_A. This leads to the equation

$$F = F_M + r_{gas} \cdot F_A, \tag{3.1}$$

where r_{gas} is a correction factor relating to the reactivity of the auxiliary gas to the film forming monomer.[Hege2014]; [dAgo2005]; [Hash2014] For HMDSO and the auxiliary gas oxygen, Hegemann and d'Agostino et al. suggest a value of 0.6 for r_{gas} [Hege2014]; [dAgo2005]. Hence, the gas flow rates range from 150

to 38 sccm for HMDSO and from 0 to 188 sccm for O_2.

Regarding the influence of the plasma pulse-on time, organosilica layers with the parameters listed in Table 3.2 are deposited. For this purpose, the process pressure of 5 Pa and the HMDSO and O_2 gas flow are kept constant at 40 and 80 sccm, respectively. This study uses microwave input powers of 1 and 2 kW, and again adjusts the coating time to fabricate layers with a thickness of about 100 nm.

Table 3.2.: PECVD coating parameters for the investigation of the microwave pulse-on length influence.

HMDSO flow [sccm]	Oxygen flow [sccm]	Pulse on/off [ms]	Microwave input power [W]
40	80	2/45	1000; 2000
40	80	3/45	1000; 2000
40	80	4/45	1000; 2000
40	80	5/45	1000; 2000

The thickness of the coatings is measured using an RC 2 variable angle spectroscopic ellipsometer from J. A. Woollam Co. Inc. (Lincoln, NE, USA) at incident angles of 65°, 70°, and 75°. The optical modeling was done with the software CompleteEASE version 6.46 (J. A. Woollam Co. Inc., Lincoln, NE, USA). The PECVD layers are modeled in a wavelength range of 250 - 1000 nm using a Cauchy type parametrization ($n(\lambda) = A + B/\lambda^2$) under consideration of the thickness non-uniformity.

X-ray photoelectron spectroscopy (XPS) determines the elemental chemical composition of the near-surface areas of the deposited layers. This study uses the spectrometer's type M-Probe from Surface Science Instruments (Mountain View, CA, USA). The evaluation is performed with the software CasaXPS (Computer Aided Surface Analysis for X-ray Photoelectron Spectroscopy) from Casa Software Ltd. (Teignmouth, UK). During the assessment, the element distribution in atomic percent (at.-%) is considered.

A Nexus 870 spectrometer from Thermo Nicolet (now Thermo Fisher Scientific)

does Fourier transform infrared spectrometry (FTIR) to investigate the structural chemical properties of the organosilica films. The infrared spectrometer operates in attenuated total reflection (ATR) mode with a diamond crystal at a fixed angle of 42° or 45° and a potassium bromide beam splitter. Gold sputtered silicon wafers served as substrate for the organosilica layers.
Membrane permeance measurements are conducted using the constant volume variable pressure approach on the setup described in Section 2.1.5. This study uses the gasses helium (He) 5.0, nitrogen (N_2 5.0), carbon dioxide (CO_2 4.5), methane (CH_4 4.5.), and propane (C_3H_8 2.5) as permeants. It keeps the feed pressure constant at 1.5 bar, the temperature at 24.5 $\pm$ 1.5 °C and repeats each measurement six times for every gas and membrane.

3.3. Results and Discussion

3.3.1. Chemical analysis

Figure 3.1 displays the elemental compositions of the fabricated organosilica layers for different O_2/HMDSO reactor gas fractions and three microwave input powers from 1000 to 3000 W gained by XPS. The elemental concentration of oxygen (O) and carbon (C) is normalized in proportion to each layer's silicon (Si) concentration. Figure 3.1a shows an increasing O/Si ratio for an increasing O_2/HMDSO fraction in the reaction gas for all three microwave input powers. The increased oxygen content of the reaction atmosphere and hence the increased chance of oxygen atom incorporation into the deposited layer explain this general trend. In addition, for pure HMDSO (O_2/HMDSO fraction = 0), the difference in oxygen content between the different input powers is the most significant. With increasing O_2 reaction gas fraction, this difference vanishes and the sample fabricated with 2000 W even shows the highest O/Si ratio. However, each data point was only measured on one sample. The error bars represent the deviations of multiple measurements on one sample. Therefore, specific data points might deviate from the actual value although the error bars are small because of variations in the deposition process or contamination during storage or transport of the samples.

Generally, the grade of fragmentation of the HMDSO precursor is lower for 1000 W, meaning there are fewer reaction sites to which an oxygen atom can bind. Furthermore, the lower the O_2 content in the reaction gas atmosphere, the lower the chance of an oxygen atom coming into contact with an open reactive site in the gas phase or at the substrate surface. [Mits2018] In contrast, the chances are high that a split-off methyl group will rebind to the reaction site instead of reacting to O_2 and H_2O in the gas phase. Hence, the chances of oxygen incorporation in the organosilica layers are lowest for low-power inputs and low O_2 content in the reaction gas atmosphere, as confirmed by the results shown in Figure 3.1a.

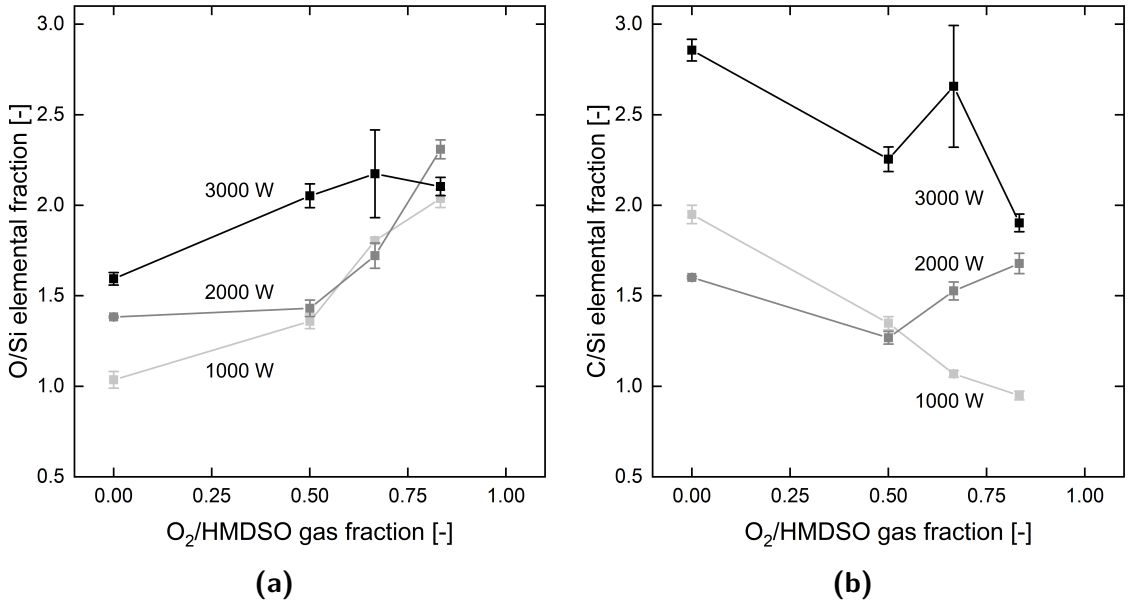


Figure 3.1.: Figures 3.1a and 3.1b show the O/Si and C/Si elemental ratios of the deposited organosilica layers over the O_2/HMDSO reactor gas fraction.

In addition to Figure 3.1a, Figure 3.1b shows an overall decreasing carbon content with increasing O_2/HMDSO gas fraction in the reaction atmosphere. As explained before, the high oxygen content in the reactor increases the chance of oxygen binding to reactive sites which emerge from removed methyl groups. An oxygen atom replaces the carbon containing methyl group. Hence, the carbon content decreases while the oxygen content increases. As in Figure 3.1a, also in

Figure 3.1b some data points deviate significantly from the trend of each input power over the varying gas fraction. Still, the overall trend is recognizable.
In summary, the XPS results clearly show the influence of microwave input power and oxygen content in the reaction gas on the organosilica's stoichiometry. Hence, the investigated parameters are suited to be used for specifically tailoring the composition of the deposited layers.

Figure 3.2 shows the O/Si and C/Si elemental ratios of organosilica layers deposited with different plasma pulse-on times from 2 to 5 seconds and microwave input powers of 1000 and 2000 W. The ratio of the reaction gas flows was 1:2 for HMDSO:Oxygen. Regarding the two microwave input powers, the O/Si ratio for 2000 W is lower than for 1000 W, which contradicts the earlier explanation. In contrast, the results show a higher C/Si ratio for higher microwave input power, similar to the results shown in Figure 3.1b. Hereby, the coatings deposited with 1000 W represent an oxidic (SiOx) layer, while the 2000 W depositions show a more organic (SiOCH) composition [Alex1997]; [Inag1999]; [Bahr2013]; [Hopp2020]. Considering the variation in plasma pulse-on length, no clear trend is visible. For both input powers, the minimum O/Si ratio is reached with 3 ms pulse-on time. Besides the maximum for the layer fabricated with 2 ms and 1000 W, all compositions show ratios around 2 and 1.5 for microwave input powers of 1000 and 2000 W, respectively, for different pulse-on times. Considering the C/Si ratio, the differences for the varying pulse-on times are even smaller. The ratios for layers deposited with a microwave input power of 1000 and 2000 W fluctuate around 1 and 1.5, respectively.
Compared to Figure 3.1, the elemental composition trend regarding the influence of the microwave input power is mostly confirmed for the C/Si ratio. In contrast, the variation of the plasma pulse-on length did neither show a clear trend for in- or decreasing the O/Si ratio nor did it significantly change the O/Si and C/Si ratios in the deposited layers.

Besides the aforementioned XPS measurements, this study investigated the influence of altered O_2/HMDSO gas fractions in the reaction atmosphere by FTIR. Figure 3.3 shows the IR spectrum with the characteristic bond types for organosilica layers deposited with 3000 W and O_2/HMDSO gas fractions from 0 to 0.83. The main peak for all layers is located between 1135 and 1072 cm^{-1} and is assigned

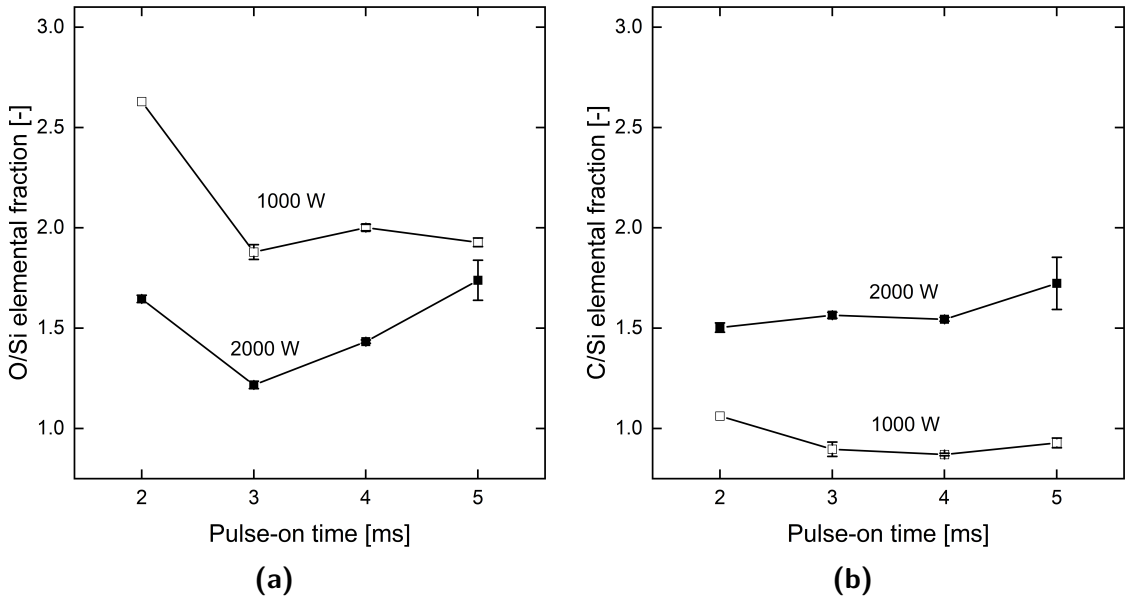


Figure 3.2.: Figures 3.2a and 3.2b show the O/Si and C/Si elemental ratios of the deposited organosilica layers over the pulse-on time of the pulsed plasma during layer deposition.

to the Si-O-Si bond. The peak for the organosilica layer fabricated with pure HMDSO is located at 1072 cm^{-1} and represents a network structure (144° bond angle). For increasing O_2 gas fractions, the peak shifts towards higher wavenumbers of up to 1135 cm^{-1} representing a cage structure (150° bond angle). Hence, the addition of oxygen leads to an increased crosslinking density of the organosilica layer, which supports the oxygen content progression in Figure 3.1a [Quee2004].

Besides the main peak assigned to Si-O-Si bonds, the FTIR progressions show two more distinct extinction areas at 1260 cm^{-1} and between 925 and 750 cm^{-1}. Those areas are assigned to bending and rocking modes of CH_3 from $Si-(CH_3)_2$ and $Si-(CH_3)_3$. The methyl group peaks are most significant for the layer deposited from pure HMDSO. With increasing O_2 content in the process gas, the area assigned to methyl groups significantly decreases in comparison to the Si-O-Si area. This carbon content depletion is also in agreement with the findings from the XPS measurement. Both methods, XPS and FTIR, show a decreasing carbon/methyl content in the organosilica layer for increasing O_2 gas fractions.

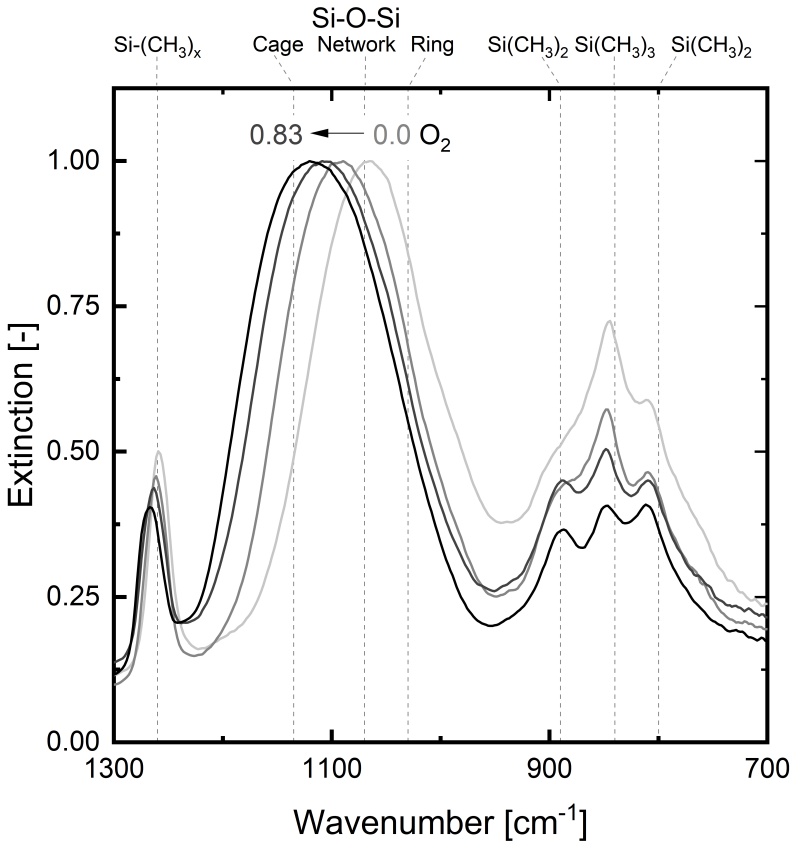


Figure 3.3.: FTIR spectra from 1300 to 700 cm^{-1} for organosilica layers deposited with 3000 W microwave input power and altered O_2 gas fractions from 0 to 0.83.

3.3.2. Pure gas permeation

The following sections investigate the pure gas permeances of the fabricated organosilica layers. The study measured the permeances of He, CO_2, N_2, CH_4, and C_3H_8. However, the following sections will focus on the permeation behavior of the smallest and biggest molecules (He and C_3H_8). Since the fabricated membranes all show a molecular size-sieving behavior, these two gases show the most distinct trends and provide better clarity for the reader. In addition, Section A.1 displays the results for the permeances of CO_2, N_2 and CH_4. Because this thesis aims for a size-sieving membrane, a high He permeance together with a high He/C_3H_8 selectivity is beneficial. It first discusses the impact of the O_2 gas fraction in the reactor on the gas permeances before focusing on the influence of the microwave input power and the plasma-on time pulse length.

Auxiliary gas impact

The influence of O_2 as an auxiliary gas in the utilized HMDSO PECVD process is studied at different microwave input powers of 1000, 2000, and 3000 W. The monomer HMDSO was mixed with four different fractions of O_2, as plotted in Table 3.1. Figure 3.4a shows the permeances of Helium, the smallest investigated gas molecule, through the fabricated organosilica membranes. Three membrane samples were measured for each fabrication parameter. The He permeance decreases with increasing O_2 content for all three microwave input powers. The increased O_2 content in the reaction chamber leads to a stronger oxidized organosilica layer (see Section 3.3.1) and thereby seems to build a more dense layer, less permeable for He.

Figure 3.4b shows the C_3H_8 permeances of the fabricated samples. C_3H_8 is the largest of the investigated gas molecules and should be retained by the organosilica layer. In contrast to the He permeances, the C_3H_8 permeances do not show a clear trend regarding the varied O_2 gas fraction, considering the displayed error bars for each fabrication parameter. On the one hand, the membranes fabricated with 2000 and 3000 W show a slightly increasing C_3H_8 permeance with increasing O_2 content. On the other hand, the permeances decrease for the membranes fabricated with 1000 W. Although no clear trend is visible, significant deviations (error bars) are present for each set of fabrication parameters. These deviations show the sensitivity of the process towards small inhomogeneities in the organosilica layer especially for the weakly permeable C_3H_8.

Figure 3.4c shows the selectivity of He to C_3H_8, calculated from the respective permeances displayed in Figures 3.4a and 3.4b. It shows increasing selectivity with decreasing O_2 content for all three microwave input powers. The membranes produced at 2000 W with pure HMDSO show the highest selectivity overall, while with added oxygen, the 1000 W microwave input power leads to the most selective layers. Although the layers fabricated with 3000 W show the lowest selectivities, they offer the least deviations and, thereby, the best reproducibility for each set of fabrication parameters. This study shows that minimizing the oxygen content in the reaction chamber leads to increased selectivity of the deposited layer combined with the highest permeances. Thus, the organosilica layers fabricated

with pure HMDSO at 1000 and 2000 W are best suited for membrane applications. Besides the gases He and C_3H_8, the permeances of CO_2, N_2, and CH_4 through the organosilica layers (see Figures in chapter A.1) confirm the findings in this section.

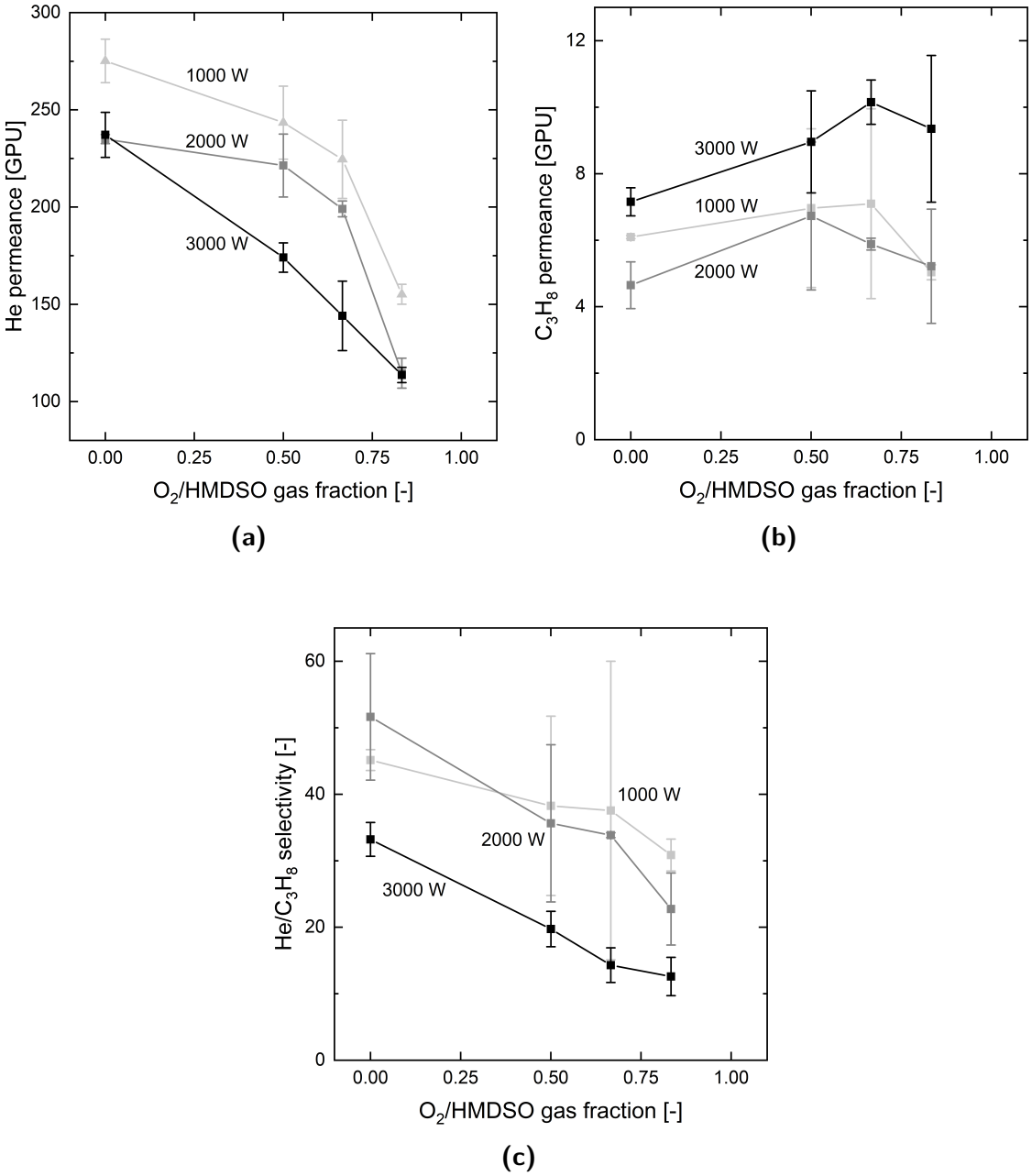


Figure 3.4.: Figures 3.4a and 3.4b show the He and C_3H_8 permeance of organosilica membranes fabricated with microwave power inputs of 1000, 2000, and 3000 W with O_2 to HMDSO gas fractions from 0 to 0.83. Figure 3.4c displays the resulting He/C_3H_8 selectivity. Each data point consists of the measurements of three membrane samples.

Microwave input power

Besides the influence of Oxygen as auxiliary gas, this thesis also investigated the effect of the microwave input power on the separation performance of the organosilica layer. Therefore, samples were fabricated with microwave input powers of 1000, 2000 and 3000 W. Their permeances for He and C_3H_8 are shown in Figure 3.4. Figure 3.4a shows the He permeance for the three different input powers over the O_2/HMDSO gas fraction. The layers deposited with 1000 W (light grey) show the highest permeances and hence the best performance for all studied gas fractions, with the maximum for pure HMDSO (P_{He}=275±11 GPU). In contrast, the permeance of C_3H_8, the biggest investigated gas molecule, has to be as low as possible. Hence, Figure 3.4b shows the best performance for layers deposited with 2000 W but closely followed by 1000 W for all gas fractions. To evaluate the overall best fabrication parameter, the selectivity of He to C_3H_8 is plotted in Figure 3.4c. It shows the highest selectivity with a mean value of around 50 for fabricating layers at 2000 W with pure HMDSO. Nevertheless, the membranes fabricated with 1000 W show nearly the same selectivity for pure HMDSO and even outperform the layers fabricated with 2000 W when O_2 is added to HMDSO. Taking into account the error bars, the layers manufactured with 1000 and 2000 W show comparable selectivity. However, the higher permeance of the 1000 W fabrication must be considered. In conclusion, the lowest possible microwave input power realizable at the LAMPS (1000 W) led to the best membrane performance for every investigated O_2 gas fractions.

Pulse length

Figure 3.5a displays the He permeance of membranes fabricated with plasma pulse-on times from 2 to 5 ms and pulse-off times of 45 ms. Organosilica layers were deposited with microwave input powers of 1000 and 2000 W, and each data point comprises three samples. The samples fabricated with 1000 W (open squares) do not show a clear trend with increasing pulse-on time. In contrast, the He permeance of the specimens deposited with 2000 W microwave input power shows a clear trend of decreasing He permeance with increasing pulse-on time.

Overall, all samples fabricated with 1000 W outperform the 2000 W samples in He permeance.

Comparing this behavior to the permeance of C_3H_8 displayed in Figure 3.5b, the samples produced with a microwave power input of 2000 W do not show any clear correlation between C_3H_8 permeance and pulse-on time. In contrast, the C_3H_8 permeances of the 1000 W samples increase by more than 100 % when increasing the pulse-on time from 3 to 4 ms. The permeances of all 2000 W samples and the 1000 W samples deposited with 2 and 3 ms show the same beneficial low permeance for C_3H_8.

Figure 3.5c shows the selectivity of He to C_3H_8. The results show increased selectivity for low pulse-on times (2 and 3 ms) for 1000 W and 2000 W. Since the He permeance is highest for the samples fabricated with 1000 W microwave input power, this is the best-performing parameter set. Furthermore, although the permeance for one specific gas might not change with varied fabrication parameters, as seen for the 1000 W samples' He permeance and the 2000 W samples' C_3H_8 permeance, there may still be drastic changes for other gases.

The findings described in this section agree with the results discussed in section 3.3.2. There, a low microwave input power positively affected the membrane performance of the deposited layers. In this section, again, a minimized microwave power input into the plasma reactor, in this case by lowering the plasma pulse-on time, reveals a positive effect. Hence, this section concludes that the membrane performance in the investigated parameter range, which was the maximum range implementable on the used LAMPS reactor, benefits from the lowest possible energy input with a microwave input power of 1000 W and a pulse-on time of 2 ms.

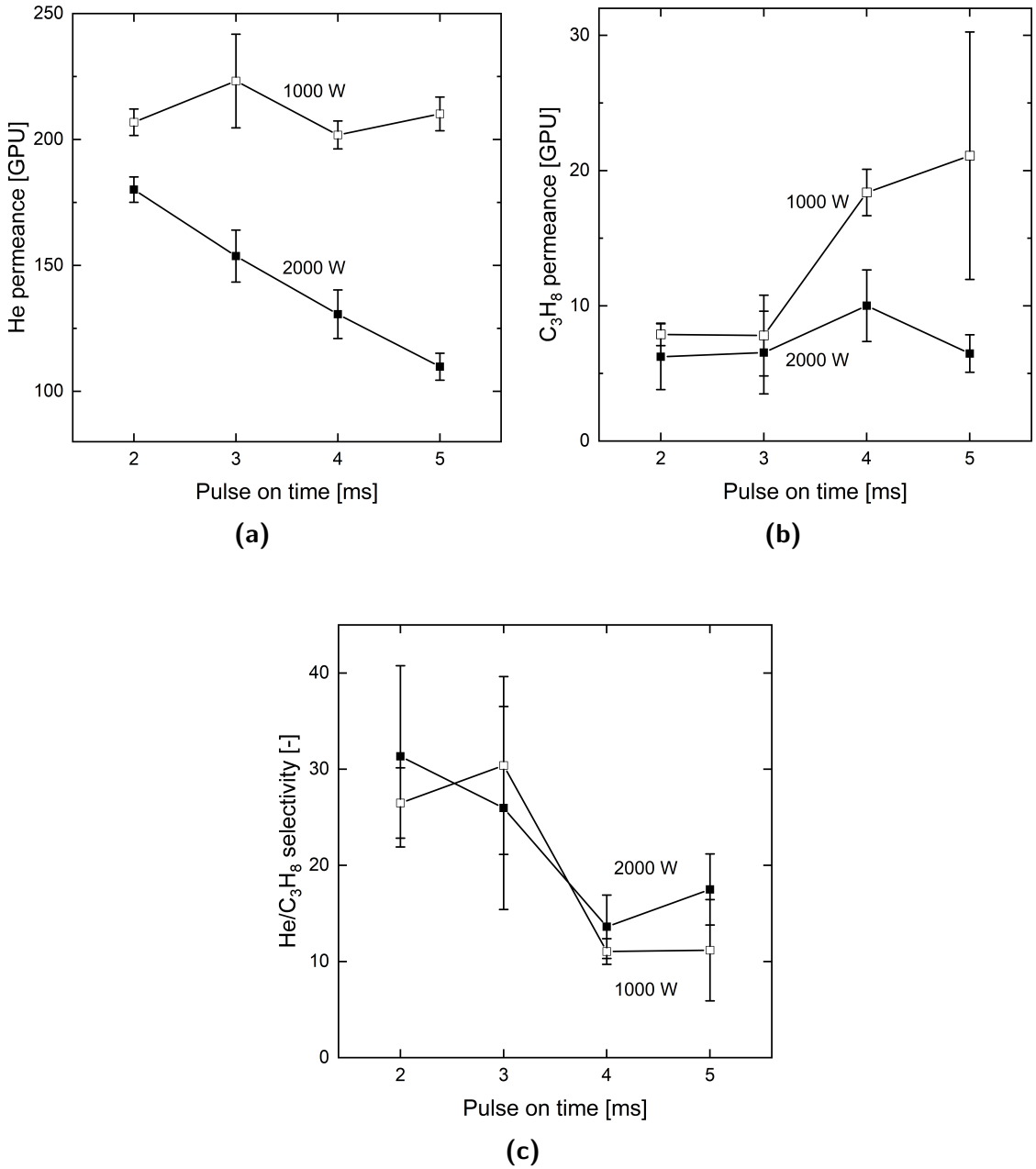


Figure 3.5.: Figures 3.5a and 3.5b show the He and C_3H_8 permeance of organosilica membranes fabricated with pulse-on times of 2 to 5 ms. Figure 3.5c displays the resulting He/C_3H_8 selectivity. Each data point consists of the measurements of three membrane samples.

3.4. Conclusion

Chapter 3 investigated the variation of fabrication parameters for organosilica layers deposited on a PDMS thin film composite membrane and their resulting membrane performance. The layers have been deposited in a plasma reactor using microwave magnetrons with a frequency of 2.45 GHz at a pressure of 5 Pa and HMDSO as the precursor. The amount of additional O_2 to the reaction gas, the microwave input power, and the plasma pulse-on length have been varied over the different samples. The aim was to optimize the molecular size-sieving behavior by increasing the He permeance and the He/C_3H_8 selectivity.

The addition of O_2 to the HMDSO in the plasma reactor exhibited the strongest influence. The He permeances and He/C_3H_8 selectivities for all studied microwave input powers are highest for pure HMDSO. However, increasing the O_2 content significantly decreases the permeance and selectivity.

The variation of the microwave input power shows similar behavior for varying O_2 fractions in the reaction gas mixture. The smaller the input power, the higher the permeance and selectivity for He.

In contrast, the alteration of the pulse-on time did not show strong effects on the selectivity for the selected microwave input powers. Nevertheless, the He permeance is highest for the lowest microwave power input.

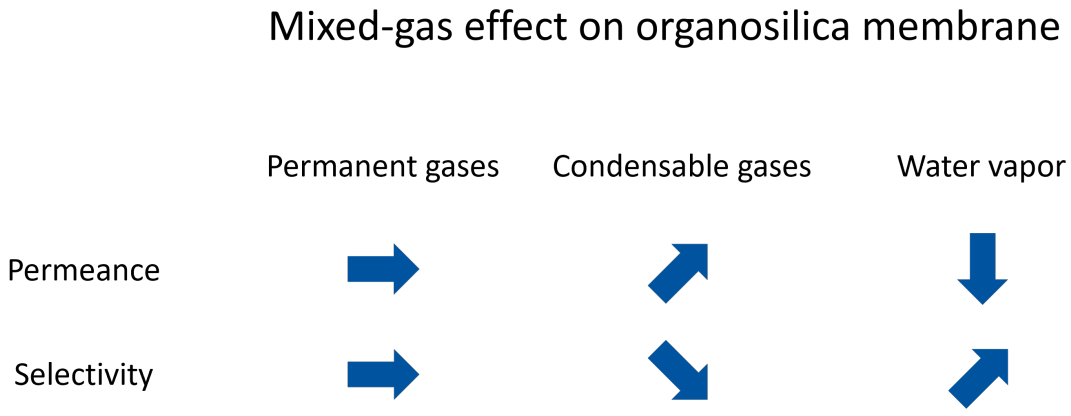
The fabrication parameters with the lowest power input per molecule (smallest Yasuda parameter) and the highest HMDSO reaction gas fraction led to the best membrane performance considering He permeance and He/C_3H_8 selectivity. Besides the investigated parameters, an increase in the HMDSO flow rate into the reactor and increased pressure in the plasma reactor could realize a further decrease in energy input per molecule. However, in additional experiments (not shown here), parameters with lower energy input resulted in unstable plasma ignitions since insufficient energy was put into the reactor. Hence, lowering the energy input per molecule would further exacerbate reproducibility issues. In addition, the deposition rates would drop significantly with decreasing energy input. Low deposition rates would reduce the membrane production rate leading to challenges in scaling up this method to a roll-to-roll process. Thus, the investigated parameters represent the optimum membrane performance achievable within the

feasible parameters for the used plasma reactor. For the transfer to another reactor or the upscaling to a roll-to-roll process, the gained insights can be used to optimize the membrane performance. Still, the limits of feasibility must be considered individually for each reactor.

3

4. On the mixed gas behavior of organosilica fabricated by plasma-enhanced chemical vapor deposition

Parts of this chapter have been published as:
Jens Rubner, Soukaina Skribbe, Hannah Roth, Lara Kleines, Rainer Dahlmann, Matthias Wessling *On the Mixed Gas Behavior of Organosilica Membranes Fabricated by Plasma-Enhanced Chemical Vapor Deposition (PECVD)* , Membranes, 2022
DOI: 10.3390/membranes12100994



4

4.1. Introduction

Since energy efficiency is crucial for mitigating global warming, the industry is forced to develop alternative processes with reduced energy demand [Mass2018]. One promising alternative for gas separation are membrane processes, which are already used in different applications like gas sweetening, hydrogen recovery and air separation [Brun2010]. These processes are up to 10 times more energy efficient than traditional separation methods [Shol2016]. As Sholl and Lively state, the full potential for the use of gas separation membranes in chemical processes has not yet been reached. Membranes with high permeances and selectivities for specific applications are needed [Shol2016]. To fulfill the need for membranes with improved permeation performances, researchers have developed many new membrane materials in recent decades. Thereby, they were able to push the Robeson upper bounds for different gas combinations to higher values [Robe2008]; [Swai2015]; [Come2019]; [Lai2022]. Although these new materials are promising, only a few materials developed decades ago are used for industrial membrane processes today due to the lack of scalable fabrication routes [Iuli2020] .

In this regard, a promising separation task for membranes is the recovery of helium. The demand and consequently also the market prices of helium rose quickly in the last decades [Scho2017b]. Helium is produced by separating it from natural gas fields with high helium contents (up to around 4%). While cryogenic distillation and pressure swing adsorption are commonly used recovery methods, in many cases separation through membrane processes present a more energy efficient alternative [Alde2017]; [Scho2016]; [Scho2017b]. Sunarso et al. and Scholes and Ghosh reviewed different membrane materials for helium recovery in detail [Suna2017]; [Scho2017a]. They found that especially silica membranes, in comparison to all other membrane materials, show high helium permeability and selectivity, which are essential for a successful implementation [Suna2017]. Although zeolites and metal organic frameworks (MOF) show similar permeabilities as silica, they suffer from low selectivity. Moreover, the loss in selectivity and also permeability significantly increases for MOF mixed matrix membranes (MMM). On the one hand, the MMMs outperform polymeric membranes in permeability, selectivity and chemical stability. On the other hand, their production process is

time consuming, hardly reproducible, difficult to upscale and hence costly. Thus, commercial membrane development for helium production still mainly focuses on polymeric membrane materials. [Iuli2020]

In addition to the previously mentioned materials, scalable plasma processes create thin selective coatings [Roua2010]. In particular, plasma-enhanced chemical vapor deposition (PECVD) has been studied for many years [Li1999]. It allows the fabrication of tailored coatings with regard to mechanical and chemical properties and, at the same time, enables low coating thicknesses in the nanometer range. The formation of organosilica layers by PECVD utilizing hexamethyldisiloxane (HMDSO) as precursor results in membranes with gas separation characteristics [Roua2017]; [Lo2010]; [Li1999]; [Kafr2010]; [Cous2014]; [Naga2015]; [Klei2020]; [Klei2021]; [Klei2022]. Inorganic [Kafr2009]; [Tsur2011]; [Naga2013]; [Haac2015] or organic substrate membranes [Li1999]; [Roua1999]; [Roua2002]; [Bosc2003]; [Ngam2013]; [Char2016]; [Wang2017]; [Klei2020]; [Klei2021]; [Klei2022] function as support for the thin organosilica layer. Besides, PECVD enables the combination of advantages of different membrane materials. Inexpensive organic membranes offering mechanical support combined with an organosilica layer result in high permeances and selectivities for helium [Naga2013]. Furthermore, PECVD is already industrially used and scalable in roll-to-roll processes and therefore can be easily applied for industrial scale membrane production [Izu1995]. Since the resulting selective layer properties are dependent on the plasma parameters [Klei2021]; [Klei2022], membranes for different separation tasks can be fabricated on the same production line, by only changing the plasma parameters. While PECVD membranes are not a new concept in the literature of the last two decades, research does not offer much information on mixed gas experiments with such membranes. The interaction effects of different gases and vapors on the permeance and selectivity of those membranes are still unknown.

To gain more knowledge about the permeation behavior of membranes fabricated by PECVD, this study closely investigates the performance of one promising organosilica membrane. Figure 4.1 shows the selectivity of helium to carbon dioxide over the helium permeance in an adapted Robeson plot. Since there is no clear linear relation between permeance and thickness in organosilica membranes fabricated by PECVD, unlike what is generally seen in conventional polymers, a

thickness of 1 µm is assumed for all polymer membranes according to Zhu et al. The solid line in Figure 4.1 represents the Robeson upper bound [Robe2008]. The filled circles show the permeation characteristics of composite membranes with selective PECVD coatings fabricated with varying coating parameters (refer to Kleines et al. [Klei2020]; [Klei2021]). Additionally, the characteristics of the used PDMS substrate for the PECVD coating and two commercially available polymers (Matrimid [Guiv2002] and P84 [Shen2010]) are plotted as reference.

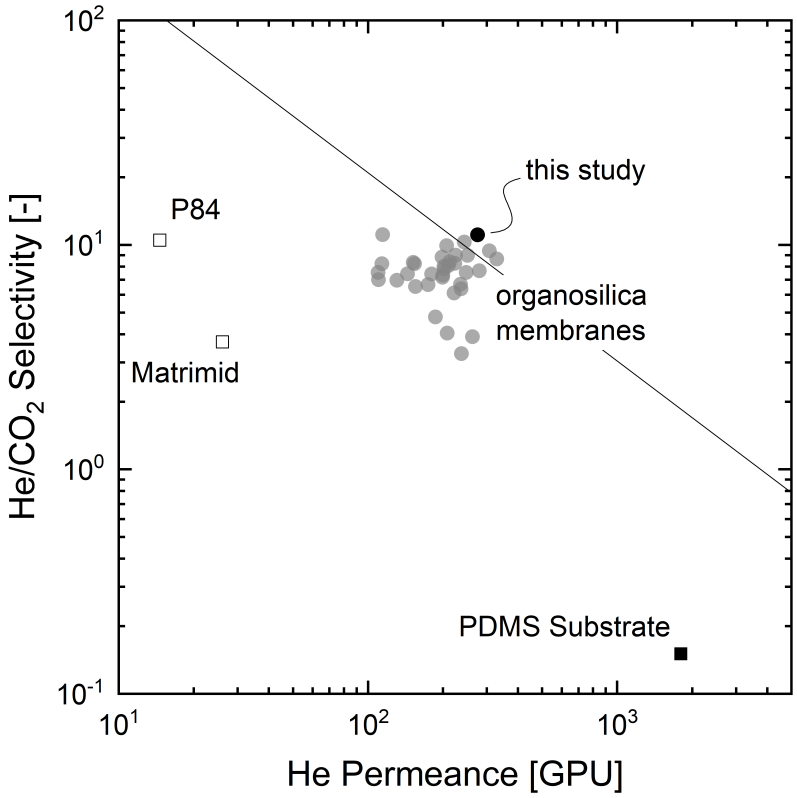


Figure 4.1.: Robeson plot for He/CO_2 with a variety of organosilica membranes fabricated via PECVD by the authors (filled circles) [Klei2020]; [Klei2021] and the uncoated PDMS substrate membrane. As reference, the plot displays two commercially available polymers (Matrimid [Guiv2002] and P84 [Shen2010]) with an assumed thickness of 1 µm. The best performing organosilica membrane, which was chosen for mixed gas experiments in this study, is plotted with a black circle.

For this study, the best performing PECVD membrane, plotted as a black circle (cf. Figure 4.1), was chosen for further investigation. First, this study determines the activation energies for pure gas permeation of four gases (He, CO_2, CH_4, and N_2) from 0 °C to 60 °C. Then, it evaluates the activation energy differences of

the four gases and compares them to published PECVD membrane data, which all show high energy values [Haac2015]; [Kafr2009]; [Kafr2010]; [Naga2013]; [Naga2016]. Afterward, the study focuses on the mixed gas behavior of equimolar mixtures of selected gases. Experiments at various temperatures will elucidate the possible occurrence of competitive sorption or other non-ideal effects of organosilica membranes. In the last step, the study assesses the influence of additional water vapor on the pure gas permeance of the most promising gas combination, He and CO_2. It further discusses the possibility of water vapor condensation or organosilica hydrolysis, previously reported for PECVD membranes [Gava1989]; [Gall1994]; [Lebo1995]; [Duke2006]; [Cast2008]; [Song2016]. This study aims to identify application windows for gas separation tasks with a scalable producible organosilica membrane.

4.2. Experimental

4.2.1. Materials

A PDMS composite membrane acts as the substrate for the deposition of the PECVD layer and was supplied by the Helmholtz-Zentrum Hereon Geesthacht. It consists of a non-woven fabric, a microporous support structure of polyacrylonitrile (PAN) and a dense, about 160 nm thin, gas-selective layer of polydimethylsiloxane (PDMS). This substrate membrane was chosen because of its smooth surface compared to porous substrates, which should enable a more homogeneous, uniform, and defect free layer growth. Furthermore, PDMS is a rubbery polymer and therefore known for its high permeance and its nearly ideal permeation behavior. For the PECVD coating, this study uses hexamethyldisiloxane (HMDSO) as monomer and oxygen as auxiliary reaction gas for the deposition of the plasma polymer layers. HMDSO with a purity of $> 98\%$ was purchased from Sigma-Aldrich. Figure 4.2 shows the schematic layer structure of the final membrane. For the permeation experiments, helium (He) and methane (CH_4) from Nippon with a purity of 99.999 vol.-% and 99.95 vol.-%, respectively, were used. Carbon dioxide (CO_2) with a purity of 99.995 vol.-%, and Nitrogen (N_2) with a purity of 99.999 vol.-% from Westfalen AG were used.

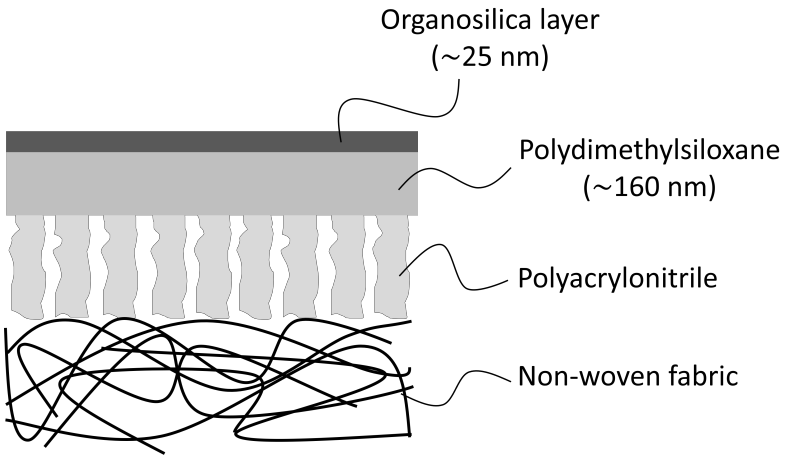


Figure 4.2.: Schematic representation of the thin film composite membrane's structure.

4.2.2. PECVD membrane fabrication

The coating deposition was conducted in the low-pressure plasma reactor (LAMPS, Large Area Microwave Plasma System) introduced and schematically presented in section 2.2.5.

A 7x7 cm piece of the PDMS composite membrane mentioned in Section 4.2.1 is installed on the substrate holder of the LAMPS to deposit the organosilica membrane on top. First, an oxygen plasma pre-treatment activates the surface before coating (see Table 4.1 for plasma parameters) [Klei2021]; [Klei2022]. Afterward, the organosilica layer is deposited using HMDSO as a precursor in the pulsed plasma with a microwave peak power of 2,000 W for 93 seconds. An organosilica layer with a thickness of about 25 nm is deposited. At the same time, a silicon wafer and a gold-sputtered silicon wafer are coated next to the membrane for subsequent ellipsometry and FTIR measurements, respectively. The pre-treatment activates the surface before coating [Klei2021]; [Klei2022]. In the coating experiment, a silicon wafer and a gold-sputtered silicon wafer were coated at the same time next to the membrane for subsequent ellipsometry and FTIR measurements, respectively.

4.2.3. XPS measurements

The X-ray photoelectron spectroscopy (XPS) measurements were carried out in an Ultra AxisTM spectrometer from Kratos Analytical (Manchester,UK). The mem-

Table 4.1.: PECVD coating parameters.

Coating type	HMDSO flow [sccm]	Oxygen flow [sccm]	Pulse on/off [ms]	Microwave peak power [W]	Coating time [ms]
Pre-Treatment	0	100	4/45	4,000	5,000
Layer Deposition	70	0	2/45	2,000	93,000

brane samples were irradiated with mono energetic Al K*1,2 radiation (1486.6 eV), and the spectra were taken at a power of 144 W (12 kV×12 mA). The aliphatic carbon at a binding energy of 285 eV (C 1s photo line) was used to determine the charging. XPS spectra were processed with dedicated software, and atomic concentrations of the elements were quantified by integration of the relevant photoelectron peaks. The information depth is about 10 nm.

4.2.4. FTIR measurements

Structural chemical properties were investigated by Fourier transform infrared spectrometry (FTIR) with a Nexus 870 spectrometer from Thermo Nicolet (now Thermo Fisher Scientific). The infrared spectrometer is operated in attenuated total reflection (ATR) mode with a diamond crystal at a fixed angle of 42° or 45° and a potassium bromide beam splitter. Gold sputtered silicon wafers served as substrate for the PDMS and PECVD layer.

4.2.5. Ellipsometry measurements

To determine the thickness of the deposited PECVD layer, this study conducted ellipsometric measurements with a Spectroscopic Ellipsometer (RC2 from J.A. Woollam Co. Inc., Lincoln, NE, USA) with a investigated spot size of 2 mm. All measurements were performed at incident angles of 65°, 70° and 75° over a wavelength range of 300 to 1000 nm with a spectral resolution of 2 nm. The optical modeling was done with the commercial software package CompleteEASE 6.46 (J.A. Woollam Co.).

The layer thickness was measured on a silicon wafer and not on the membrane itself to avoid thickness deviations originating from the slightly varying PDMS layer

thickness of the membrane. Material data for silicon were taken from Herzinger et al. [Herz1998]. To determine the PECVD layer thickness, a Cauchy-type parametrization ($n(\lambda) = A + B/\lambda^2$) was used and fitted to the data. The determined thickness of the deposited layer is stated in Table 4.1.

4.2.6. Permeation measurements

This study conducted all permeation measurements with a constant pressure/variable volume method on the gas permeation setup (GPS) introduced in Section 2.1.5 similar to the one used by Logemann et al. [Loge2020]. This study conducts experiments in the temperature range from -20 °C to 60 °C. The diameter of the membrane is 65 mm. The feed pressure is regulated with an automated back pressure regulator (Bürkert GmbH) and set to 2 bara for all experiments. The permeate pressure is always ambient pressure (1 bara).

The gas mixtures are produced from pure gas cylinders with the required composition controlled through mass flow controllers (Bronkhorst EL-Flow). To determine the gas compositions of the feed, retentate and permeate stream, a gas chromatograph (Agilent Technologies 7890A) is connected to the gas permeation setup which consists of a thermal conductivity detector and argon as carrier gas. For experiments with water vapor, a controlled evaporation and mixing device (CEM Evaporator W-101A from Bronkhorst GmbH) is used. The water vapor content is measured using dew point mirrors (Michell Optidew) in the feed, retentate and permeate channels. The measured dew points are converted into water vapor pressures using the Antoine equation [Anto1888]. With this value, the water activity a_w is calculated as follows:

$$a_w = \frac{p_{H2O,gas}}{p_{H2O,sat}(T)}, \tag{4.1}$$

where $p_{H2O,gas}$ is the water vapor pressure of the gas stream measured with the dew point sensor and $p_{H2O,max}(T)$ is the saturation water vapor pressure at the temperature of the gas stream.

A manual bubble flow meter was used to determine the permeate flux. The permeances are calculated with:

$$Q_i = \frac{\dot{V}_P x_{P_i} \left(\frac{T_F}{273.15+T_R}\right)}{A_m \left(p_{F_i} - p_{P_i}\right)}, \tag{4.2}$$

where Q_i is the permeance [GPU] (1 GPU=10^{-6} cm^3(STP)/cm^2· s· cmHg), $\dot{V}_P$ the average permeate volume flux, x_{P_i} the mole fraction of gas i in the permeate stream, T_F the feed temperature, T_R the room temperature, A_m the membrane surface area and $(p_{F_i} - p_{P_i})$ the partial pressure difference between feed and permeate side.

The apparent activation energies of permeation for the gases i, $E_{P,i}$, were calculated using the Arrhenius-type equation:

$$Q_i(T) = Q_{0,i} \cdot \exp \frac{-E_P}{RT}, \tag{4.3}$$

where $Q_i(T)$ is the permeance of gas i at temperature T, $P_{0,i}$ a pre-exponential factor for gas i, R the ideal gas constant and T the absolute temperature.

4.3. Results and discussion

4.3.1. Chemical analysis of the organosilica layer

The elemental composition of the PDMS substrate membrane and the organosilica layer fabricated by PECVD is determined by XPS at three different spots of the membrane. Table 4.2 displays the elemental composition of the PDMS and the organosilica layer. Each has a thickness significantly higher than 10 nm to avoid influences of the underlying PAN and PDMS layer, respectively. Since the XPS can not detect hydrogen atoms, the content of this atom is disregarded in Table 4.2 and the following paragraph.

The measured atomic composition of the investigated PDMS membrane layer ($SiO_{1.1}C_{2.3}$) is in accordance with its theoretical composition $SiOC_2$. Consider-

Table 4.2.: Elemental composition of the PECVD layer and PDMS substrate in at. % by XPS.

Layer	Si2p	O1s	C1s	Composition
PDMS	22.51 ± 0.18	25.11 ± 0.24	52.39 ± 0.38	$SiO_{1.1}C_{2.3}$
Organosilica	24.95 ± 0.70	27.38 ± 0.13	47.67 ± 0.57	$SiO_{1.1}C_{1.9}$

ing the organosilica layer, the atomic composition of it ($SiO_{1.1}C_{1.9}$) only deviates marginally from the theoretical PDMS and the measured PDMS membrane composition. Compared to the used monomer HMDSO ($SiO_{0.5}C_3$), the deposited organosilica layer shows a significantly lower carbon and a higher oxygen amount. The change in carbon content can be attributed to a depletion of the methyl groups in the PECVD process. In contrast, the increase in oxygen content can not be induced by the PECVD process, since there is no additional oxygen present. Rather, it could be attributed to the contact with atmospheric oxygen or water vapor after the coating process, possibly leading to slow post-oxidation promoted by free radicals incorporated in the organosilica layer during film growth [Yasu1977].

Figure 4.3 displays the FTIR spectra from 1,300 to 700 cm^{-1} of the PDMS and the PECVD-deposited organosilica layer. To allow comparability, the main peak of the PDMS, and the organosilica spectra at about 1,040, and 790 cm^{-1}, respectively, is normalized to a value of 1. The characteristic wave numbers of the functional groups of organosilica layers are marked in Figure 4.3 for easier assessment [Gril2003]; [Lenz2001]; [Mota1995].

The infrared (IR) spectrum of the PDMS coating exhibits characteristic IR bands [Efim2002]; [Khor1996]. The absorption band at around 1,010 cm^{-1} can be attributed to the -Si-O-Si- group of the PDMS. The absorption bands at around 790 and 1,270 cm^{-1} represent the valence vibrations of the -Si-C- and -C-H groups, respectively. [Khor1996]
The IR spectrum of the organosilica layer has an absorption band at around 1,270 cm^{-1} as well. However, in contrast to the PDMS, the organosilica layer has its main peak at around 1,040 cm^{-1} correlating with the Si-O-Si vibration mode [Gril2003]. Figure 4.3 also shows absorption peaks at 845, and 805 cm^{-1} representing the

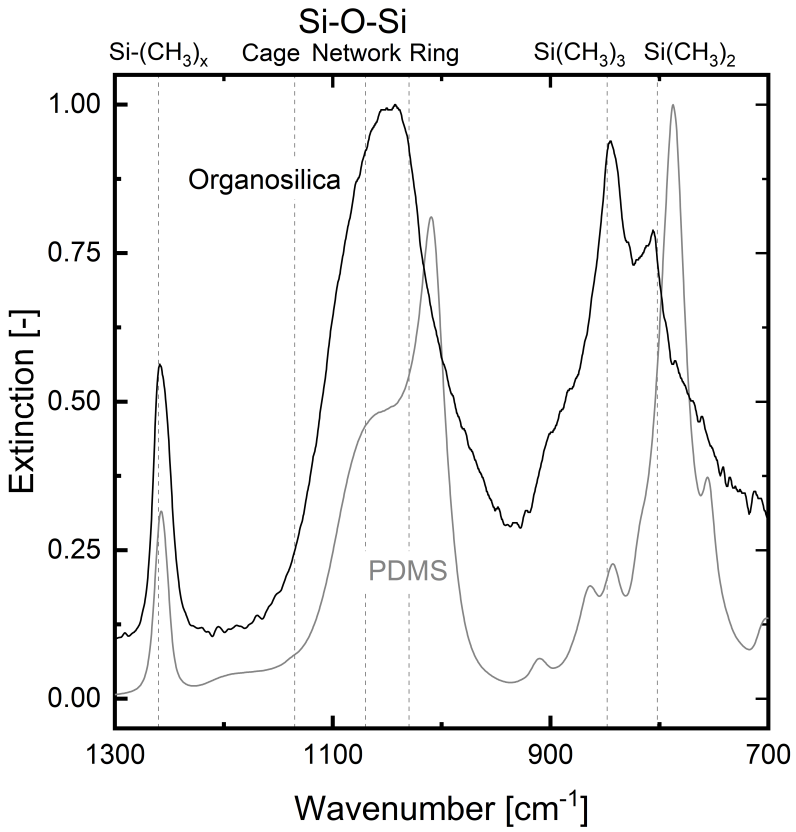


Figure 4.3.: Infrared spectra from 1,300 to 700 cm^{-1} of the PDMS (grey), and the PECVD-deposited organosilica layer (black). Wave numbers of the organosilica's characteristic functional groups are marked by dashed lines [Gril2003]; [Lenz2001]; [Mota1995].

methyl group contribution. These results are in accordance with measurements for pure HMDSO PECVD-fabricated layers published by Kleines et al. [Klei2021]. Together with the carbon content of nearly 50 % measured with XPS, this result confirms the strong organic character of the studied organosilica layer.

4.3.2. Temperature dependent permeation behavior

The pure gas permeance of the organosilica membrane was measured for He, CO_2, CH_4 and N_2 at four different temperatures (0, 20, 40, 60 °C) and is depicted in figure 5. The individual permeances are plotted over 1,000/(RT). The dashed lines show the best fit for each gas, which represent an Arrhenius-type function. This enables the determination of the activation energy for permeation according to equation 4.3.

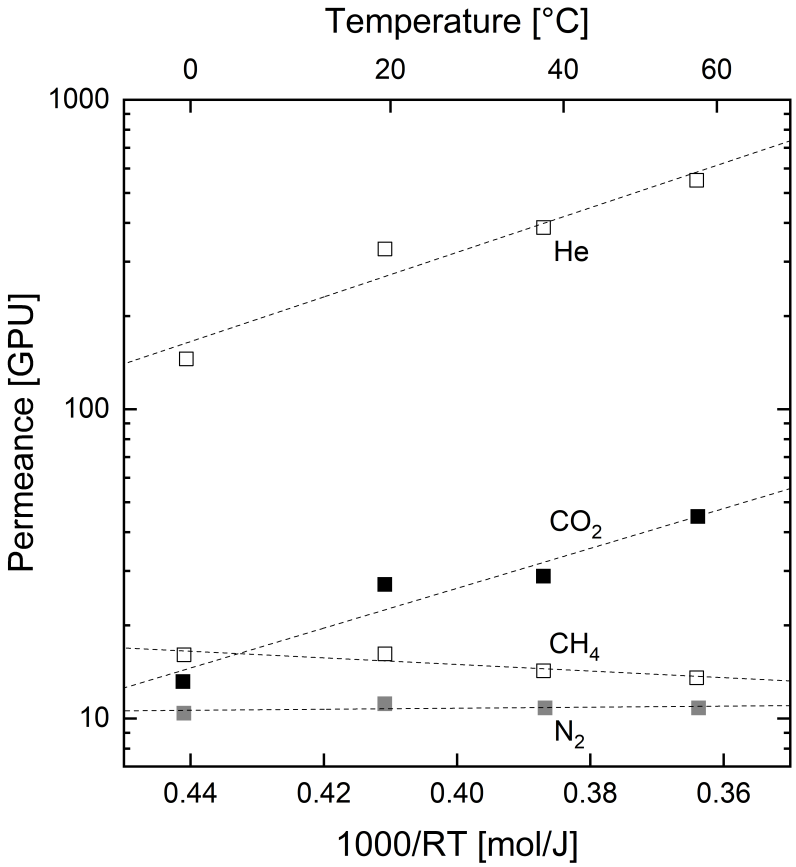


Figure 4.4.: Permeances for He, CO_2, CH_4 and N_2 of the studied organosilica membrane fabricated by PECVD. Permeances are plotted over $1,000/(RT)$ to determine the activation energies for permeation for the different gases.

He and CO_2 show a clear increase in permeance over time and their activation energies are 16.6 ± 3.1 kJ/mol and 14.8 ± 2.8 kJ/mol, respectively. In comparison, the activation energies for N_2 and CH_4, being 0.4 ± 0.5 kJ/mol and -2.5 ± 0.8 kJ/mol, respectively, are significantly lower. This distinct temperature dependent behavior for He accompanied with a low or even negative activation energy for N_2 compares well to other publications of membranes fabricated by PECVD [Kafr2009]; [Kafr2010]; [Naga2013]; [Haac2015]; [Naga2016]. Those substantial differences in activation energies are due to the microporous structure of the organosilica layer. The molecules with small kinetic diameters (He and CO_2) are small enough to permeate through the micropores/free-volumes of the membrane following the solution-diffusion mechanism. At the same time, the bigger molecules can not access those micropores but only permeate through defects

(meso- and macropores) in the organosilica layer following Knudsen diffusion. Whilst Knudsen diffusion is only weekly temperature dependent, a temperature increase leads to a substantially increased diffusivity and hence also permeation for gases following the solution-diffusion behavior. [Kafr2009]; [Naga2015] This permeation behavior leads to a remarkably strong selectivity increase with increasing temperature for CO_2 to CH_4, which has, to the best of my knowledge, not been reported for any gas separation membrane before. Furthermore, the differences in activation energies for the investigated gases lead to the assumption that the average pore/free-volume size of the studied organosilica layer is between the kinetic diameter of CO_2 (330 pm [Brec1973]) and N_2 (364 pm [Kiha1951]) [Kafr2009]; [Naga2015].

4.3.3. Mixed gas behavior

Non-ideal effects can potentially occur and drastically alter the separation performance of the membrane. The following section evaluates the gas pairs He/CH_4, He/CO_2 and CO_2/CH_4 with regard to their mixed gas behavior in comparison to the aforementioned pure gas experiments.

Permanent gases

First, the mixed gas behavior of the two permanent gases, He and CH_4, is discussed. Figures 4.5a and 4.5b show the permeances and the resulting selectivity for the pure and mixed gas experiments from 0 to 60 °C.

For mixed gases, the permeance of both gases drops slightly in comparison to the pure gas results. Nevertheless, the selectivity in the mixed gas stays the same as for the pure gas experiments. Hence, the organosilica membrane shows no significant non-ideal behavior in the investigated temperature and pressure range for permanent gases. The same behavior can also be expected for the mixture of the two permanent gases He and N_2 which was not investigated in this study.

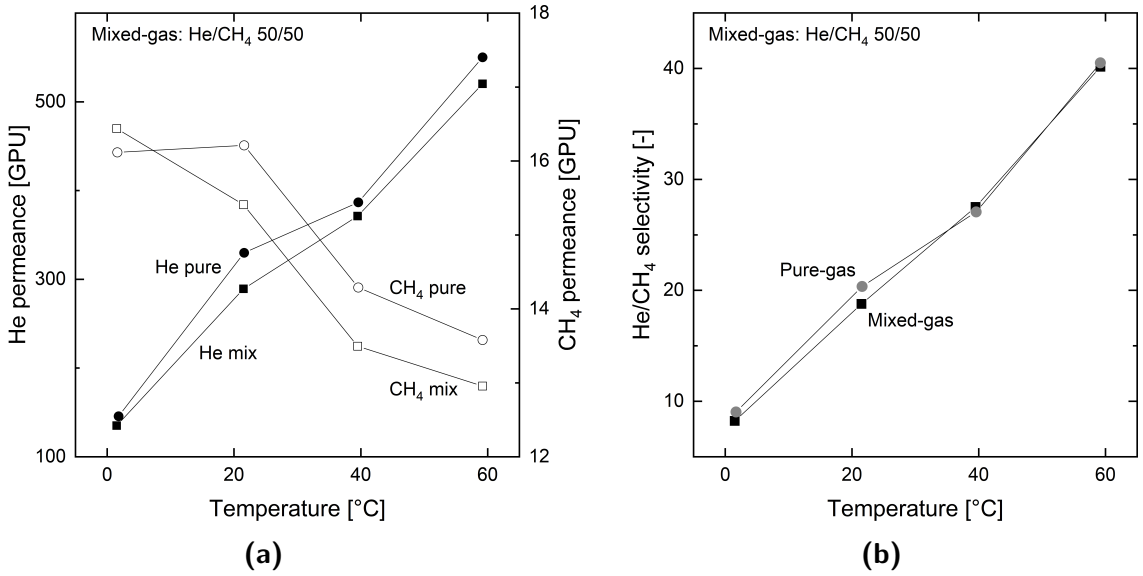


Figure 4.5.: Permeance (a) and selectivity (b) of the organosilica membrane for He and CH_4, pure gas (circles) and mixed gas (squares) experiments with feed and permeate absolute pressures of 2 and 1 bar, respectively.

Condensable gases

Permeation experiments with CO_2 reveal the influence of a condensable gas on the permeation behavior of the organosilica membrane. This section shows the results of the addition of CO_2 to both He and CH_4.
Figures 4.6a and 4.6b illustrate the permeances and selectivities of the pure and mixed gas experiments with He and CO_2. In these experiments, the condensable CO_2 is the retained compound.

As can be seen, the temperature dependent behavior of both gases is the same for pure and mixed gas experiments. But Figure 4.6a also shows a decrease in mixed gas permeance for He and an increase for CO_2 compared to their pure gas values. This effect results in a significantly decreased mixed gas selectivity of He to CO_2 (cf. Figure 4.6b). This behavior was also observed in other studies and is attributed to effects of plasticization and/or competitive sorption [Bos1999]; [Viss2005]; [Viss2007]; [Ricc2020]. However, as Genduso, Ghanem, and Pinnau recently showed, in case of 6FDA-mPDA, the depression of the size sieving capability of the polymer causes this decrease in selectivity. Hence, to elucidate the origin of this phenomenon, further studies on the sorption and diffusion behavior

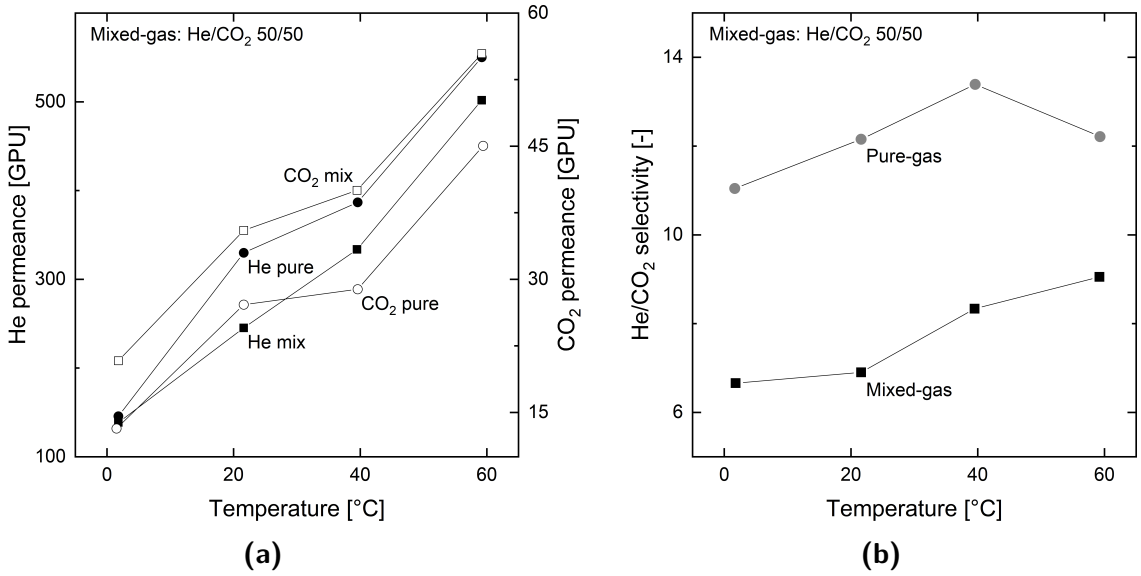


Figure 4.6.: Permeance (a) and selectivity (b) of pure, and mixed gas (50:50) He and CO_2 for the organosilica membrane for 0, 20, 40 and 60 °C with feed and permeate pressures of 2 and 1 bar, respectively.

4

of the organosilica membrane need to be conducted.
Regardless of the selectivity loss for mixed gases, the trend of an increasing permeance and selectivity over temperature is maintained for the investigated gas mixture. Thus, this organosilica membrane favors the application at elevated temperatures.

Besides the mixed gas He and CO_2, a 50:50 mixture of CH_4 and CO_2 also functions as feed. Figure 4.7 displays the permeances and selectivities for pure and mixed gas experiments of CO_2 and CH_4 from -20 to 60 °C.
A unique feature of the organosilica membrane is the inversion of selectivity for CH_4 and CO_2 pure gases with respect to temperature (see Figure 4.7b). This effect is based on the strongly differing activation energies for both gases (see Section 4.3.2). The permeance of CO_2 strongly increases with temperature, whereas the permeance of CH_4 slightly drops. This behavior leads to an inversion of selectivity between 20 and 40 °C in the pure gas experiment. In contrast, the CO_2/CH_4 selectivity for the mixed gas experiments does not show this inversion of selectivity but always remains above one (see Figure 4.7b), even for temperatures as low as -20 °C.

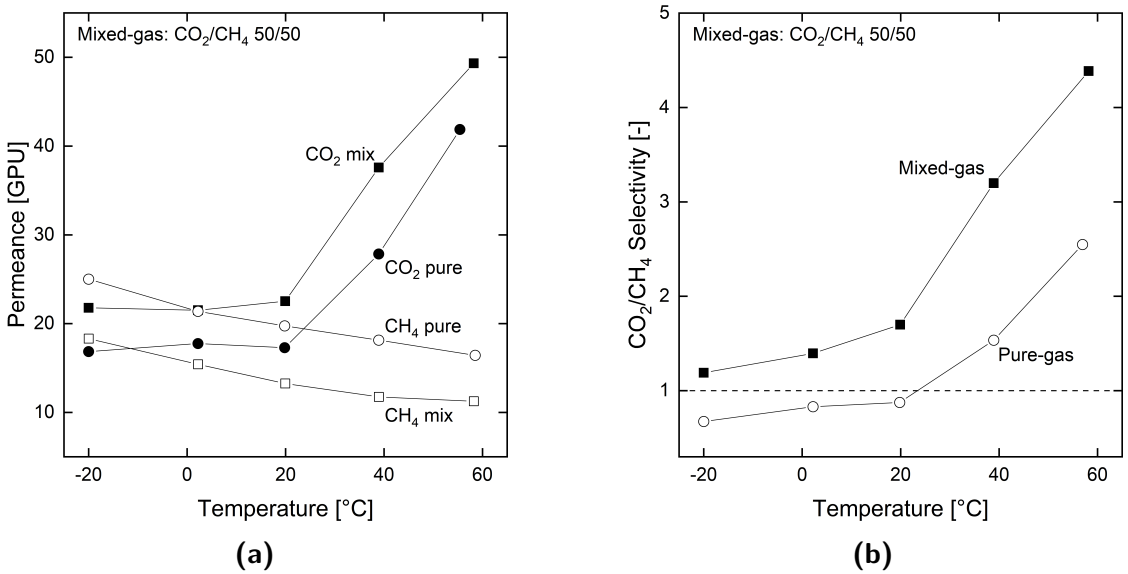


Figure 4.7.: Permeability (a) and selectivity (b) of pure and mixed gas (50:50) CO_2 and CH_4 for the organosilica membrane. Results are plotted for -20, 0, 20, 40 and 60 °C with feed and permeate pressures of 2 and 1 bar, respectively.

Figure 4.7a shows the course of the permeances of the two gases. Here, the mixed gas permeances of CO_2 surpass the values of the pure gas experiments, whereas the permeances for CH_4 lay below their pure gas values. This mixed gas effect can be attributed to the above mentioned competitive sorption effect [Vopi2014]; [Ricc2020]. As with He and CO_2, the condensable CO_2 apparently sorbs preferentially into the membrane, thereby mitigating the sorption of CH_4. In concrete terms, this leads to an in- and decrease of the CO_2 and CH_4 permeance, respectively, preventing the inversion of selectivity. Further studies on the sorption and diffusion behavior of the organosilica layer are needed to gain more insights into the exact phenomena.

Water vapor

Figures 4.8a and 4.8b show the permeance of pure He and CO_2 in dependence on the feed gas water activity in the respective gas at 25 °C. Before the membrane came into contact with water vapor, the He and CO_2 permeances were at 330 and 37.5 GPU, respectively. As soon as water vapor contacts the membrane, the permeance drops by about 60 % to around 100 and 10 GPU, respectively, for

low water activities. When going back to pure gases, the permeance does not increase back to the original value. Even an extensive drying time (50 hours) under vacuum and elevated temperatures (60 °C) does not regain the original value (data not shown).

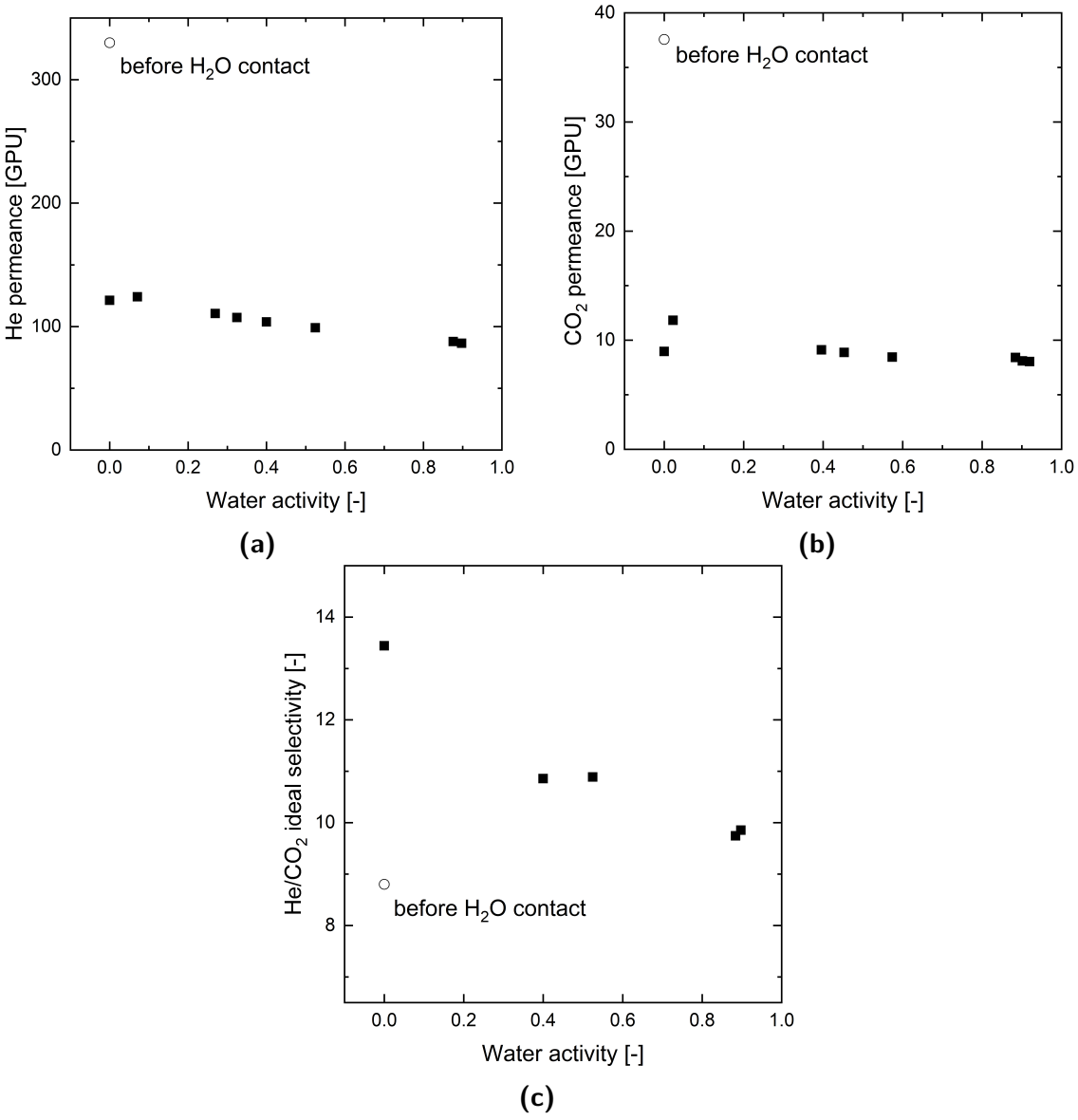


Figure 4.8.: He permeance (a), CO_2 permeance (b), and ideal He/CO_2 selectivity (c) in dependence of water activity in the feed gas stream of the gas mixture. Values of the membrane before contact with H_2O vapor are displayed with open symbols as reference.

At the same time, Figure 4.8c shows an increase in ideal selectivity for He to CO_2 after contact with water vapor. Starting at a value of 8.8, the selectivity

increases to 10 for high water activity and even reaches a value of more than 13 for dry gases after the organosilica membrane has been in contact with water vapor.
Various authors also reported a decreasing permeance when contacting (organo)silica membranes with water vapor [Gava1989]; [Gall1994]; [Lebo1995]; [De V1998]; [Duke2006]; [Cast2008]; [Song2016]. Gavalas, Megiris, and Nam and Gallaher and Liu attributed the permeance drop to moist air adsorbed in the pores and reversed this effect by heating above 600 °C [Gava1989]; [Gall1994]. Since the support membrane of this study is not stable in those conditions, only a temperature of 60 °C under vacuum was used but a reversal of the drop in permeance could not be achieved.
However, Leboda et al.; Duke et al.; Castricum et al. and Song et al. attribute the change in permeance to hydrothermal instability of the silica membrane. The membranes lack inherent microstructural stability and hence exposure to water leads to hydrolysis of siloxane groups on the surface. Thereby, the mobile groups coming from bigger pores condense in small pores which leads to pore closure. In the end, this effect leads to an increased permeance and decreased selectivity of the silica membranes. [Lebo1995]; [Duke2006]; [Cast2008]; [Song2016]
In contrast, the membrane in this work shows the opposite behavior compared to the latter and hence seems to not be affected by hydrolysis. This is also in agreement with the findings of Duke et al. There, organic methyl groups, which are also present in the studied organosilica membranes, led to a stabilization of the membrane. Comparable to the findings of this study, they still discovered a drop in permeance but observed a stable selectivity. [Duke2006]
Nevertheless, the possible presence of condensed water vapor in the studied organosilica membranes can not be ruled out completely. To get a better understanding of the aforementioned behavior, detailed investigations should be carried out following this work.

n summary, Figure 4.9 schematically shows all effects on permeance and selectivity induced by mixed gas compared to the pure gas results for the organosilica membrane. For permanent gases, this study did not see any mixed gas effects. In contrast, the condensable CO_2 leads to an increase in permeance and a selectivity

loss for mixed gases. Conversely, the addition of water vapor induces a significant drop in gas permeance together with increased selectivity.

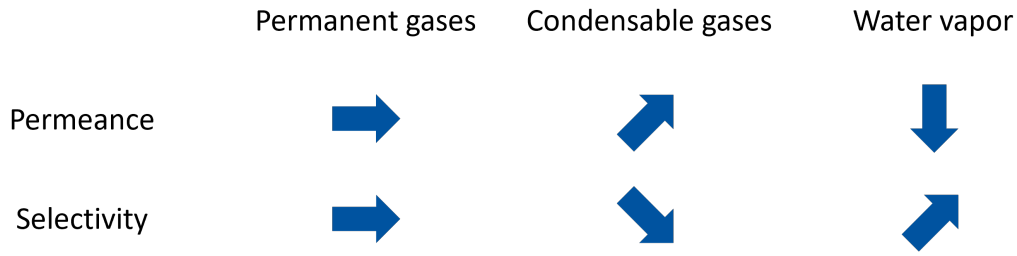


Figure 4.9.: Effect of mixed gas on the separation behavior of organosilica membranes

4.4. Conclusion

Organosilica membranes fabricated via PECVD have the potential to combine the advantages of silica and polymeric membranes. Thereby, they offer both high permeabilities and selectivities like silica membranes and low production costs compared to polymeric membranes. The presented in-depth investigation of a selected organosilica membrane with pure and mixed gas feeds at different temperatures reveals promising non-ideal permeation behavior.

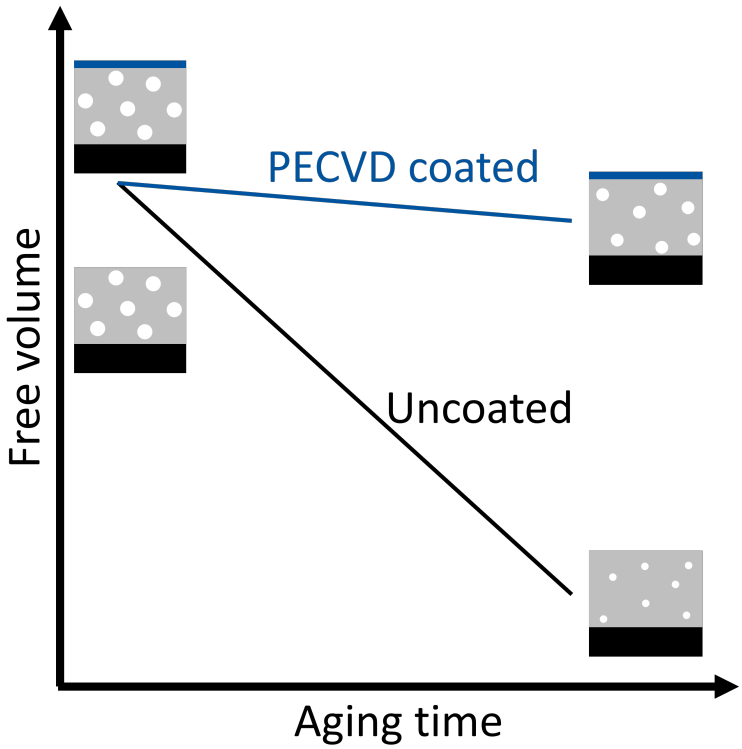
For pure gases, He and CO_2 permeance for the organosilica membrane are strongly temperature dependent. In contrast, N_2 and CH_4 permeances stay constant or even decrease slightly with increasing temperature. This leads to a strong increase in ideal selectivity with increasing temperature. The studied organosilica membrane, for example, shows a substantial increase in selectivity from α_{He/CH_4}= 9 at 0 °C to α_{He/CH_4}= 40 at 60 °C, accompanied by a He permeance of up to 300 GPU.

Furthermore, mixed gas permeation effects with equimolar mixtures of He/CH_4, He/CO_2 and CO_2/CH_4 were studied. For the combination of two permanent gases (He and CH_4), only minor changes in the permeance and a mixed gas selectivity equal to the ideal selectivity were observed. However, when mixing a permanent and condensable gas, the membrane exhibits a significantly decreased selectivity compared to ideal conditions, which is attributed to competitive sorption. The same phenomenon also seems to affect the CO_2/CH_4 selectivity. While the pure

gas experiments show an inversion of selectivity over temperature, this behavior was not apparent for mixed gas. A selectivity above 1 for CO_2/CH_4 occurs over the investigated temperature range of -20 to 60 °C.
Besides, water vapor induces a strong effect on the permeances of He and CO_2. A significant, irreversible drop in permeance appeared for both gases. But at the same time, the organosilica membrane shows an increase in the ideal He/CO_2 selectivity. The reason for this behavior might be water condensation in the organosilica membrane, but hydrolysis of siloxane groups in the membrane can be excluded.
All in all, the investigated organosilica membrane shows a promising mixed gas behavior. For the separation of helium or similar permanent gases with small kinetic diameters from other bigger gas molecules, this study identified a promising operational window at elevated temperatures.
Nevertheless, the selectivities and permeances at ambient conditions still need to be improved to outperform known membranes under those conditions. Hence, further research on the fabrication parameters of PECVD membranes is necessary. Here, especially a deeper understanding of the PECVD process is needed. The ability to fabricate coatings with narrower free volume size distributions and to adjust the free volume size would allow the fabrication of tailored selective layers for specific separation tasks by size sieving. In continuation of this work, the assessment of the interaction of water vapor and other easily condensable components like higher hydrocarbons with the organosilica membrane has to be studied in more detail to fully understand short and long-term effects on the membrane performance.

5. Physical aging mitigation by plasma-polymerized organosilica layers

Parts of this chapter have been published as:
Jens Rubner, Leonie Stellmann, Ann-Kathrin Mertens, Maik Tepper, Hannah Roth, Lara Kleines, Rainer Dahlmann, and Matthias Wessling *Organosilica coating layer prevents aging of a polymer with intrinsic microporosity*, Plasma processes and polymers, 2022 DOI: 10.1002/ppap.202200016



5.1. Introduction

Glassy polymers are used in widespread applications such as amorphous pharmaceuticals [Lee1984]; [Hanc1997]; [Mazi2009], organic semiconductors [Müll2015]; [Shib2015]; [Snyd2018] , corrosion-protective coatings [Mera2017]; [Hill2020] and membrane technology [Gome2005]; [Sand2013]; [Loge2020]. In contrast to rubbery polymers, they are in a thermodynamically nonequilibrium state. Therefore, a slow relaxation of the glassy polymer towards its equilibrium state takes place which is called physical aging [Kova1964]; [Stru1976]. During this process, the polymer partly loses its free volume over time and thereby changes its mechanical, physical and transport properties.[Hill2020]

Especially in membrane applications, this is an unwanted behavior. Since the amount of free volume directly relates to the polymer's permeability, the permeance of a glassy polymer membrane strongly decreases over time. At the same time, the size distribution of the free volumes changes, leading to an increase in selectivity of the membrane.[Huan2004]

Because a time dependent membrane performance (i.e. permeance and selectivity) is unacceptable for industrial applications, many promising polymers are still not industrially used. For this reason, numerous recent studies deal with the mitigation of physical aging. Low et al. and Ahmad, Castro-Muñoz, and Budd name a variety of presented approaches in their articles. Thereof, mainly the design of polymers (i.e. backbone or structure modification), postmodification of membranes and blending polymers with nanofillers are investigated in literature [Low2018]; [Ahma2020]. Although some of the approaches show a significant retardation of physical aging, their application fails due to lacking upscalability [Smit2020]. In many cases, the synthesis of the polymer is complex or the yield is low, making them very costly. Also, they are often not applicable for ultra-thin films used in industry since their filler particle size is too big.

In physical aging studies, up to now, only little attention has been drawn to the connection between thickness dependence and free film surface. Huang and Paul and Rowe, Freeman, and Paul reported the dependence of the aging rate on the polymer film thickness, i.e. thinner films age faster[Huan2007]; [Rowe2009a]. They attribute this to the increased surface area to volume ratio leading to a higher

polymer chain mobility because of better access to the film surface [Huan2007]. At the same time, the shorter way of the free volume elements to diffuse to the surface affects the dynamics [Huan2006a]. Moreover, positron annihilation lifetime spectroscopy (PALS) measurements of polysulfone showed a decrease in free volume element size at the film surface compared to the bulk polymer although the number of elements stayed the same. This indicates a faster densification at/near the surface of the polymer due to a higher chain mobility[Rowe2009b]. Contrarily, PALS results of polycarbonate showed a decrease in the number of free volume elements at the film surface but no size decrease, which is explained by the diffusion of free volume to the surface [Cang2003]; [Cang2004]. Hence, the exact phenomena of physical aging are still not fully understood.

Lately, it has also been suggested that the presence of a free surface with faster dynamics promotes hole diffusion in thin films. It has been claimed that the free volume release in thin films and thus, the confined polymer dynamics can be modulated by changing the free surface properties of the films. [Zha2021] All in all, the cited studies show a clear coherence between physical aging and polymer chain mobility at the film surface. Plasma-enhanced chemical vapor deposition (PECVD) is a scalable process and has the ability to fabricate tailored coatings with regard to mechanical and chemical structure as well as low coating thicknesses in the nanometer range. Among others, hexamethyldisiloxane (HMDSO) is a commonly used starting substance for the production of durable coatings by plasma polymerization. Multiple studies report the use of plasmapolymeric coatings in the field of gas separation membranes. [Roua2017]; [Lo2010]; [Li1999]; [Kafr2010]; [Cous2014]; [Naga2015]; [Klei2021]. Coatings are typically deposited on inorganic [Kafr2009]; [Tsur2011]; [Naga2013]; [Haac2015] or on organic substrate membranes [Li1999]; [Roua1999]; [Roua2002]; [Bosc2003]; [Ngam2013]; [Char2016]; [Wang2017]; [Klei2020]. Up to now, the influence of PECVD coatings on the aging behavior of the underlying polymer has not been studied.

Ellipsometry is a non-destructive optical technique allowing precise and accurate analysis of optical properties of thin film systems. In recent years, it has been increasingly used in the field of thin polymer film characterization. Especially, the interaction between polymer thin films and varying ambient conditions attracted the attention of researchers.[Ogie2015] Different studies show the capability of

ellipsometry to precisely monitor the changes in thickness and refractive index (i.e. swelling behavior) of various polymers in liquids[Kapp2019]; [Ogie2013]; [Hill2003], vapors [Ogie2017a]; [Secr2011] and gases [Raai2015]; [Horn2012]; [Sira2001]; [Ogie2020]. Furthermore, it enables the observation of dynamic polymer behavior like relaxation phenomena [Ogie2014b]; [Lópe2011]; [Wind2003] or glass transition [Ogie2014a]. Huang et al. even showed the capability to observe long term changes in the polymer caused by physical aging [Huan2006a] and quantified those by connecting them to the free volume amount [Huan2006b].

This study proposes to mitigate physical aging of poly(1-trimethylsilyl-1-propyne) (PTMSP) thin films by applying thin top layer coatings. By binding to the PTMSP polymer chains, I hypothesize that the coating restricts the movement of the polymer chains at the surface and thereby suppresses the loss of free volume. The scalable PECVD process creates a thin top layer coating. Two different coating layers cover sub µm PTMSP layers.

Spectroscopic ellipsometry with its unique capabilities tracks the physical aging behavior of the films. The chemical composition and the thickness of the top layer coating shows to have a significant influence on the physical aging of PTMSP thin films. Such a scalable process for the mitigation of polymer ageing is highly desired in membrane and coating applications.

5.2. Experimental

PTMSP film preparation

Poly[1-(trimethylsilyl)-1-propyne] (PTMSP) was purchased from abcr GmbH and toluene (purity $> 99.9\%$ VWR International S.A.S.) is used as solvent. The polymer solution contains 1.35 wt.% PTMSP in toluene and is stirred for at least 24 hours. Afterwards, the solutions are filtered through a 1 µm PTFE syringe filter to avoid any particles in the solution. A spin coater creates thin films (WS-650MZ-23NPP/LITE Laurell Technologies Corporation). Silicon wafers (MicroChemicals GmbH) with a 500 nm oxide surface layer are used as substrate. Pieces of 2×2 cm are placed on the spin coater and coated with 300 µL of the polymer solution at 2500 rpm for 45 s. Afterwards, the samples dry at ambient conditions for at

least 12 hours.

Rejuvenation

All samples are rejuvenated before usage to ensure a consistent high free volume state for each experimental series. For this, the samples are submerged in methanol (Sigma-Aldrich) with a purity of $> 99.5\%$ for 10 minutes. Afterwards, they are transferred onto a heating plate ($165°C$) for two minutes to fully evaporate the methanol and subsequently quenched to room temperature.

PECVD coating

Coating deposition is conducted in the low-pressure plasma reactor (LAMPS, Large Area Microwave Plasma System) introduced in Section 2.2.5. This study uses hexamethyldisiloxane (HMDSO) as monomer and oxygen as auxiliary reaction gas for the deposition of the plasma polymer layers. HMDSO with a purity of $> 98\%$ was purchased from Sigma-Aldrich. Two different parameter sets create two distinct coating types. In particular, films are created with and without oxygen as additional reactive gas resulting in oxidized (SiOx) and organic-like (SiOCH) layers, respectively. The exact coating parameters are listed in Table 5.1. The thickness of the coatings measured by ellipsometry is tuned by adjusting the coating time. For the investigated thickness range, the relationship between thickness and coating time is assumed to be linear. All samples with PTMSP films were rejuvenated directly before the coating procedure. In each coating experiment, a wafer with PTMSP film and a reference wafer without PTMSP film are coated at the same time next to each other in the reaction chamber.

Table 5.1.: PECVD coating parameters.

Coating type	HMDSO flow [sccm]	O_2 flow [sccm]	Pulse on/off [ms]	Microwave peak-power [kW]	Coating time [s]	Approx. thickness [nm]
SiOx	20	200	5/45	4	10	10
SiOx	20	200	5/45	4	30	30
SiOCH	100	0	2/45	2	80	25
SiOCH	100	0	2/45	2	160	50

XPS measurements

The XPS measurements are carried out in an Ultra AxisTM spectrometer (Kratos Analytical, Manchester,UK). The samples are irradiated with mono energetic Al Kα1,1 radiation (1486.6 eV), and the spectra are taken at a power of 144 W (12 kV$\times$12 mA). The aliphatic carbon at a binding energy of 285 eV (C 1s photo line) is used to determine the charging. XPS spectra are processed with dedicated software, and atomic concentrations of the elements are quantified by integration of the relevant photoelectron peaks.

FTIR measurements

Structural chemical properties are investigated by Fourier transform infrared spectrometry. The used instrument is a Nexus 870 spectrometer from Thermo Nicolet (now Thermo Fisher Scientific). The infrared spectrometer is operated in attenuated total reflection (ATR) mode with a diamond crystal with a fixed angle of 42° or 45° and potassium bromide beam splitter. The PECVD coatings were deposited on gold sputtered silicon wafers.

SEM images

Scanning electron microscopy (SEM) is performed with a Hitachi SU-9000 scanning electron microscope. The acceleration voltage is 5.0 kV. The PECVD coatings are measured on a PTMSP film on top of a silicon wafer. The PTMSP film is spincoated on the wafer with a solution of 0.4 wt.% PTMSP in toluene. This leads to a polymer film of about 40 nm and therefore an increased SEM image quality. The PECVD coating is deposited together with the samples for the ellipsometric study to guarantee the same fabrication conditions.

Ellipsometry measurements

For all ellipsometric measurements, a Spectroscopic Ellipsometer (RC2 from J.A. Woollam Co. Inc., Lincoln, NE, USA) with a spot size of 2 mm is used. All measurements are performed at incident angles of 65°, 70° and 75° over a wavelength

range of 192 to 1000 nm with a spectral resolution of 2 nm. The optical modeling is conducted with the commercial software package CompleteEASE 6.46 (J.A. Woollam Co.).
Silicon wafer pieces with a 500 nm thick thermally grown silicon oxide layer (Microchemicals, Germany) are used to enhance the interference effect of the measurements. This improves the accuracy of the data modeling especially for the thin films used here and has been thoroughly described elsewhere [Ogie2017b]; [Ogie2018]; [Ogie2019].

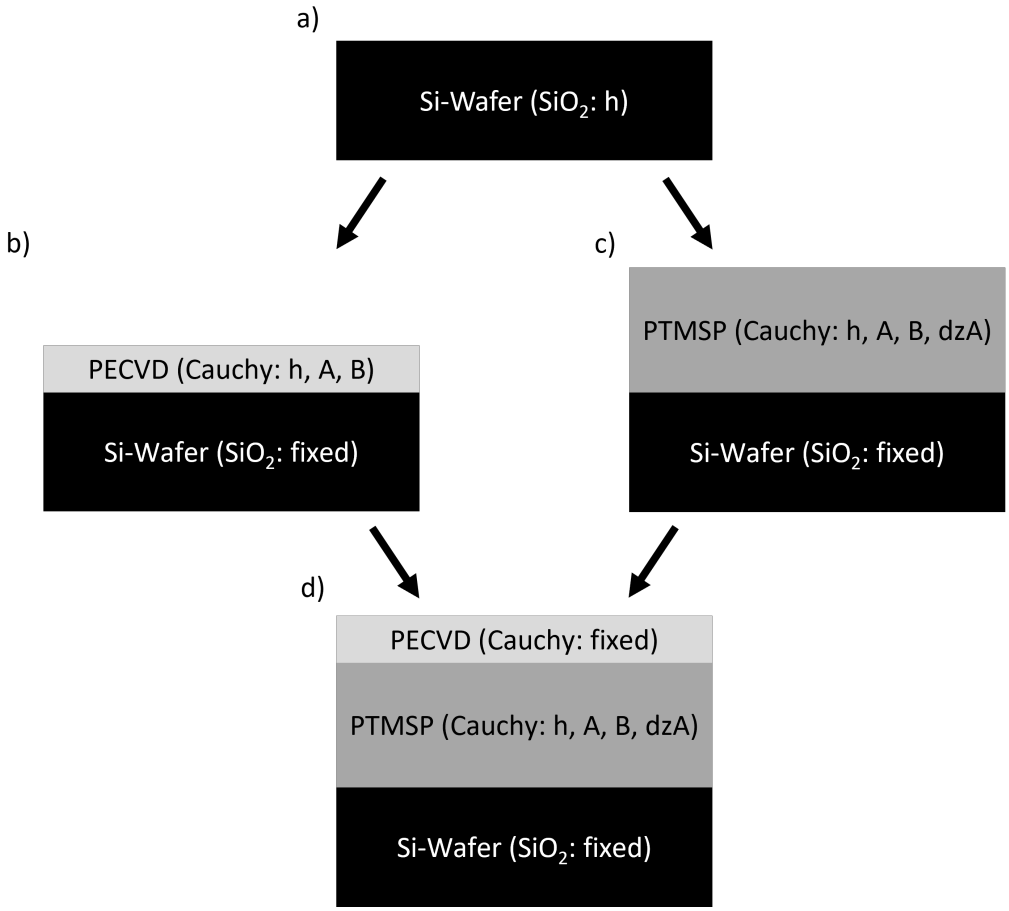


Figure 5.1.: Scheme of the prepared samples and their layer models for ellipsometry. Fitted parameters of the layers are listed in brackets. Parameter h stands for the height and A, B and dzA for the Cauchy parameters of the respective layer.

The stepwise ellipsometric modeling approach is shown schematically in Figure 5.1. All silicon wafer samples are measured before any coating to gain the exact silicon oxide thicknesses h (see Figure 5.1 a)), which was fixed for the following

measurements. Optical properties of the silicon oxide and underlying silicon layer rely on literature values [Herz1998]. For the subsequent PTMSP layer (see Figure 5.1 c)), a Cauchy-type parametrization ($n(\lambda) = A + B/\lambda^2$) in a wavelength range of 300-1000 nm is used to calculate its refractive index n. The PECVD top layer was modeled using a Cauchy-type parametrization ($n(\lambda) = A + B/\lambda^2$). To avoid inaccuries due to thickness fluctuations of the underlying PTMSP layer, the thickness and the parameters A and B of the PECVD coating were determined from the reference wafer without polymer coating (see Figure 5.1 b)).
For the ellipsometric study of the PTMSP physical aging, the parameters of the PECVD coating are kept constant over time since they did not show any significant time dependent behavior on the reference wafer (see section 5.3.2). Furthermore, the influence of the refractive index of the thin PECVD coating layer compared to the much thicker PTMSP layer is only minor. Hence, during aging only the PTMSP-layer parameters A, B and the thickness are fitted (see Figure 5.1 d)). All measurements besides the first one after the PECVD coating were conducted at three different sample spots.

5.3. Results and discussion

First, this study presents the analysis of the chemical composition of the two different PECVD coatings. Subsequently, it discusses the ellipsometric measurements of the PTMSP films with and without PECVD coating in depth and evaluates the impact of the coatings on the physical aging behavior.

5.3.1. Chemical analysis

The elemental composition of the two different PECVD coating types is determined with XPS measurements. The penetration depth of the XPS measurements is around 10 nm. Table 5.2 displays the elemental composition of coatings significantly thicker than 10 nm in order to avoid influences of the underlying layer.

As expected, the SiOx layer shows a high O/Si (2.4) and a low C/O (0.2) ratio. Comparable values for high oxygen to HMDSO ratios in the PECVD processing

Table 5.2.: Elemental composition in atomic percentage (at.%), resulting composition and atomic ratios of the PECVD coatings by XPS.

Coating	Si2p	O1s	C1s	Composition	O/Si	C/O	C/Si
SiOx	26.3	60.8	12.8	$SiO_{2.4}C_{0.5}$	2.4	0.2	0.5
SiOCH	24.6	24.4	50.9	$SiO_{1.0}C_{2.1}$	1.0	2.1	2.1

gas are reported in literature [Alex1997]; [Inag1999]; [Bahr2013].
In contrast, the SiOCH layer shows a significantly lower oxygen content, since no oxygen is present in the processing gas. They also display a higher ratio of C/Si (2.1), the same C/Si ratio as in the pure precursor HMDSO (2.1).

Figure 5.2 displays the FTIR spectra from 1300 to 700 cm^{-1} of the two PECVD coatings for qualitative assessment of the produced layers. The main peak at 1200 - 1050 cm^{-1} is normalized to a height of 1 to allow comparability. The characteristic positions of the functional groups of organosilicon layers listed in Table 5.3 are marked in Figure 5.2 for easier assessment.

5

The main peak correlates with the Si-O-Si vibration mode for both layers and shifts towards smaller wavenumbers for the SiOCH layer. On the one hand, this can be caused by the Si-O-Si bond changing from a cage structure to a network structure [Gril2003]. On the other hand, the shift to smaller wavenumbers can be explained by neighboring group effects due to the bound methyl groups.[Klei2022] Besides the shift of the main peak, Figure 5.2 shows strong differences in peaks representing methyl groups. Whereas the SiOCH spectrum shows clear peaks at the wavenumbers 1263, 890, 850 and 800 cm^{-1}, the SiOx spectrum shows only a minor peak at about 800 cm^{-1}. Together with the high C content measured via XPS, those peaks display the significantly higher methyl group content of the SiOCH layer. Hence, the PECVD coatings represent two structurally differing coatings: SiOx resembles a ceramic-like coating, while SiOCH forms a polymer-like top layer.

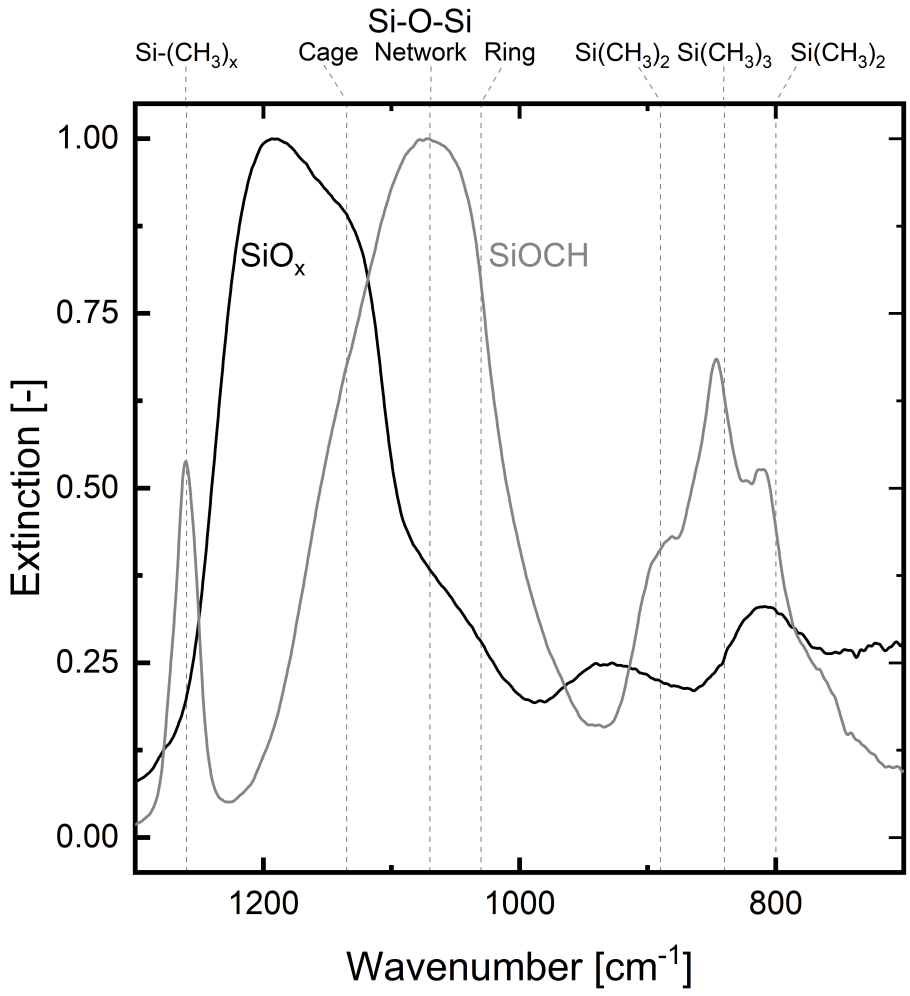


Figure 5.2.: IR spectra from 1300 to 700 cm^{-1} of the SiOx and SiOCH PECVD coatings.

Table 5.3.: Characteristic location of functional groups of organosilicon layers in the FT-IR spectrum (s=stretching, b=bending, r=rocking; anti=antisymmetric, sym= symmetric) [Gril2003]; [Lenz2001]; [Mota1995]

Vibration mode	Wavenumber [cm-1]
s CH_x	2875-2970
s_{sym} $Si(CH_3)_x$	1263
s_{anti} Si-O-Si (cage structure)	1135
s_{anti} Si-O-Si (network structure)	1072
s_{anti} Si-O-Si (suboxide structure)	1010-1035
s_{sym} Si-(OH)	930-950
r_{sym} Si-$(CH_3)_2$ b H-Si-O s Si-C	890
b Si-$(CH_3)_3$ r Si-CH_3	840-850
r Si-$(CH_3)_2$ b Si-O-Si s Si-C	800
b Si-CH_2	765

Figure 5.3 shows SEM images of a 6.3 nm SiOx and a 26 nm SiOCH layer on a PTMSP coated silicon wafer. All images show a smooth and homogeneous surface.

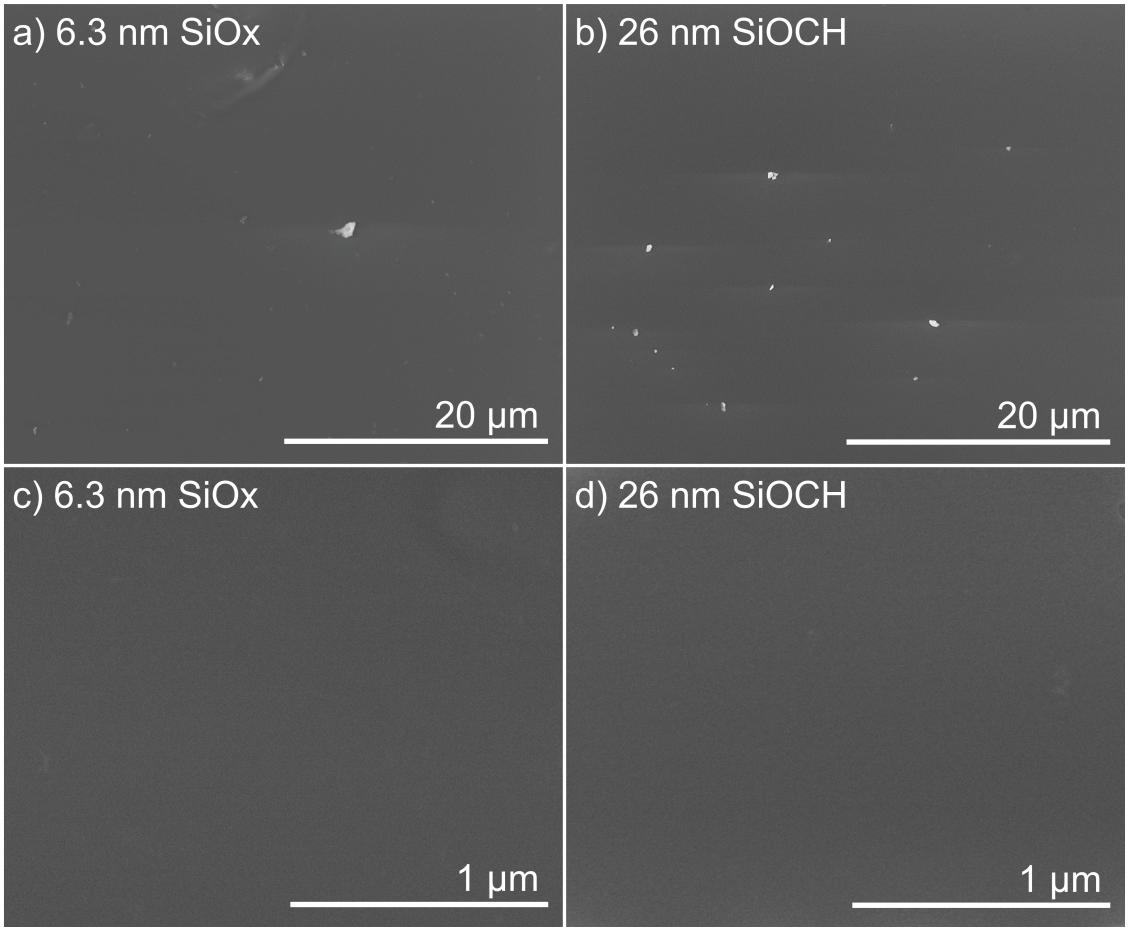


Figure 5.3.: SEM images of a 6.3 nm SiOx and a 26 nm SiOCH layer on top of a PTMSP coated silicon wafer with 2.5k (a) and b)) and 20k (c)and d)) magnification.

5.3.2. Physical aging monitoring via ellipsometric analysis

The subsequent sections present the results of the ellipsometric measurements for samples coated with PTMSP and different PECVD coatings. The sections show refractive index progressions without and with rejuvenation after the PECVD coating, which is regaining the original high free volume amount of PTMSP. The model approach shown in Figure 5.1 gains the refractive index of the PTMSP layers.

Optically, the PTMSP layer is a mixture of two parts: polymer chains and free vol-

ume. The refractive indices of polymer chains ($n_{polymer\ chain} \gg 1.0$) differ strongly from the refractive index of free volume ($n_{void} = 1.0$). Since free volume is lost during physical aging, a shift in composition towards a higher amount of polymer chains occurs. Hence, the refractive index of the polymer layer increases in a well measurable manner[Huan2006a]. The resulting refractive index progressions are examined in the following sections.

Physical aging of PECVD coatings

Figure 5.4 displays the refractive index progression over time. A 51 nm SiOCH and a 37 nm SiOx layer were deposited on silicon wafer. After the deposition, the samples were tracked by ellipsometry. Both refractive indices show only minor refractive index changes over time. Hence, a constant refractive index can be assumed for the PECVD layer in the multi layer model used in this study and will not lead to significant changes in PTMSP's optical properties.

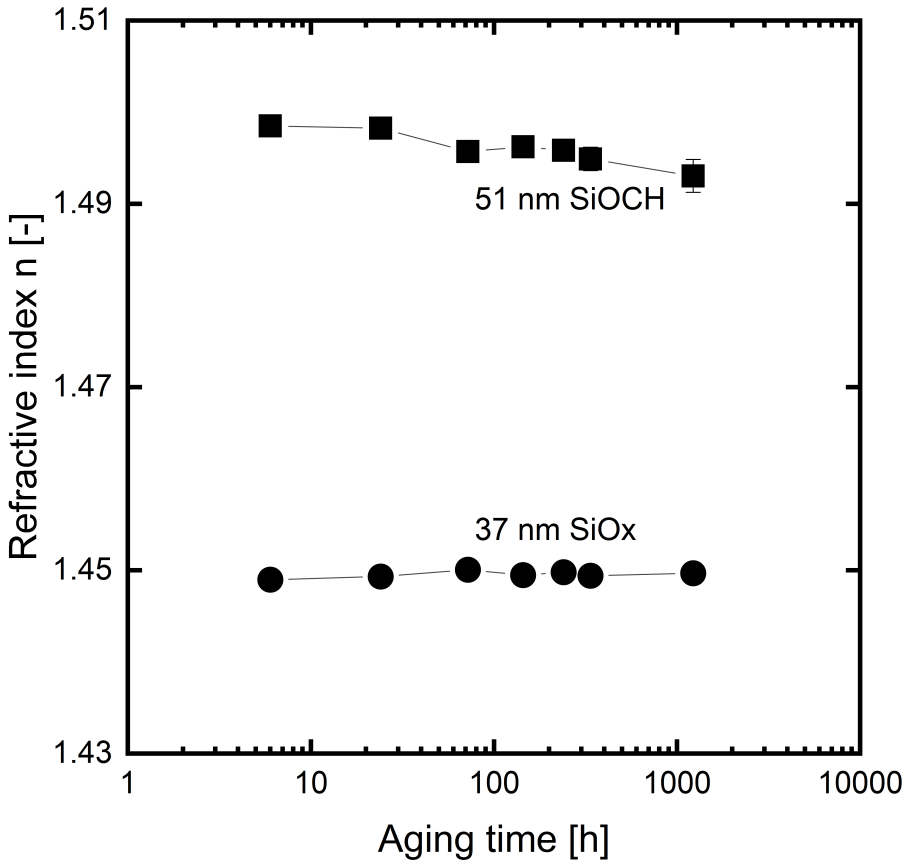


Figure 5.4.: Refractive index n over aging time for of a 51 nm SiOCH and a 37 nm SiOX layer after deposition by PECVD.

PECVD coated PTMSP films

Figure 5.5 shows the refractive index (n) progression for the PTMSP layer of an uncoated reference sample and four samples with different coating thicknesses of around 200 nm. All samples show an increase of refractive index over time. After 1000 hours, they all reach a refractive index value of more than 1.52. Since a constant value means no more loss of free volume, as seen for the uncoated sample, and all samples show comparable refractive indices for PTMSP, this state can be attributed to a quasi fully aged PTMSP layer. Hence, the uncoated, 210 nm thick PTMSP layer is fully aged after merely 66 hours.

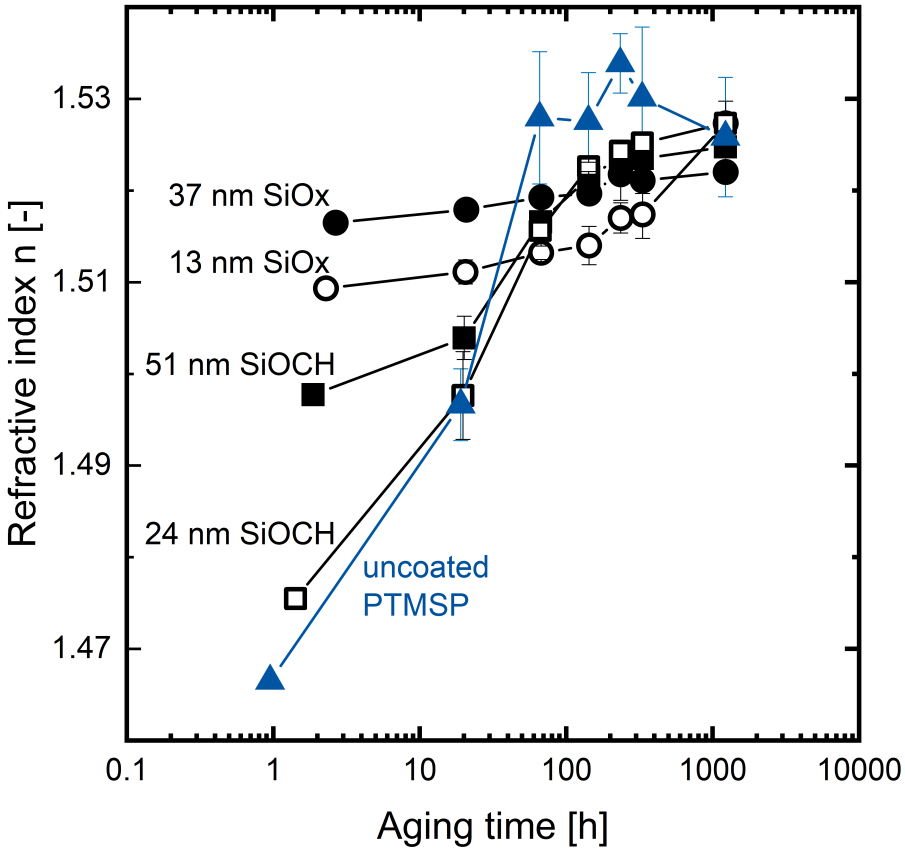


Figure 5.5.: Refractive index n of the PTMSP layer over aging time without coating and with 24 and 51 nm SiOCH and 13 and 37 nm of SiOx coating via PECVD without rejuvenation after PECVD coating.

Comparing the absolute values of the refractive indices (measurements at t $\approx 1\ h$) of the PTMSP samples after the PECVD coating, they tremendously deviate from each other. They were all rejuvenated before the coating and I expected

them to have refractive indices in the same range as the uncoated PTMSP sample ($n(t = 1\ h) = 1.467$).
While the thin SiOCH coating ($n(t = 1.4\ h) = 1.476$) only shows a slightly higher refractive index than the uncoated PTMSP reference, the PTMSP layer coated with a 37 nm SiOx layer nearly displays a fully aged PTMSP state directly after coating ($n(t = 2.7\ h) = 1.517$).
For both, the SiOx and the SiOCH layer, this study shows an increase in refractive index (loss of free volume) with increased coating time. Since all samples were treated the same way, effects of the heat treatment during rejuvenation or the time in vacuum during the plasma coating can be excluded.In contrast, all samples are exposed to different energy input during the plasma coating. Therefore, the initial refractive index differences are clearly attributed to the energy input by the plasma. Furthermore, a combination of increased microwave peak-power and pulse-on time (compare SiOx to SiOCH) leads to an increase in the refractive index. Concluding, glassy polymers can be aged intentionally using high energy plasmas for a certain time. Nevertheless, more experiments have to be carried out to find the correlation between plasma parameters and loss of free volume in polymers.

Comparing the gradients of the refractive index progressions, the samples differ significantly from each other. Figure 5.6 displays the linear gradient fits of the refractive index n of the PTMSP layer over aging time without and with the different coatings. The gradients of the slopes in this case represent the rate of physical aging. The biggest gradient and therefore fastest aging can be seen for the uncoated PTMSP with a gradient of $0.0315\ \mathrm{h}^{-1}$.
In comparison, the SiOCH coatings show a small increase in time until they are fully aged (approx. after 100 h). Nevertheless, the gradients of the 24 nm and 51 nm SiOCH layer ($0.019\ \mathrm{h}^{-1}$ and $0.011\ \mathrm{h}^{-1}$) decreased by a factor of 1.7 and 2.9 compared to the uncoated sample, respectively. Hence, a slower physical aging is achieved, especially for the thicker SiOCH coating. Nevertheless, this retarded physical aging can not only be attributed to the top layer coating, but could also be caused by the increased layer thickness alone [Huan2007]. At the same time, Rauscher et al. studied the effect of an adjacent rubbery layer on the

physical aging of glassy polystyrene. They used the rubbery polymer as substrate and did not see any effect on the aging rate of the glassy polymer[Raus2013]. In comparison, the studied SiOCH top layer coating, which covers the PTMSP free surface, alters the aging rate of the polymer at least to a measurable amount.

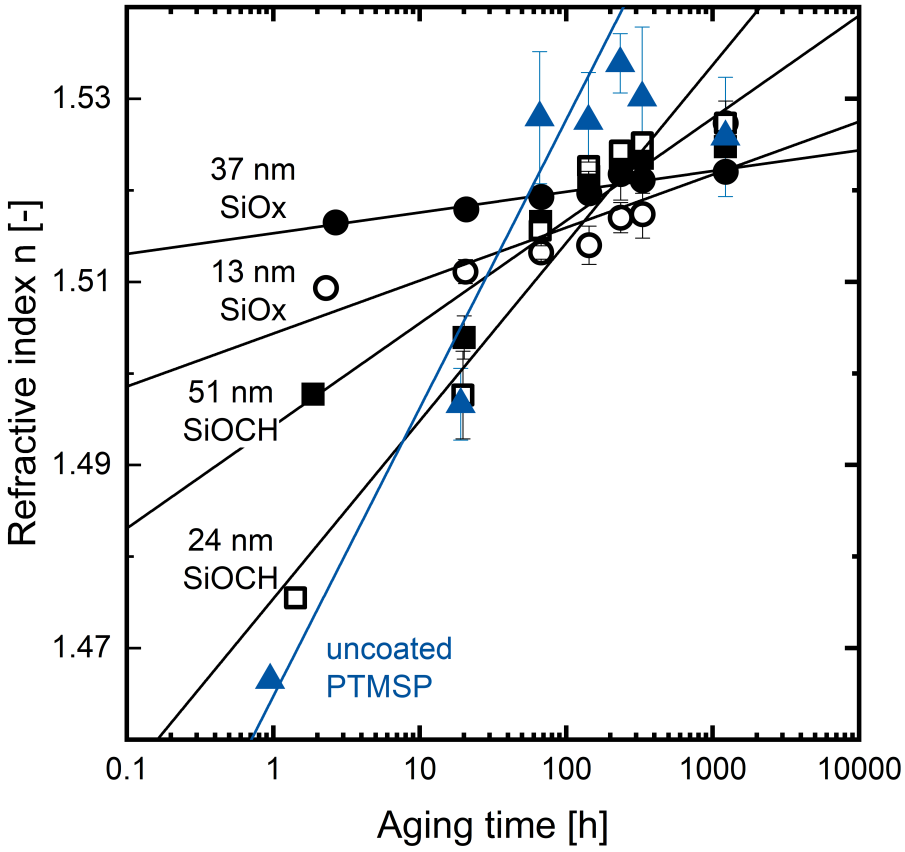


Figure 5.6.: Refractive index n of the PTMSP layer over aging time without coating and with 24 and 51 nm SiOCH and 13 and 37 nm of SiOx coating via PECVD without rejuvenation after PECVD coating. Lines represent the best linear fits of the increasing refractive index progressions.

Regarding the SiOx layers, the reduction of the refractive index gradient is much more pronounced. For the thin SiOx layer, it takes about 1000 h (42 days) to reach a refractive index of more than 1.52. The gradient is reduced to $0.0058\ \mathrm{h}^{-1}$, which is less than 18% of the original PTMSP value. The thicker, 37 nm thick SiOx coating even outperforms this reduction with a decreased gradient of $0.0023\ \mathrm{h}^{-1}$. For this sample, aging is 14 times slower than the uncoated reference sample. Nevertheless, as stated before, both coatings have already an elevated refractive index after the PECVD coating. This leads to a reduced driving force for phys-

ical aging. Hence, both, the coating layer and the different starting points, can attribute to the refractive index gradient reduction and are investigated in more detail in the next section.
All in all, the different coating types (SiOx and SiOCH) show strongly differing refractive index progressions. Roth et al. reported a similar behavior for the glass transition temperature of ultra-thin polystyrene and poly(2-vinylpyridine) layers closely related to physical aging [Roth2007]. Depending on the adjacent layer and the resulting attractive interactions, they observed differing influences on the glass transition temperature. Figure 5.5 as well shows a differing impact of the two fabricated PECVD coating types on the refractive index progression.

PECVD coated, rejuvenated PTMSP films

Since the refractive indices for PTMSP with the most promising coatings (SiOx) were nearly at a fully aged state directly after the PECVD process, this section investigates the effect of a rejuvenation of the PTMSP layer after plasma coating. First, this study investigates the influence of the time on the heating plate on the aging behavior of the PTMSP films. Figure 5.7 shows the refractive index progression over aging time of a PTMSP sample without (blue) and with a 8.3 nm SiOx layer top coating. The samples were soaked in Methanol for 10 minutes and afterwards placed on a heating plate at 165 °C for different amounts of time as stated next to the data points. The blue reference displays the same progression as shown in figure 5.5 and was heat treated for 2 minutes. Every data point is the average of three different measurement spots.

Directly after the heat treatment, the refractive indices of the coated samples differ strongly from each other. The refractive index of the 20 seconds treated sample is only 1.473 and the lowest of the four. This can be attributed to residual Methanol (n=1.33) in the PTMSP matrix. The other three samples range at about 1.5. Besides the low index of the 20 second sample, the results do not show a trend of increasing refractive index by increased heat treatment duration for the other samples.
Taking a look at the refractive index progression, the gradients of all SiOx coated

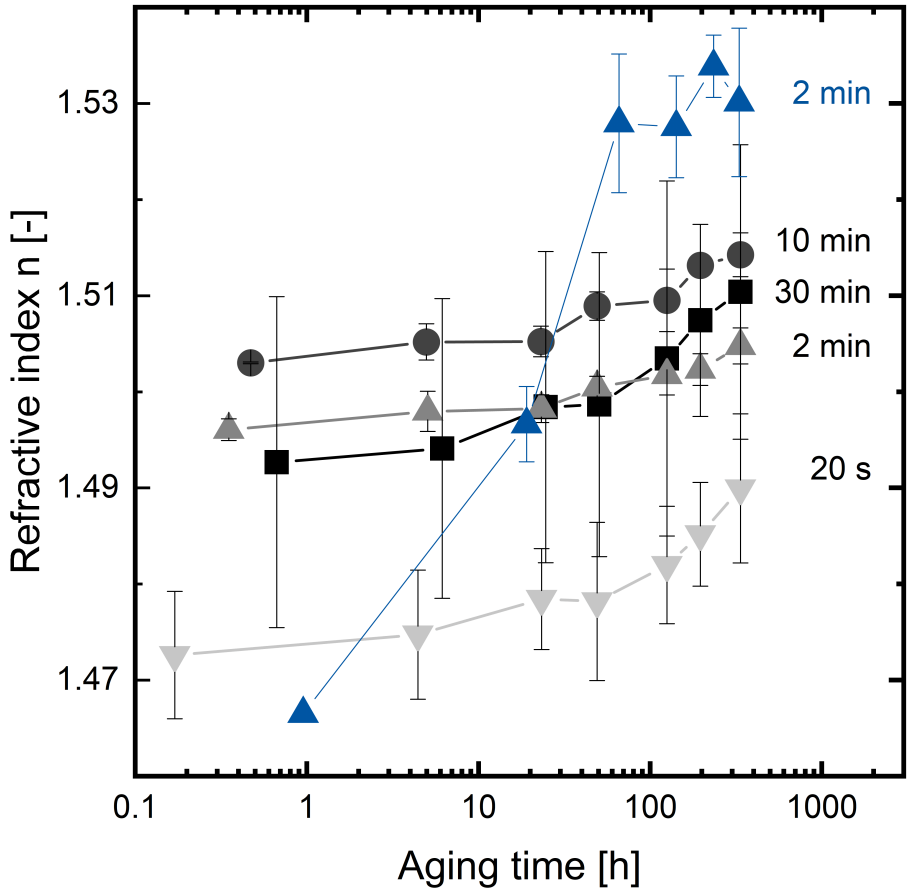


Figure 5.7.: Refractive index over aging time after rejuvenation for a PTMSP sample without coating (blue), and samples with PTMSP and a 8.3 nm SiOx coating layer. After 10 minutes of Methanol soaking, the samples were placed on the heating plate (165°C) for different amounts of time as stated next to the data points.

samples are in the same range. Nevertheless, the 20 second and 30 minute sample show a slightly increasing gradient over time whereas the gradients of the two other samples are nearly linear in the logarithmic plot. All in all, besides the strong deviation in refractive index of the 20 seconds treated sample, the other samples show a comparable physical aging behavior. Although this study can not prove the absence of any residual methanol in the PTMSP matrix, the results in Figure 5.7 show a clear difference in the refractive index progression between the uncoated and SiOx coated samples. Based on these results, a treatment time of 2 minutes was chosen for the investigations carried out in this study.

Besides the heat treatment, this study also investigates the swelling behavior of PTMSP in Methanol during rejuvenation. Therefore, experiments involving

methanol were carried out in a trapezoidal sample cell. It consists of quartz glass with windows angled perpendicular to the probing light. The cell enabled measurements with an incident angle of 65°. The window Δ offsets introduced by the quartz glass and the angle offset, resulting from an imperfect cell symmetry, were corrected by the software. The temperature for the swelling experiments was held constant at $23 \pm 1°C$. The ambient refractive index of methanol was taken from Kozma, Krok, and Riedle [Kozm2005]. Further details on the setup can be found elsewhere. [Ogie2018].
Figure 5.8 shows the thickness (filled circles) and refractive index (open circles) of a PTMSP layer coated with a 30 nm SiOx layer. The first data point is representing the PTMSP film in the dry state.

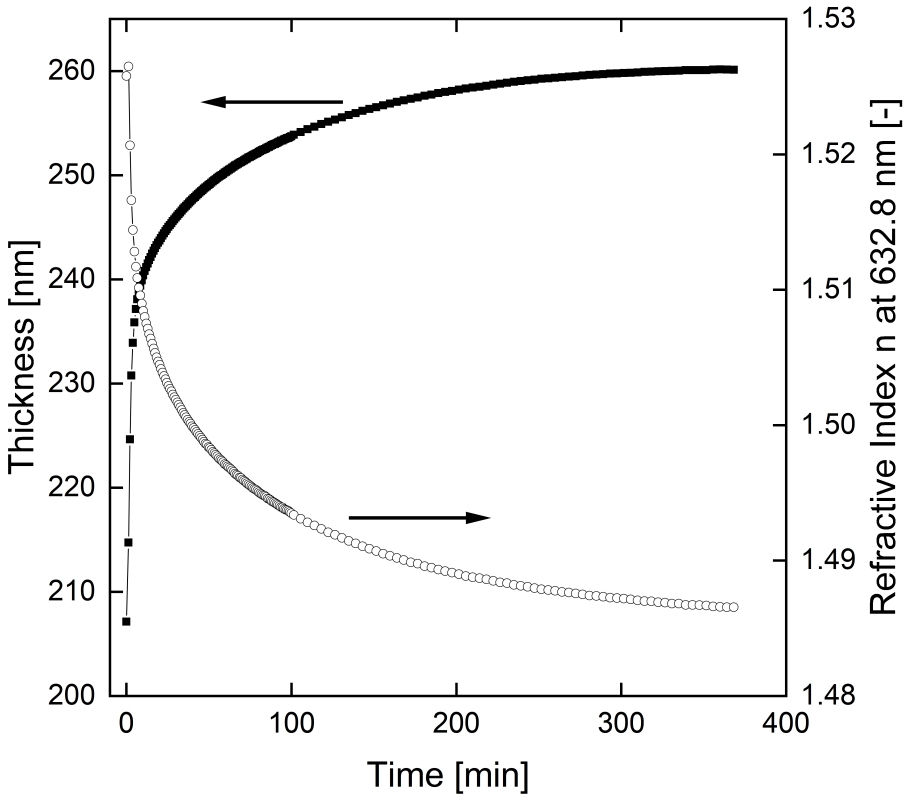


Figure 5.8.: Thickness and refractive index progression of a PTMSP layer coated with a 30 nm SiOx layer immersed in Methanol. The values for t=0 are measured in a dry state.

After immersion of the PTMSP film in methanol a rather fast swelling can be seen for the first 10 minutes. Nevertheless, it takes about 6 hours for this film to reach a quasi-equilibrium swelling state in methanol. In comparison, an

uncoated PTMSP film swells instantaneously, making it too fast to measure with the present setup.
Table 5.4 shows the thicknesses and refractive indices of the uncoated and organo-silica-coated PTMSP layer in dry and wet quasi-equilibrium state. The values of the swollen samples are averaged over a period of 10 minutes. The swelling degree shows the thickness increase of the samples due to immersion in methanol.

Table 5.4.: Thickness, refractive index and swelling degree of PTMSP in dry state and after immersion quasi-equilibrated in methanol.

Coating	Thickness (dry) [nm]	Refractive index (dry) [-]	Thickness (wet) [nm]	Refractive index (wet) [-]	Swelling degree (dry/wet) [%]
Uncoated PTMSP	245.48	1.529	347.08	1.45	41.4
SiOx coated PTMSP	207.13	1.526	260.15	1.4866	25.6

Finally, figure 5.9 shows the refractive index progression of rejuvenated PTMSP samples with and without SiOx coating. Compared to Figure 5.5, the refractive indices of the rejuvenated, SiOx coated PTMSP films are drastically lower. Nevertheless, they still do not reach the initial value of the uncoated PTMSP.

The reason for not reaching as low values as the uncoated PTMSP layer might be due to insufficient rejuvenation time in methanol for the coated polymer. As previously discussed, uncoated PTMSP nearly swells instantaneously close to its equilibrium state, whereas a much slower swelling behavior was detected for the SiOx coated PTMSP. This is either caused by the additional diffusion barrier of the PECVD coating for methanol and/or decreased polymer chain mobility of the PTMSP caused by the double-sided confinement effect.
Besides the swelling rate, also the swelling degree, which is the ratio of the thickness of the swollen compared to the unswollen sample, differs for the samples. Whereas the uncoated PTMSP immediately swells by 41 %, the SiOx coated sample only reaches 25 % after 6 hours (see Table 5.4). Since the swollen thicknesses are taken from quasi-equilibrium states, the diffusion barrier behavior of the PECVD coating does not play an important role in this case. The difference in swelling degree rather emphasizes the effect of the decreased chain mobility for

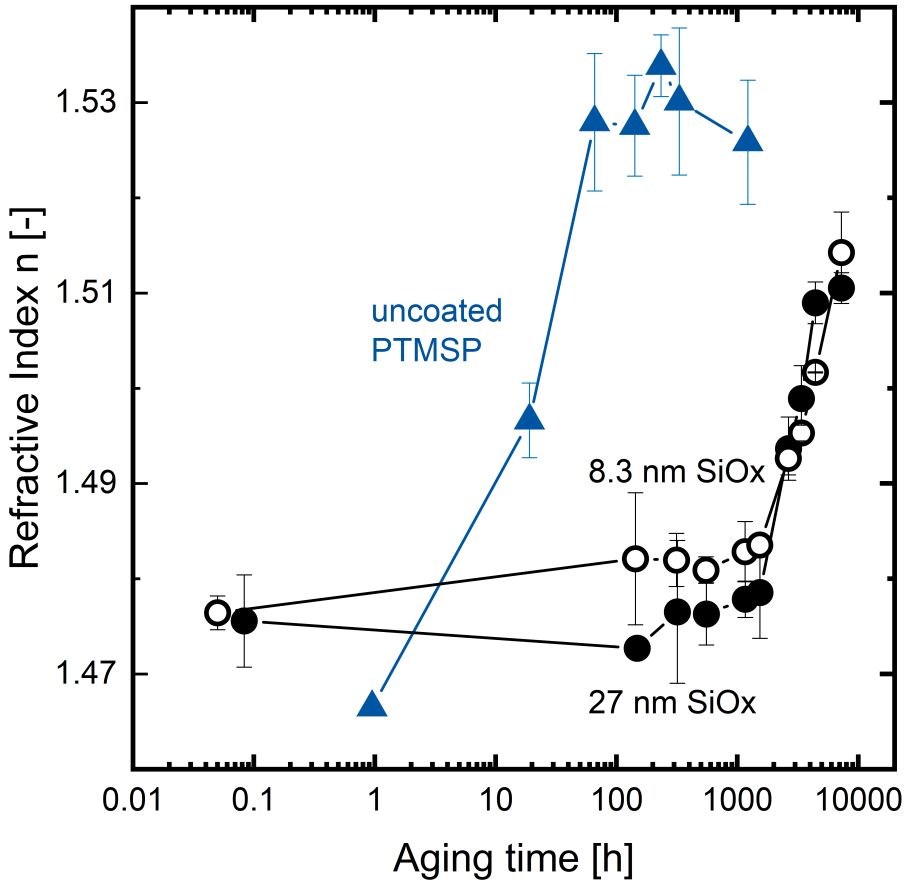


Figure 5.9.: Refractive index n of the PTMSP layer over logarithmic aging time without coating and with 8.3 and 27 nm of SiOx coating via PECVD after rejuvenation.

the coated PTMSP, hindering the polymer chains to reach a state comparable to the chains at a free surface.

Focusing the refractive index progression in Figure 5.9, the coated layers show nearly no increase in refractive index for the first 1000 hours compared to the uncoated PTMSP reference layer. During this time, their gradients are $0.0014\ \mathrm{h}^{-1}$ and $0.0003\ \mathrm{h}^{-1}$ for the 8.3 and 27 nm thick SiOx layers, respectively. Hence, the gradient of the refractive index increase is suppressed to 5 % and 1 % of the uncoated PTMSP, respectively.
After about 1000 hours, the refractive index progression changes significantly. This is in agreement with the report of Kelman et al. for their crosslinked and uncrosslinked PTMSP. However, their so called initial aging time is only 24 hours.[Kelm2008] In comparison, optical aging studies of other polymers do not show this behavior but rather follow a linear progression on a log t scale. [Robe1998];

[Kim2006]; [Tani2006]; [Huan2006a] In contrast to the refractive index progressions in literature, the results propose a linear behavior over t instead of log t for the aging of PTMSP, which is plotted in figure 5.10. The lines show linear gradient fits for increasing values of the refractive index. With R^2 of at least 0.986, they well represent the refractive index progression. While the uncoated PTMSP has a gradient of $6.7 \cdot 10^{-4}\ \mathrm{h}^{-1}$, the 27 nm and 8.3 nm SiOx coated layer have a gradient of only $8.2 \cdot 10^{-6}\ \mathrm{h}^{-1}$ and $5.6 \cdot 10^{-6}\ \mathrm{h}^{-1}$, respectively. This means a reduction of the aging speed of more than two orders of magnitude. Furthermore, the refractive index progressions of both SiOx coatings show comparable impact on the aging mitigation. Hence, the confinement effect of a 10 nm thin non-polymeric layer is already sufficient to drastically mitigate physical aging.

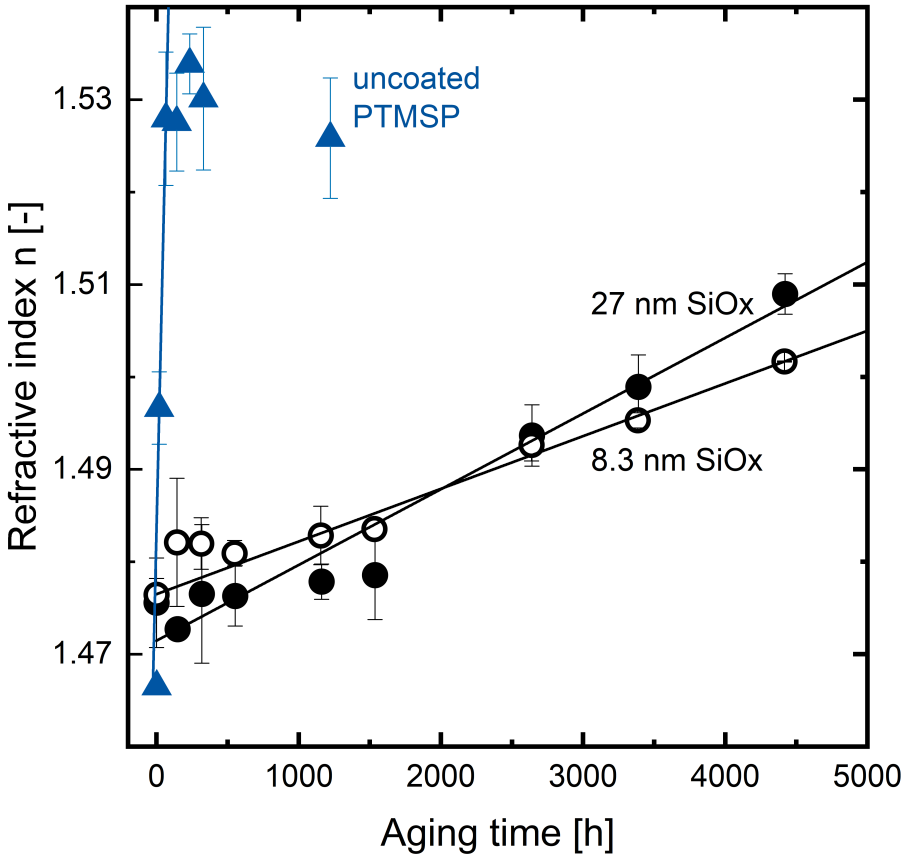


Figure 5.10.: Refractive index n of the PTMSP layer over aging time without coating and with 8.3 and 27 nm of SiOx coating via PECVD after rejuvenation. Lines are best linear fits of the refractive index over time.

The underlying PTMSP films are successfully rejuvenated after PECVD coat-

ing. Furthermore, the presented PECVD top layer coating effectively mitigates physical aging of a more than 200 nm thick PTMSP film by a double-sided confinement effect. In comparison, Priestley et al. showed the confinement impact of a substrate interface on the relaxation rate of poly(methyl methacrylate) to mainly range about 25 nm into the polymer. At 100 nm from the surface only a small effect of aging mitigation could be detected. [Prie2005]
In contrast, this study shows the impact of a double-sided instead of a one-sided confinement effect. Even though the middle of the studied film is slightly over 100 nm away from the surface and should, referring to Priestley et al., only see minor aging mitigation, the results demonstrate a strong impact on the whole film.
Concluding, a double-sided confinement effect, as shown here, amplifies the aging mitigation impact drastically compared to a single-sided confinement, as shown by Priestley et al. Hence, an effective physical aging mitigation can be implemented for films significantly thicker than 25 nm, which is the reported impact distance of a substrate interface [Prie2005]. Nevertheless, the exact reason for the strong amplification of the aging mitigation by the double-sided confinement effect and how far it can reach has to be studied in further experiments.

5.4. Conclusion

Coating ultra-thin polymer films with intrinsic microporosity with a top layer of a few nanometers using plasma-enhanced chemical vapor deposition (PECVD) mitigates physical aging successfully. Instead of tuning the intrinsic properties of the polymer, this study takes advantage of interfacial confinement effects. The results show the difference in aging mitigation impact of a weakly (SiOCH) and highly (SiOx) oxidised PECVD coating layer on a 200 nm thick polymer with intrinsic microporosity. On the one hand, the SiOCH coating did not show significant impact compared to the aging of the uncoated PTMSP reference sample. On the other hand, a SiOx coating of less than 10 nm suppressed the refractive index gradient by more than two orders of magnitude compared to the reference sample. This shows the enormous capability of a top layer coating to effectively mitigate physical aging of polymers with intrinsic microporosity.

Although many studies investigate the physical aging behavior, the exact influence of interfaces on polymer behavior are not yet fully understood. Especially, the amplification of the double-sided compared to the one-sided confinement effect needs to be investigated in further studies to determine the full potential of this approach.
This study also shows accelerated physical aging of a glassy polymer by treating it with a microwave plasma. This approach can be used to intentionally age glassy polymers in a fraction of the usual period of time.

Concluding, the PECVD-coated films stand out with their superior anti-aging behavior compared to untreated PTMSP films. Since industrial roll-to-roll manufacturing processes already use PECVD, the studied approach opens a new path for the commercial application of high free volume polymers minimizing their properties' time dependency.

In the future, the plasma coating conditions, as well as the used monomer, can be varied to further investigate the influence on the anti-aging behavior beyond SiOx and SiOCH chemistry and different layer thicknesses. Additionally to the outstanding physical aging mitigation, the permeation resistance of those coatings is a key factor for membrane applications, which needs to be investigated in future studies. Furthermore, the relationship between aging mitigation and permeation resistance depending on the thickness and degree of oxidation of the coating needs to be studied more closely.

6. Conclusion and perspectives

Parts of this chapter have been published as:

Jens Rubner, Soukaina Skribbe, Hannah Roth, Lara Kleines, Rainer Dahlmann, Matthias Wessling
On the Mixed Gas Behavior of Organosilica Membranes Fabricated by Plasma-Enhanced Chemical Vapor Deposition (PECVD) , Membranes, 2022
DOI: 10.3390/membranes12100994

Jens Rubner, Leonie Stellmann, Ann-Kathrin Mertens, Maik Tepper, Hannah Roth, Lara Kleines, Rainer Dahlmann, and Matthias Wessling
Organosilica coating layer prevents aging of a polymer with intrinsic microporosity, Plasma processes and polymers, 2022
DOI: 10.1002/ppap.202200016

6.1. Summary

This thesis' goal was to use PECVD as a process to fabricate highly selective thin film composite polymeric membranes for gas separation and physical aging mitigators for polymers with intrinsic microporosity.

PECVD fabrication parameter

Chapter 3, therefore, investigated three parameters influencing the molecular composition or the energy density in the PECVD and examined their influence on the chemical composition and the membrane performance.
The microwave's magnetron frequency of 2.45 GHz, a pressure of 5 Pa, and HMDSO as the precursor were constant parameters. The amount of additional O_2 to the reaction gas, the microwave input power, and the plasma pulse-on length have been varied for the different fabrications. The aim was to optimize the molecular size-sieving behavior of the membrane by increasing the He permeance and the He/C_3H_8 selectivity.
The addition of O_2 to the HMDSO in the plasma reactor showed the strongest influence. The He permeances and He/C_3H_8 selectivities for all studied microwave input powers are highest for pure HMDSO. Conversely, increasing the O_2 content significantly decreases the permeance and selectivity. The variation of the microwave input power shows similar behavior for all tested O_2 fractions in the reaction gas mixture. The smaller the input power, the higher the permeance and selectivity for He. In contrast, the alteration of the pulse-on time did not show a strong and clear trend on the selectivity for the used microwave input powers. Nevertheless, the He permeance was highest for the lowest microwave power inputs.
Concluding, the fabrication parameters with the lowest power input per molecule (smallest Yasuda parameter) and the highest HMDSO reaction gas fraction led to the best membrane performance considering He permeance and He/C_3H_8 selectivity.

PECVD membrane performance

Chapter 3 studied the membrane performance of the organosilica layer deposited under the optimal conditions determined in Chapter 3. It investigated the pure and mixed gas permeation behavior for temperatures from 0 °C to 60 °C for four gases (helium, methane, carbon dioxide, and nitrogen) and water vapor. For the two permanent gases helium and methane, the studied organosilica membrane shows a substantial increase in selectivity from α_{He/CH_4}= 9 at 0 °C to α_{He/CH_4}= 40 at 60 °C for pure as well as mixed gases with helium permeance of up to 300 GPU. In contrast, a condensable gas like CO_2 leads to a decrease in selectivity and an increase in permeance compared to its pure gas performance. When water vapor is present in the feed gas, the organosilica membrane shows even more substantial deviations from pure gas behavior with a permeance loss of about 60 %, but accompanied by an increase in ideal selectivity α_{He/CO_2} from 8 to 13. All in all, the studied organosilica membrane shows promising results for mixed gases. Especially for elevated temperatures, there is a high potential for separation by size exclusion.

Nevertheless, the selectivities and permeances at ambient conditions still need to be improved to outperform known membranes under those conditions. Furthermore, the differences in the temperature dependent permeation behavior of CH_4 and N_2 in comparison to He and CO_2 leads to the presumption of the occurrence of defects in the organosilica layer. Hence, closing the defects either by further optimizing the fabrication parameters to gain a defect free organosilica layer or by coating a subsequent protective layer on the membrane could drastically increase the selectivity of the PECVD-fabricated organosilica membrane.
In addition, the utilization of other monomers with more complex structures than HMDSO could allow to finely tune the permeation behavior of certain molecules by facilitating their transport through the membrane. Apart from this, a narrower microporosity distribution of the organosilica layer would lead to a more distinct permeation cut-off enabling the selective transport of molecules with only slight size differences. The improved selectivity could enable the application of membranes for separation tasks not feasible yet.

Physical aging mitigator

In addition to the studies considering the selective permeation behavior of organosilica layers, Chapter 5 tracked the physical aging behavior of coated and uncoated ultra-thin Poly(1-trimethylsilyl-1-propyne) (PTMSP) films. It observed the aging of the polymer on top of silicon wafers based on the refractive index using ellipsometry over several weeks. The measured refractive index directly correlates with the free volume and hence the physical aging progression of the PTMSP. PECVD creates coatings with different thicknesses and oxidation degrees onto PTMSP films. Compared to uncoated PTMSP films, the PECVD-coated films show a reduction of the refractive index increase of more than two orders of magnitude for less than 10 nm strongly oxidized (SiOx) coatings. In contrast, weakly oxidized (SiOCH) films show only a minor impact. The results reveal the superior physical aging behavior of PECVD-coated films compared to untreated PTMSP films.

In the future, the plasma coating conditions and the used monomer can be varied to investigate further the influence on the anti-aging behavior beyond SiOx and SiOCH chemistry and different layer thicknesses. Additionally to the outstanding physical aging mitigation, the permeation resistance of those coatings is a crucial factor for membrane applications, which needs to be investigated in future studies. Furthermore, the relationship between aging mitigation and permeation resistance depending on the thickness and degree of oxidation of the coating needs to be studied more closely.

A. Appendix

Parts of this chapter have been published as:

Kleines, L., Wilski, S., Alizadeh, P., Rubner, J., Wessling, M., Hopmann, C., & Dahlmann, R.
Structure and gas separation properties of ultra-smooth PE-CVD silicon organic coated composite membranes, Surface and Coatings Technology, 2021
DOI: 10.1016/j .surfcoat.2021.127338

Kleines, L., Wilski, S., Alizadeh, P., Rubner, J., Wessling, M., Hopmann, C., & Dahlmann, R.
Evaluation of the membrane performance of ultra-smooth silicon organic coatings depending on the process energy density, Thin Solid Films, 2022
DOI: 10.1016/j .tsf.2022.139169

A.1. Pure gas permeation

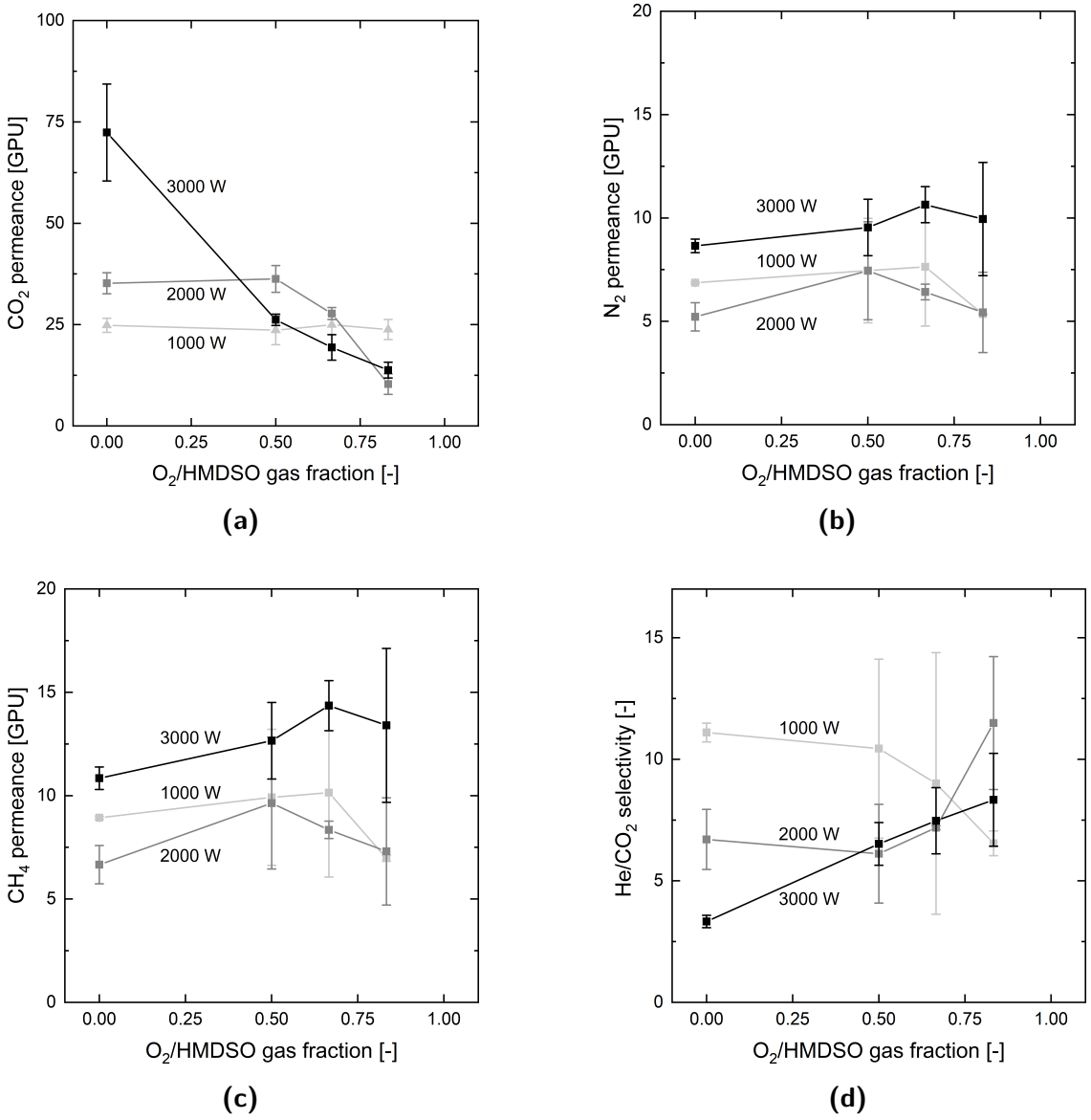


Figure A.1.: Figures A.1a, A.1b and A.1c show the CO_2, N_2 and CH_4 permeance of organosilica membranes fabricated with microwave power inputs of 1000, 2000, and 3000 W with O_2 to HMDSO gas fractions from 0 to 0.83. Figure A.1d displays exemplarily the resulting He/CO_2 selectivity. Each data point consists of the measurements of three membrane samples.

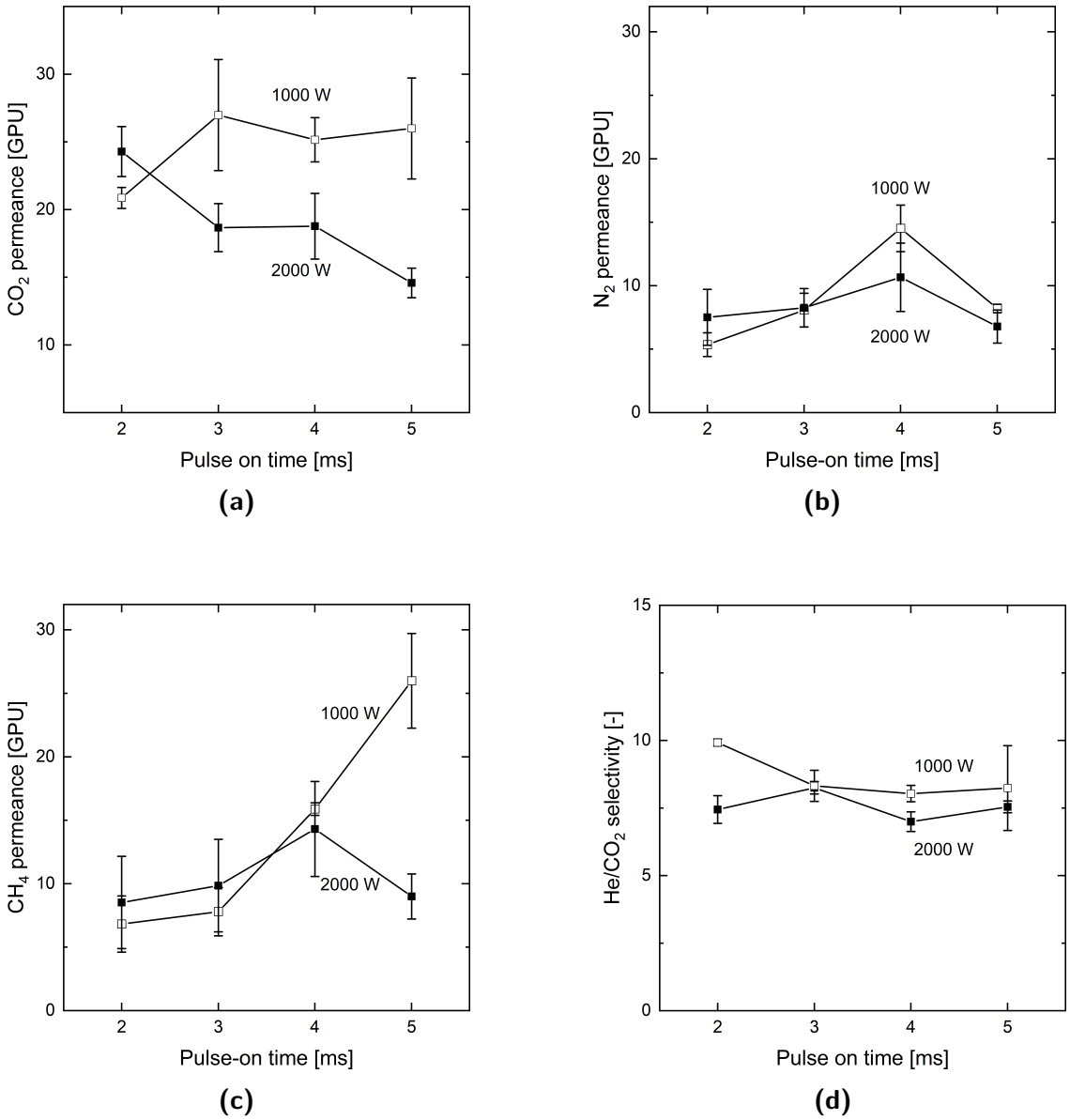


Figure A.2.: Figures A.2a, A.2b and A.2c show the CO_2, N_2 and CH_4 permeance of organosilica membranes fabricated with pulse-on times of 2 to 5 ms. Figure A.2d displays examplarily the resulting He/CO_2 selectivity. Each data point consists of the measurements of three membrane samples.

Bibliography

[Ahma2020] M. Z. Ahmad, R. Castro-Muñoz, and P. M. Budd. "Boosting gas separation performance and suppressing the physical aging of polymers of intrinsic microporosity (PIM-1) by nanomaterial blending". *Nanoscale* 12.46 (2020). (Cit. on p. 79).

[Alde2017] M. Alders, D. Winterhalder, and M. Wessling. "Helium recovery using membrane processes". *Separation and Purification Technology* 189 (2017). (Cit. on p. 57).

[Alex1997] M. Alexander, F. Jones, and R. Short. "Radio-frequency hexamethyldisiloxane plasma deposition: a comparison of plasma-and deposit-chemistry". *Plasmas and polymers* 2.4 (1997). (Cit. on pp. 43, 86).

[Anto1888] M. C. Antoine. "Nouvelle relation entre les tensions et les temperatures". *C. r. held Seanc. Acad. Sci. Paris* 107 (1888). (Cit. on pp. 22, 63).

[Arqu1962] G. J. Arquette and R. Leo. *Insolubilization of coatings*. US Patent 3,061,458. Oct. 1962 (cit. on p. 25).

[Bahr2013] K. Bahroun et al. "Influence of layer type and order on barrier properties of multilayer PECVD barrier coatings". *Journal of Physics D: Applied Physics* 47.1 (2013). (Cit. on pp. 32, 43, 86).

[Bake2014] R. W. Baker and B. T. Low. "Gas separation membrane materials: a perspective". *Macromolecules* 47.20 (2014). (Cit. on pp. 15, 19).

[Baxa2009] S. H. Baxamusa and K. K. Gleason. "Random copolymer films with molecular-scale compositional heterogeneities that interfere with protein adsorption". *Advanced Functional Materials* 19.21 (2009). (Cit. on p. 37).

[Behm2016] H. Behm. "Investigation of plasma processes and their influence on the composite properties of polypropylene coated by means of plasma polymerization". PhD thesis. RWTH Aachen University, 2016 (cit. on pp. 32, 37).

[Bos1999] A. Bos et al. "CO2-induced plasticization phenomena in glassy polymers". *Journal of membrane science* 155.1 (1999). (Cit. on p. 69).

[Bosc2003] F. Bosc et al. "Sorption and permeation characteristics of hybrid organosilicon thin films deposited by PECVD". *Separation and purification technology* 32.1-3 (2003). (Cit. on pp. 31, 58, 80).

[Brad1963] A. Bradley and J. P. Hammes. "Electrical properties of thin organic films". *Journal of The Electrochemical Society* 110.1 (1963). (Cit. on p. 25).

[Brec1973] D. W. Breck and D. W. Breck. *Zeolite molecular sieves: structure, chemistry, and use*. John Wiley & Sons, 1973 (cit. on p. 68).

[Brow1976] W. R. Browall. *Method for sealing breaches in multi-layer ultrathin membrane composites*. US Patent 3,980,456. Sept. 1976 (cit. on p. 15).

[Brun2010] A. Brunetti et al. "Membrane engineering: Progress and potentialities in gas separations". *Membrane Gas Separation* 6 (2010). (Cit. on p. 57).

[Cang2003] D. Cangialosi et al. "Positron annihilation lifetime spectroscopy for measuring free volume during physical aging of polycarbonate". *Macromolecules* 36.1 (2003). (Cit. on p. 80).

[Cang2004] D. Cangialosi et al. "Physical aging of polycarbonate far below the glass transition temperature: Evidence for the diffusion mechanism". *Physical review B* 70.22 (2004). (Cit. on p. 80).

[Cast2008] H. L. Castricum et al. "Hydrothermally stable molecular separation membranes from organically linked silica". *Journal of Materials Chemistry* 18.18 (2008). (Cit. on pp. 60, 73).

[Char2016] R. Charifou et al. "SiOx and SiOxCzHw mono-and multi-layer deposits for improved polymer oxygen and water vapor barrier properties". *Journal of Membrane Science* 500 (2016). (Cit. on pp. 31, 58, 80).

[Chen2003] L.-Y. Chen and F. Chau-Nan Hong. "Diamond-like carbon nanocomposite films". *Applied Physics Letters* 82.20 (2003). (Cit. on p. 33).

[Cohe1959] M. H. Cohen and D. Turnbull. "Molecular transport in liquids and glasses". *The Journal of Chemical Physics* 31.5 (1959). (Cit. on pp. 18–20).

[Cole1962] J. H. Coleman. *Polymerizing method and apparatus*. US Patent 3,068,510. Dec. 1962 (cit. on p. 25).

[Come2019] B. Comesaña-Gándara et al. "Redefining the Robeson upper bounds for CO 2/CH 4 and CO 2/N 2 separations using a series of ultrapermeable benzotriptycene-based polymers of intrinsic microporosity". *Energy & Environmental Science* 12.9 (2019). (Cit. on pp. 13, 57).

[Cous2014] R. Coustel et al. "An insight into the structure–property relationships of PECVD SiCxNy (O): H materials". *Microporous and mesoporous materials* 191 (2014). (Cit. on pp. 37, 58, 80).

[Croo1879] W. Crookes. "ART. XXXV.–On Radiant Matter; A Lecture delivered to the British Association for the Advancement of Science, at Sheffield, Friday, August 22, 1879". *American Journal of Science and Arts (1820-1879)* 18.106 (1879). (Cit. on p. 24).

[dAgo1990] P. d'Agostino. *Treatment and Etching of Polymers*. 1990 (cit. on p. 37).

[dAgo2005] R. d'Agostino et al. "Plasma Processes and Polymers: 16th International Symposium on Plasma Chemistry Taormina, Italy June 22-27, 2003". In*Plasma Processes and Polymers: 16th International Symposium on Plasma Chemistry Taormina*. 2005, p. 545 (cit. on p. 39).

[De V1998] R. M. De Vos and H. Verweij. "High-selectivity, high-flux silica membranes for gas separation". *Science* 279.5357 (1998). (Cit. on p. 73).

[Duke2006] M. C. Duke et al. "Hydrothermally robust molecular sieve silica for wet gas separation". *Advanced Functional Materials* 16.9 (2006). (Cit. on pp. 60, 73).

[Efim2002] K. Efimenko, W. E. Wallace, and J. Genzer. "Surface modification of Sylgard-184 poly (dimethyl siloxane) networks by ultraviolet and ultraviolet/ozone treatment". *Journal of colloid and interface science* 254.2 (2002). (Cit. on p. 65).

[Enna2010] A. Ennajdaoui et al. "Membranes produced by plasma enhanced chemical vapor deposition technique for low temperature fuel cell applications". *Journal of Power Sources* 195.1 (2010). (Cit. on p. 37).

[Förc2007] R. Förch et al. "Recent and expected roles of plasma-polymerized films for biomedical applications". *Chemical Vapor Deposition* 13.6-7 (2007). (Cit. on p. 37).

[Gall1994] G. Gallaher and P. Liu. "Characterization of ceramic membranes I. Thermal and hydrothermal stabilities of commercial 40 Å membranes". *Journal of membrane science* 92.1 (1994). (Cit. on pp. 60, 73).

[Gava1989] G. Gavalas, C. Megiris, and S. Nam. "Deposition of H2-permselective SiO2 films". *Chemical engineering science* 44.9 (1989). (Cit. on pp. 60, 73).

[Gend2019] G. Genduso, B. S. Ghanem, and I. Pinnau. "Experimental mixed-gas permeability, sorption and diffusion of CO2-CH4 mixtures in 6FDA-mPDA polyimide membrane: unveiling the effect of competitive sorption on permeability selectivity". *Membranes* 9.1 (2019). (Cit. on p. 69).

[Gome2005] D. Gomes, S. P. Nunes, and K.-V. Peinemann. "Membranes for gas separation based on poly (1-trimethylsilyl-1-propyne)–silica nanocomposites". *Journal of Membrane Science* 246.1 (2005). (Cit. on p. 79).

[Grah1866] T. Graham. "LV. On the absorption and dialytic separation of gases by colloid septa". *The London, Edinburgh, and Dublin Philosophical Magazine and Journal of Science* 32.218 (1866). (Cit. on p. 10).

[Gril2003] A. Grill and D. A. Neumayer. "Structure of low dielectric constant to extreme low dielectric constant SiCOH films: Fourier transform infrared spectroscopy characterization". *Journal of applied physics* 94.10 (2003). (Cit. on pp. 65, 66, 86, 88).

[Guiv2002] M. D. Guiver et al. "Structural characterization and gas-transport properties of brominated matrimid polyimide". *Journal of Polymer Science Part A: Polymer Chemistry* 40.23 (2002). (Cit. on p. 59).

[Haac2015] M. Haacké et al. "Optimization of the molecular sieving properties of amorphous SiC XNY: H hydrogen selective membranes prepared by PECVD". *The european physical journal special topics* 224.9 (2015). (Cit. on pp. 37, 58, 60, 67, 80).

[Hanc1997] B. C. Hancock and G. Zografi. "Characteristics and significance of the amorphous state in pharmaceutical systems". *Journal of pharmaceutical sciences* 86.1 (1997). (Cit. on p. 79).

[Hash2014] S. Hashmi. *Comprehensive materials processing*. Newnes, 2014 (cit. on p. 39).

[Hege2014] D. Hegemann. "4.09–Plasma polymer deposition and coatings on polymers". *Comprehensive materials processing* (2014). (Cit. on pp. 32, 39).

[Heni1980] J. M. Henis and M. K. Tripodi. "A novel approach to gas separations using composite hollow fiber membranes". *Separation science and technology* 15.4 (1980). (Cit. on pp. 15, 16).

[Henr1803] W. Henry. "III. Experiments on the quantity of gases absorbed by water, at different temperatures, and under different pressures". *Philosophical Transactions of the Royal Society of London* 93 (1803). (Cit. on p. 12).

[Herz1998] C. Herzinger et al. "Ellipsometric determination of optical constants for silicon and thermally grown silicon dioxide via a multi-sample, multi-wavelength, multi-angle investigation". *Journal of Applied Physics* 83.6 (1998). (Cit. on pp. 63, 85).

[Hill2003] J. Hiller and M. F. Rubner. "Reversible molecular memory and pH-switchable swelling transitions in polyelectrolyte multilayers". *Macromolecules* 36.11 (2003). (Cit. on p. 81).

[Hill2020] A. Hill et al. "Role of free volume in molecular mobility and performance of glassy polymers for corrosion-protective coatings". *Corrosion Engineering, Science and Technology* 55.2 (2020). (Cit. on p. 79).

[Hipp2008] R. Hippler et al. "Low temperature plasmas". *Eds R Hippler et al, Berlin: Wiley* 787 (2008). (Cit. on p. 37).

[Hopp2020] C. Hoppe et al. "Characterisation of micropores in plasma deposited SiOx films by means of positron annihilation lifetime spectroscopy". *Journal of Physics D: Applied Physics* 53.47 (2020). (Cit. on p. 43).

[Horn2012] N. R. Horn and D. Paul. "Carbon dioxide sorption and plasticization of thin glassy polymer films tracked by optical methods". *Macromolecules* 45.6 (2012). (Cit. on p. 81).

[Huan2004] Y. Huang and D. R. Paul. "Physical aging of thin glassy polymer films monitored by gas permeability". *Polymer* 45.25 (2004). (Cit. on p. 79).

[Huan2006a] Y. Huang and D. R. Paul. "Physical aging of thin glassy polymer films monitored by optical properties". *Macromolecules* 39.4 (2006). (Cit. on pp. 80, 81, 90, 99).

[Huan2006b] Y. Huang, X. Wang, and D. R. Paul. "Physical aging of thin glassy polymer films: Free volume interpretation". *Journal of Membrane Science* 277.1-2 (2006). (Cit. on p. 81).

[Huan2007] Y. Huang and D. R. Paul. "Effect of film thickness on the gas-permeation characteristics of glassy polymer membranes". *Industrial & engineering chemistry research* 46.8 (2007). (Cit. on pp. 79, 80, 92).

[Hube1997] F. Huber, J. Springer, and M. Muhler. "Plasma polymer membranes from hexafluoroethane/hydrogen mixtures for separation of oxygen and nitrogen". *Journal of applied polymer science* 63.12 (1997). (Cit. on p. 37).

[Inag1999] N. Inagaki, S. Tasaka, and H. Hiramatsu. "Preparation of oxygen gas barrier poly (ethylene terephthalate) films by deposition of silicon oxide films plasma-polymerized from a mixture of tetramethoxysilane and oxygen". *Journal of applied polymer science* 71.12 (1999). (Cit. on pp. 43, 86).

[Inag2014] N. Inagaki. *Plasma surface modification and plasma polymerization*. CRC press, 2014 (cit. on pp. 27, 28).

[Iuli2020] A. Iulianelli and E. Drioli. "Membrane engineering: Latest advancements in gas separation and pre-treatment processes, petrochemical industry and refinery, and future perspectives in emerging applications". *Fuel Processing Technology* 206 (2020). (Cit. on pp. 57, 58).

[Izu1995] M. Izu, B. Dotter, and S. Ovshinsky. "Roll-to-roll microwave PECVD machine for high-barrier film coatings". *Journal of Photopolymer Science and Technology* 8.1 (1995). (Cit. on p. 58).

[Kafr2009] W. Kafrouni et al. "Synthesis of PECVD a-SiCXNY: H membranes as molecular sieves for small gas separation". *Journal of Membrane Science* 329.1-2 (2009). (Cit. on pp. 37, 58, 60, 67, 68, 80).

[Kafr2010] W. Kafrouni et al. "Synthesis and characterization of silicon carbonitride films by plasma enhanced chemical vapor deposition (PECVD) using bis (dimethylamino) dimethylsilane (BDMADMS), as membrane for a small molecule gas separation". *Applied Surface Science* 257.4 (2010). (Cit. on pp. 37, 58, 60, 67, 80).

[Kapp2019] E. J. Kappert et al. "Swelling of 9 polymers commonly employed for solvent-resistant nanofiltration membranes: A comprehensive dataset". *Journal of membrane science* 569 (2019). (Cit. on p. 81).

[Kelm2008] S. D. Kelman et al. "Crosslinking poly [1-(trimethylsilyl)-1-propyne] and its effect on physical stability". *Journal of Membrane Science* 320.1-2 (2008). (Cit. on p. 98).

[Khor1996] M. Khorasani, H. Mirzadeh, and P. Sammes. "Laser induced surface modification of polydimethylsiloxane as a super-hydrophobic material". *Radiation Physics and Chemistry* 47.6 (1996). (Cit. on p. 65).

[Kiha1951] T. Kihara. "The second virial coefficient of non-spherical molecules". *Journal of the Physical Society of Japan* 6.5 (1951). (Cit. on p. 68).

[Kim2003] Y. Kim et al. "N2 doped SiO2–SiON planar waveguides deposited by PECVD method". *Surface and Coatings Technology* 174 (2003). (Cit. on p. 28).

[Kim2006] J. H. Kim, W. Koros, and D. Paul. "Physical aging of thin 6FDA-based polyimide membranes containing carboxyl acid groups. Part II. Optical properties". *Polymer* 47.9 (2006). (Cit. on p. 99).

[Klei2020] L. Kleines et al. "Enhancing the separation properties of plasma polymerized membranes on polydimethylsiloxane substrates by adjusting the auxiliary gas in the PECVD processes". *Journal of Physics D: Applied Physics* 53.44 (2020). (Cit. on pp. 31, 58, 59, 80).

[Klei2021] L. Kleines et al. "Structure and gas separation properties of ultra-smooth PE-CVD silicon organic coated composite membranes". *Surface and Coatings Technology* 421 (2021). (Cit. on pp. 58, 59, 61, 66, 80).

[Klei2022] L. Kleines et al. "Evaluation of the membrane performance of ultra-smooth silicon organic coatings depending on the process energy density". *Thin Solid Films* (2022). (Cit. on pp. 58, 61, 86).

[Kova1964] A. J. Kovacs. "Transition vitreuse dans les polymères amorphes. Etude phénoménologique". In*Fortschritte der hochpolymeren-forschung*. Springer, 1964. Pp. 394–507. (Cit. on p. 79).

[Kozm2005] I. Z. Kozma, P. Krok, and E. Riedle. "Direct measurement of the group-velocity mismatch and derivation of the refractive-index dispersion for a variety of solvents in the ultraviolet". *JOSA B* 22.7 (2005). (Cit. on p. 96).

[Lai2022] H. W. Lai et al. "Hydrocarbon ladder polymers with ultrahigh permselectivity for membrane gas separations". *Science* 375.6587 (2022). (Cit. on p. 57).

[Lam1976] D. K. Lam, R. F. Baddour, and A. F. Stancell. "A mechanisms and kinetics study of polymeric thin-film deposition in glow discharge". *Journal of Macromolecular Science—Chemistry* 10.3 (1976). (Cit. on p. 26).

[Lebo1995] R. Leboda et al. "Hydrothermal modification of silica gels (xerogels) 2. Effect of the duration of treatment on their porous structure". *Colloids and Surfaces A: Physicochemical and Engineering Aspects* 105.2-3 (1995). (Cit. on pp. 60, 73).

[Lee1984] P. I. Lee. "Novel approach to zero-order drug delivery via immobilized nonuniform drug distribution in glassy hydrogels". *Journal of pharmaceutical sciences* 73.10 (1984). (Cit. on p. 79).

[Lenz2001] R. F. Lenza and W. L. Vasconcelos. "Structural evolution of silica sols modified with formamide". *Materials Research* 4.3 (2001). (Cit. on pp. 65, 66, 88).

[Li1999] K. Li and J. Meichsner. "Gas-separating properties of membranes coated by HMDSO plasma polymer". *Surface and Coatings Technology* 116 (1999). (Cit. on pp. 37, 58, 80).

[Lin2006] H. Lin and B. D. Freeman. "Gas permeation and diffusion in cross-linked poly (ethylene glycol diacrylate)". *Macromolecules* 39.10 (2006). (Cit. on p. 20).

[Lo2009] C.-H. Lo et al. "Investigation on the variation in the fine structure of plasma-polymerized composite membrane by positron annihilation spectroscopy". *Journal of Membrane Science* 337.1-2 (2009). (Cit. on p. 37).

[Lo2010] C.-H. Lo et al. "Control of pore structure and characterization of plasma-polymerized SiOCH films deposited from octamethylcyclotetrasiloxane (OMCTS)". *Journal of Membrane Science* 365.1-2 (2010). (Cit. on pp. 31, 37, 58, 80).

[Loge2020] M. Logemann et al. "How is mixed-gas permeation through poly (1-trimethylsilyl-1-propyne) membranes influenced by elevated temperatures?" *Journal of Membrane Science* 615 (2020). (Cit. on pp. 63, 79).

[Lópe2011] Í. López García, J. Keddie, and M. Sferrazza. "Probing the early stages of solvent evaporation and relaxation in solvent-cast polymer thin films by spectroscopic ellipsometry". *Surface and interface analysis* 43.11 (2011). (Cit. on p. 81).

[Low2018] Z.-X. Low et al. "Gas permeation properties, physical aging, and its mitigation in high free volume glassy polymers". *Chemical reviews* 118.12 (2018). (Cit. on p. 79).

[Magn2001] D. Magni et al. "Oxygen diluted hexamethyldisiloxane plasmas investigated by means of in situ infrared absorption spectroscopy and mass spectrometry". *Journal of Physics D: Applied Physics* 34.1 (2001). (Cit. on p. 33).

[Mass2018] V. Masson-Delmotte et al. "Global warming of 1.5 C". *An IPCC Special Report on the impacts of global warming of* 1.5 (2018). (Cit. on p. 57).

[Mazi2009] N. A. Mazied, S. A. Ismail, and M. F. Abou Taleb. "Radiation synthesis of poly [(dimethylaminoethyl methacrylate)-co-(ethyleneglycol dimethacrylate)] hydrogels and its application as a carrier for anticancer delivery". *Radiation Physics and Chemistry* 78.11 (2009). (Cit. on p. 79).

[Meno2008] I. Menous et al. "Silicon nitride film for solar cells". *Renewable Energy* 33.10 (2008). (Cit. on p. 37).

[Mera2017] D. Merachtsaki et al. "Corrosion protection of steel by epoxy-organoclay nanocomposite coatings". *Coatings* 7.7 (2017). (Cit. on p. 79).

[Mitc1995] J. K. Mitchell. "On the penetrativeness of fluids". *Journal of Membrane Science* 100.1 (1995). (Cit. on p. 10).

[Mits2018] F. Mitschker et al. "Comparative study on the deposition of silicon oxide permeation barrier coatings for polymers using hexamethyldisilazane (HMDSN) and hexamethyldisiloxane (HMDSO)". *Journal of Physics D: Applied Physics* 51.23 (2018). (Cit. on p. 42).

[Mota1995] R. P. Mota et al. "HMDSO plasma polymerization and thin film optical properties". *Thin Solid Films* 270.1-2 (1995). (Cit. on pp. 65, 66, 88).

[Müll2015] C. Müller. "On the glass transition of polymer semiconductors and its impact on polymer solar cell stability". *Chemistry of Materials* 27.8 (2015). (Cit. on p. 79).

[Naga2013] H. Nagasawa et al. "Characterization and gas permeation properties of amorphous silica membranes prepared via plasma enhanced chemical vapor deposition". *Journal of membrane science* 441 (2013). (Cit. on pp. 31, 37, 58, 60, 67, 80).

[Naga2014] H. Nagasawa et al. "High-temperature stability of PECVD-derived organosilica membranes deposited on TiO2 and SiO2–ZrO2 intermediate layers using HMDSO/Ar plasma". *Separation and Purification Technology* 121 (2014). (Cit. on p. 37).

[Naga2015] H. Nagasawa et al. "Microporous organosilica membranes for gas separation prepared via PECVD using different O/Si ratio precursors". *Journal of Membrane Science* 489 (2015). (Cit. on pp. 37, 58, 68, 80).

[Naga2016] H. Nagasawa et al. "Plasma-enhanced chemical vapor deposition of amorphous carbon molecular sieve membranes for gas separation". *RSC advances* 6.64 (2016). (Cit. on pp. 60, 67).

[Ngam2013] P. H. Ngamou et al. "Plasma-deposited hybrid silica membranes with a controlled retention of organic bridges". *Journal of Materials Chemistry A* 1.18 (2013). (Cit. on pp. 31, 58, 80).

[Niem2012] F. v. F. und Niemsdorff. *Wechselwirkungen zwischen Plasmaprozessen und thermoplastischen Oberflächen: Interactions between plasma processes and thermoplastic surfaces*. Mainz, 2012 (cit. on p. 25).

[Ogie2013] W. Ogieglo et al. "Temperature-induced transition of the diffusion mechanism of n-hexane in ultra-thin polystyrene films, resolved by in-situ Spectroscopic Ellipsometry". *Polymer* 54.1 (2013). (Cit. on p. 81).

[Ogie2014a] W. Ogieglo, M. Wessling, and N. E. Benes. "Polymer relaxations in thin films in the vicinity of a penetrant-or temperature-induced glass transition". *Macromolecules* 47.11 (2014). (Cit. on p. 81).

[Ogie2014b] W. Ogieglo et al. "Effects of time, temperature, and pressure in the vicinity of the glass transition of a swollen polymer". *Journal of membrane science* 464 (2014). (Cit. on p. 81).

[Ogie2015] W. Ogieglo et al. "In situ ellipsometry studies on swelling of thin polymer films: A review". *Progress in polymer science* 42 (2015). (Cit. on p. 80).

[Ogie2017a] W. Ogieglo et al. "How do organic vapors swell ultrathin films of polymer of intrinsic microporosity PIM-1?" *The Journal of Physical Chemistry B* 121.29 (2017). (Cit. on p. 81).

[Ogie2017b] W. Ogieglo et al. "Mixed-penetrant sorption in ultrathin films of polymer of intrinsic microporosity PIM-1". *The Journal of Physical Chemistry B* 121.43 (2017). (Cit. on p. 84).

[Ogie2018] W. Ogieglo et al. "High-pressure CO2 sorption in polymers of intrinsic microporosity under ultrathin film confinement". *ACS applied materials & interfaces* 10.13 (2018). (Cit. on pp. 84, 96).

[Ogie2019] W. Ogieglo et al. "Thin composite carbon molecular sieve membranes from a polymer of intrinsic microporosity precursor". *ACS applied materials & interfaces* 11.20 (2019). (Cit. on p. 84).

[Ogie2020] W. Ogieglo et al. "CO2/CH4 Pure-and Mixed-Gas Dilation and Sorption in Thin (500 nm) and Ultrathin (50 nm) Polymers of Intrinsic Microporosity". *Macromolecules* 53.20 (2020). (Cit. on p. 81).

[Pete2009] J. Peter and K.-V. Peinemann. "Multilayer composite membranes for gas separation based on crosslinked PTMSP gutter layer and partially crosslinked Matrimid® 5218 selective layer". *Journal of Membrane Science* 340.1-2 (2009). (Cit. on p. 15).

[Pinn1988] I. Pinnau et al. "Gas permeation through composite membranes". *Journal of membrane science* 37.1 (1988). (Cit. on p. 15).

[Poll1976] H.-U. Poll, M. Arzt, and K.-H. Wickleder. "Reaction kinetics in the polymerization of thin films on the electrodes of a glow-discharge gap". *European Polymer Journal* 12.8 (1976). (Cit. on p. 26).

[Prie2005] R. D. Priestley et al. "Structural relaxation of polymer glasses at surfaces, interfaces, and in between". *Science* 309.5733 (2005). (Cit. on p. 100).

[PUBC2022] PUBCHEM. *Hexamethyldisiloxane*. 2022. URL: `https://pubchem.ncbi.nlm.nih.gov/compound/Hexamethyldisiloxane` (visited on 10/26/2012) (cit. on p. 32).

[Quee2004] K. Queeney et al. "Infrared spectroscopic analysis of an ordered Si/SiO 2 interface". *Applied physics letters* 84.4 (2004). (Cit. on p. 44).

[Raai2015] M. J. Raaijmakers et al. "Sorption behavior of compressed CO2 and CH4 on ultrathin hybrid poly (POSS-imide) layers". *ACS applied materials & interfaces* 7.48 (2015). (Cit. on p. 81).

[Raus2013] P. M. Rauscher et al. "Effect of adjacent rubbery layers on the physical aging of glassy polymers". *Macromolecules* 46.24 (2013). (Cit. on pp. 92, 93).

[Ricc2020] E. Ricci et al. "Competitive sorption in CO2/CH4 separations: the case of HAB-6FDA polyimide and its TR derivative and a general analysis of its impact on the selectivity of glassy polymers at multicomponent conditions". *Journal of Membrane Science* 612 (2020). (Cit. on pp. 69, 71).

[Robe1991] L. M. Robeson. "Correlation of separation factor versus permeability for polymeric membranes". *Journal of membrane science* 62.2 (1991). (Cit. on pp. 13, 14).

[Robe1998] C. G. Robertson and G. L. Wilkes. "Refractive index: a probe for monitoring volume relaxation during physical aging of glassy polymers". *Polymer* 39.11 (1998). (Cit. on p. 98).

[Robe2008] L. M. Robeson. "The upper bound revisited". *Journal of membrane science* 320.1-2 (2008). (Cit. on pp. 13, 14, 57, 59).

[Roth2007] C. B. Roth et al. "Eliminating the enhanced mobility at the free surface of polystyrene: fluorescence studies of the glass transition temperature in thin bilayer films of immiscible polymers". *Macromolecules* 40.7 (2007). (Cit. on p. 94).

[Roua1999] S. Roualdes et al. "Gas separation properties of organosilicon plasma polymerized membranes". *AIChE journal* 45.7 (1999). (Cit. on pp. 31, 37, 58, 80).

[Roua2002] S. Roualdes, J. Sanchez, and J. Durand. "Gas diffusion and sorption properties of polysiloxane membranes prepared by PECVD". *Journal of membrane science* 198.2 (2002). (Cit. on pp. 37, 58, 80).

[Roua2010] S. Roualdes, V. Rouessac, and J. Durand. *Plasma membranes*. 2010 (cit. on pp. 27, 58).

[Roua2017] S. Roualdes and V. Rouessac. "1.10 Plasma Membranes". *Comprehensive Membrane Science and Engineering* (2017). (Cit. on pp. 25, 29, 30, 37, 58, 80).

[Roue2004] V. Rouessac, P. Tuluc, and J. Durand. "Composite plasma-polymerized organosiloxane-based material for hydrocarbon vapor selectivity". *Journal of membrane science* 230.1-2 (2004). (Cit. on p. 37).

[Rowe2009a] B. W. Rowe, B. D. Freeman, and D. R. Paul. "Physical aging of ultrathin glassy polymer films tracked by gas permeability". *Polymer* 50.23 (2009). (Cit. on p. 79).

[Rowe2009b] B. W. Rowe et al. "A variable energy positron annihilation lifetime spectroscopy study of physical aging in thin glassy polymer films". *Polymer* 50.25 (2009). (Cit. on p. 80).

[Sadr2018] M. Sadrzadeh, M. Rezakazemi, and T. Mohammadi. "Fundamentals and measurement techniques for gas transport in polymers". In *Transport properties of polymeric membranes*. Elsevier Amsterdam, 2018. Pp. 391–423. (Cit. on p. 20).

[Sand2013] D. F. Sanders et al. "Energy-efficient polymeric gas separation membranes for a sustainable future: A review". *Polymer* 54.18 (2013). (Cit. on p. 79).

[Scho2016] C. A. Scholes and U. Ghosh. "Helium separation through polymeric membranes: selectivity targets". *Journal of Membrane Science* 520 (2016). (Cit. on p. 57).

[Scho2017a] C. A. Scholes and U. K. Ghosh. "Review of membranes for helium separation and purification". *Membranes* 7.1 (2017). (Cit. on p. 57).

[Scho2017b] C. A. Scholes, U. K. Gosh, and M. T. Ho. "The economics of helium separation and purification by gas separation membranes". *Industrial & Engineering Chemistry Research* 56.17 (2017). (Cit. on p. 57).

[Secr2011] K. E. Secrist and A. J. Nolte. "Humidity swelling/deswelling hysteresis in a polyelectrolyte multilayer film". *Macromolecules* 44.8 (2011). (Cit. on p. 81).

[Shen2010] Y. Shen and A. C. Lua. "Effects of membrane thickness and heat treatment on the gas transport properties of membranes based on P84 polyimide". *Journal of applied polymer science* 116.5 (2010). (Cit. on p. 59).

[Shib2015] M. Shibata, Y. Sakai, and D. Yokoyama. "Advantages and disadvantages of vacuum-deposited and spin-coated amorphous organic semiconductor films for organic light-emitting diodes". *Journal of Materials Chemistry C* 3.42 (2015). (Cit. on p. 79).

[Shol2016] D. S. Sholl and R. P. Lively. "Seven chemical separations to change the world". *Nature* 532.7600 (2016). (Cit. on pp. 1, 57).

[Sira2001] S. Sirard, P. F. Green, and K. P. Johnston. "Spectroscopic ellipsometry investigation of the swelling of poly (dimethylsiloxane) thin films with high pressure carbon dioxide". *The Journal of Physical Chemistry B* 105.4 (2001). (Cit. on p. 81).

[Sloc2006] J. M. Slocik et al. "Site-Specific Patterning of Biomolecules and Quantum Dots on Functionalized Surfaces Generated by Plasma-Enhanced Chemical Vapor Deposition". *Advanced Materials* 18.16 (2006). (Cit. on p. 37).

[Smit2020] S. J. Smith et al. "Control of physical aging in super-glassy polymer mixed matrix membranes". *Accounts of Chemical Research* 53.7 (2020). (Cit. on p. 79).

[Snyd2018] C. R. Snyder and D. M. DeLongchamp. "Glassy phases in organic semiconductors". *Current Opinion in Solid State and Materials Science* 22.2 (2018). (Cit. on p. 79).

[Soll2002] C. Soll. "Plasmapolymerisation von Hexamethyldisiloxan zur Abscheidung von quarzähnlichen Schichten bei gepulster Leistungszufuhr". PhD thesis. Universität Wuppertal, Fakultät für Elektrotechnik, Informationstechnik und ..., 2002 (cit. on p. 25).

[Song2016] H. Song et al. "Pd-doped organosilica membrane with enhanced gas permeability and hydrothermal stability for gas separation". *Journal of Materials Science* 51.13 (2016). (Cit. on pp. 60, 73).

[Ster1965] H. Sterling and R. Swann. "Chemical vapour deposition promoted by rf discharge". *Solid-State Electronics* 8.8 (1965). (Cit. on p. 25).

[Stor1997] T. Storgaard-Larsen and O. Leistiko. "Plasma-Enhanced Chemical Vapor Deposited Silicon Oxynitride Films for Optical Waveguide Bridges for Use in Mechanical Sensors". *Journal of the Electrochemical Society* 144.4 (1997). (Cit. on p. 28).

[Stru1976] L. Struik. "Physical aging in amorphous glassy polymers". *Annals of the New York Academy of Sciences* 279.1 (1976). (Cit. on p. 79).

[Stua1963] M. Stuart. "Dielectric properties of cross-linked polystyrene film formed in the glow discharge". *Nature* 199.4888 (1963). (Cit. on p. 25).

[Suna2017] J. Sunarso et al. "Membranes for helium recovery: An overview on the context, materials and future directions". *Separation and Purification Technology* 176 (2017). (Cit. on p. 57).

[Swai2015] R. Swaidan, B. Ghanem, and I. Pinnau. *Fine-tuned intrinsically ultramicroporous polymers redefine the permeability/selectivity upper bounds of membrane-based air and hydrogen separations*. 2015 (cit. on pp. 13, 14, 57).

[Swan1967] R. G. Swann, R. Mehta, and T. Cauge. "The Preparation and Properties of Thin Film Silicon-Nitrogen Compounds Produced by a Radio Frequency Glow Discharge Reaction". *Journal of The Electrochemical Society* 114.7 (1967). (Cit. on p. 25).

[Tani2006] N. Tanio and T. Nakanishi. "Physical aging and refractive index of poly (methyl methacrylate) glass". *Polymer journal* 38.8 (2006). (Cit. on p. 99).

[Theo2006] D. N. Theodorou. "Principles of molecular simulation of gas transport in polymers". *Materials science of membranes for gas and vapor separation* (2006). (Cit. on p. 17).

[Tsur2011] T. Tsuru et al. "2-Step plasma-enhanced CVD for low-temperature fabrication of silica membranes with high gas-separation performance". *Chemical Communications* 47.28 (2011). (Cit. on pp. 37, 58, 80).

[Vasu2013] M. C. Vasudev et al. "Exploration of plasma-enhanced chemical vapor deposition as a method for thin-film fabrication with biological applications". *ACS applied materials & interfaces* 5.10 (2013). (Cit. on p. 37).

[Viss2005] T. Visser, G. Koops, and M. Wessling. "On the subtle balance between competitive sorption and plasticization effects in asymmetric hollow fiber gas separation membranes". *Journal of Membrane Science* 252.1-2 (2005). (Cit. on p. 69).

[Viss2007] T. Visser, N. Masetto, and M. Wessling. "Materials dependence of mixed gas plasticization behavior in asymmetric membranes". *Journal of Membrane Science* 306.1-2 (2007). (Cit. on p. 69).

[Vopi2014] O. Vopička, M. G. De Angelis, and G. C. Sarti. "Mixed gas sorption in glassy polymeric membranes: I. CO2/CH4 and n-C4/CH4 mixtures sorption in poly (1-trimethylsilyl-1-propyne)(PTMSP)". *Journal of membrane science* 449 (2014). (Cit. on p. 71).

[Wang2017] M. Wang et al. "Gas selective ultrathin organic covalent networks synthesized by iPECVD: does the central metal ion matter?" *Advanced Functional Materials* 27.29 (2017). (Cit. on pp. 31, 58, 80).

[Wang2018] J. Wang et al. "Plasma modification and synthesis of membrane materials—a mechanistic review". *Membranes* 8.3 (2018). (Cit. on p. 37).

[Wijm1995] J. G. Wijmans and R. W. Baker. "The solution-diffusion model: a review". *Journal of membrane science* 107.1-2 (1995). (Cit. on p. 10).

[Wind2003] J. D. Wind et al. "Relaxation dynamics of CO2 diffusion, sorption, and polymer swelling for plasticized polyimide membranes". *Macromolecules* 36.17 (2003). (Cit. on p. 81).

[Yamp2006] Y. Yampolskii, I. Pinnau, and B. D. Freeman. *Materials science of membranes for gas and vapor separation*. 2006 (cit. on p. 19).

[Yasu1977] H. Yasuda and T. Hsu. "Some aspects of plasma polymerization investigated by pulsed RF discharge". *Journal of Polymer Science: Polymer Chemistry Edition* 15.1 (1977). (Cit. on p. 65).

[Yasu1984] H. Yasuda. "Plasma polymerization for protective coatings and composite membranes". *Journal of membrane science* 18 (1984). (Cit. on p. 31).

[Yasu1985] H. Yasuda. "Plasma polymerization Academic Press". *Inc., Orando, Florida* (1985). (Cit. on p. 25).

[Yasu2000] H. Yasuda and T. Yasuda. "The competitive ablation and polymerization (CAP) principle and the plasma sensitivity of elements in plasma polymerization and treatment". *Journal of Polymer Science Part A: Polymer Chemistry* 38.6 (2000). (Cit. on p. 26).

[Yasu2012] H. K. Yasuda. *Plasma polymerization*. Academic press, 2012 (cit. on p. 26).

[Zani2007] S. Zanini et al. "Characterisation of SiOxCyHz thin films deposited by low-temperature PECVD". *Vacuum* 82.2 (2007). (Cit. on p. 25).

[Zha2021] H. Zha et al. "Enhanced Free Surface Mobility Facilitates the Release of Free-Volume Holes in Thin-Film Polymer Glasses". *Macromolecules* 54.4 (2021). (Cit. on p. 80).

[Zhu2021] L. Zhu et al. "Scalable Polymeric Few-Nanometer Organosilica Membranes with Hydrothermal Stability for Selective Hydrogen Separation". *ACS nano* 15.7 (2021). (Cit. on p. 59).

[Zuza2022] D. Zuza et al. "Characterization of hexamethyldisiloxane plasma polymerization in a DC glow discharge in an argon flow". *Vacuum* (2022). (Cit. on p. 37).